Mechanisms of PTTH signaling and steroid hormone biosynthesis in *Bombyx mori* and *Drosophila melanogaster*

A DISSERTATION
SUBMITTED TO THE FACULTY OF THE GRADUATE SCHOOL
OF THE UNIVERSITY OF MINNESOTA
BY

Rachel Jeanne Herder

IN PARTIAL FULFILLMENT OF THE REQUIREMENTS
FOR THE DEGREE OF
DOCTOR OF PHILOSOPHY

Dr. Michael B. O'Connor

August 2012

ACKNOWLEDGEMENTS

I am very grateful to my advisor, Dr. Michael B. O'Connor for allowing me to work in his lab over the past several years and for his helpful feedback and support. He was extremely patient and flexible with me while I navigated the joint degree path and I am extremely appreciative of that. I would also like to thank all past and present members of the O'Connor lab for their thoughtful ideas on my project and their technical assistance. Mary Jane O'Connor was very helpful with troubleshooting and with the development of several reagents and fly lines used in this thesis. Dr. Aidan Peterson has been wonderful to work with and has provided me with extensive technical assistance, from fly crosses to microscope work to proof-reading drafts; he has helped guide my graduate school experience. Dr. Naoki Yamanaka has provided extremely valuable insight for design and implementation of ecdysone-related experiments and was always patient with my endless questions.

I would like to thank the members of my committee for their helpful guidance and throughout my graduate school career. They provided great feedback on my preliminary examination that helped me become a better writer and have provided helpful comments at my annual committee meetings. My committee members include: Dr. Mike O'Connor (advisor), Dr. Ann Rougvie (committee chair), Dr. Hiroshi Nakato, Dr. Anna Petryk, and Dr. Jeff Simon. Dr. Howard Towle was also a member of my committee during my preliminary examination and he attended annual committee meetings and provided feedback throughout my time at the University of Minnesota.

I would like to thank members of the University of Minnesota's Developmental Biology Center for providing support and helpful feedback on my project. I would also like to acknowledge the University of Minnesota's Developmental Training Grant for supporting two years of my graduate studies.

I am grateful to the University of Minnesota's Joint Degree Program in Law, Health and the Life Sciences for providing support as I pursued a joint degree program. In particular, I would like to thank Carol Rachac. Dean Erin Keyes and Sue Knoblauch for their assistance in helping me navigate the dual degrees.

Chapter 2: I would like to thank Christina Brakken-Thal for analyzing the voluminous Illumina data. I am thankful to Dr. Naoki Yamanaka for his expertise in raising and dissecting *Bombyx mori*. I am grateful for the technical support from the University of Minnesota's Biomedical Genomics Center; specifically Nichole Peterson and Aaron Becker. I am also grateful for the technical support from the Minnesota Supercomputing Institute; particularly Ying Zhang.

Chapter 3: I would like to thank Dr. Kim Rewitz who started the *phantom* enhancer project. I also would like to thank MaryJane O'Connor for her help developing many of the *phantom* and *spookier* enhancer-GFP reporter lines. I would also like to thank David Zhitomirsky for his assistance with cloning.

Chapter 4: I would like to thank Dr. Naoki Yamanaka for providing and translating the initial MSBP data used to begin this project and for his assistance and patience with my many questions.

Appendix A: I am grateful to Mary Jane O'Connor for helping me begin the dSmad2F4 sequencing analysis and Dr. Aidan Peterson for his guidance throughout this project.

Appendix B: I would like to thank Dr. Mu Sun for helping me begin this project while I was still a rotation student. I am also grateful to Dr. Bob Hafner and Alice Ressler of the EM Characterization Facility at the University of Minnesota for their technical helping preparing and analyzing electron microscope sections.

I am grateful to Drs. Naoki Yamanaka, Aidan Peterson, and Maggie O'Meara for their thoughtful comments on early drafts of my thesis and my committee readers, Drs. Mike O'Connor, Anna Petryk and Hiroshi Nakato for their extremely helpful suggestions on my first draft.

DEDICATION

This dissertation is dedicated to my parents, John and Jeanne Herder. Without their endless support and love this would have never been possible.

ABSTRACT

Animals use steroid hormones to regulate the timing of development and growth. In insects, the developmental processes of hatching, molting, metamorphosis and eclosion are all regulated by a steroid hormone, 20-hydroxyecdysone (20E). Biosynthesis of ecdysone (E), the immediate precursor to 20E, is thought to be regulated, in part, by a small neuropeptide called prothoracicotropic hormone (PTTH).

PTTH is produced by neurons that innervate the prothoracic gland (PG) and signals to this tissue to up-regulate biosynthesis of E in insects, including *Drosophila melanogaster* (fruit fly) and *Bombyx mori* (silk worm). When PTTH signaling is disrupted, developmental timing is altered. This thesis focuses on further elucidating the role of PTTH signaling in development through three separate but related aims.

First, to better understand the global effects of PTTH signaling on transcriptional regulation in the PG, we used Illumina Next Generation sequencing to compare the transcriptome of PTTH-stimulated and –unstimulated PGs. This was used as an unbiased approach to determine what genes are up and down regulated in response to PTTH stimulation. At the time of this thesis writing, the sequencing reactions have been completed, however, the bioinformatics analysis is still underway.

Second, to better understand how PTTH acts to up-regulate gene expression, we analyzed regulatory elements in target genes using a promoter-bashing approach. Using this approach, we uncovered three minimal enhancer regions from *phantom*, *spookier* and *disembodied*, members of the Halloween family of E biosynthetic genes that are expressed in the PG. Additionally, we have discovered several small, highly conserved, sequence motifs that are necessary for reporter gene expression in the PG.

Third, we examined a single PTTH-responsive gene, called Membrane Steroid Binding Protein (MSBP), with the goal of elucidating its role in ecdysone biosynthesis. We have confirmed that MSBP is expressed in ecdysone producing tissues and that *MSBP* expression changes in response to PTTH. However, $MSBP^{-/-}$ animals show no obvious phenotype, suggesting either redundancy or no requirement of MSBP in regulating developmental timing.

TABLE OF CONTENTS

List of Tables

List of Figures

CHAPTER 1: INTRODUCTION

I. Introduction

a. Developmental timing

Precise timing of multiple gene programs is essential for the proper development of higher organisms. Animals use multiple and diverse timing mechanisms to coordinate proper development with growth. In order for an animal to develop correctly, there must be extensive integration of timing mechanisms with various downstream regulatory mechanisms [1]. Endocrine hormones are critical coordinators of developmental timing because they act systemically, thereby eliciting coordinated morphological, physiological, biochemical, and molecular events throughout the entire body [2].

b. Steroid hormones

Steroid hormones are one class of endocrine molecules that signal developmental change. Steroid hormones act as timing cues and steroid hormone pulses of a defined duration are important for gene regulation both in higher organisms and in insects [3,4]. Disruption of steroid hormone levels can have catastrophic consequences in the development of an organism, including birth defects or fatality [1]. In humans, steroid hormones regulate the timing of several developmental and biological processes, including: stress responses, metabolic regulation, salt and water balance, fetal development, pregnancy, puberty, and the menstrual cycle [2]. In insects, the timing of hatching, molting,

and metamorphosis are regulated by a steroid hormone called 20-hydroxyecdysone (20E) [5,6]. The downstream effects of steroid hormones on developmental timing have been studied for decades [7,8], however, much is still to be learned about how steroid hormone biosynthesis is regulated and how steroid hormone signals are coordinated with growth.

c. Significance

Basic research of steroid hormone production in insects can benefit society in two major ways. First, understanding insect steroid hormone biosynthesis can advance the design of new insect control agents for use in agriculture [9] and to control insects that act as vectors for the spread of human disease [10]. Second, genetic and molecular studies in the common fruit fly, *Drosophila melanogaster*, have been instrumental for the advancement of understanding several human pathologies and diseases [6,11-15]. By better understanding the basic mechanisms underlying regulation of steroid hormone biosynthesis during development in insects, we hope to advance underlying knowledge of how steroid hormone biosynthesis is controlled in higher organisms.

II. Model organisms: *Drosophila melanogaster* and *Bombyx mori*

a. Drosophila melanogaster

The two insect model organisms we chose to study steroid hormone biosynthesis are *D. melanogaster* from the order Diptera, and a close relative, the silkworm, *Bombyx mori* from the order Lepidoptera. *D. melanogaster* has been a model

organism for genetics for over a century and the genome has been fully sequenced and annotated for over the last decade [16-18]. There are many genetic tools available to manipulate and study *Drosophila*, including: marked balancer chromosomes, P-element (transposon) insertion/imprecise excision tools, chemical mutagenesis protocols, and the GAL4/UAS induction system that is useful for tissue-specific RNAi knockdown and over-expression studies [14,18]. Several human diseases have been modeled in *Drosophila* and many genes and signaling pathways are highly conserved between flies and humans [14,18,19]. Studies of steroid hormones in *Drosophila* are particularly advantageous because *Drosophila* has a relatively short and predictable lifecycle; development from egg to adult takes only nine days at 25 ºC, whereas the developmental lifecycle of higher organisms like mice or humans is on the timescale of months or years. Just as in humans, many developmental transitions in *Drosophila* are immediately preceded by a pulse of steroid hormones called ecdysteroids. However, unlike humans which have many signaling steroid hormones molecules, *Drosophila* has only two known steroid hormone molecules that elicit a response: 20-hydroxyecdysone (20E), which is thought to be the major signaling molecule, and its immediate precursor, ecdysone (E) [6]. It is thought that 20E is synthesized in a linear pathway, making analysis of each step simpler than in mammals where several parallel biosynthetic pathways occur. Another advantage of *Drosophila* as a model organism to study steroidogenesis is that *Drosophila*, unlike mammals, cannot synthesize cholesterol de novo from

acetate. Instead, cholesterol or plant sterols must be digested; making radio labeled feeding experiments possible. Since steroid hormones are instrumental in regulating and coordinating *Drosophila* development, understanding the basics of steroid hormone biology is essential for a more broad understanding of *Drosophila* as a model organism.

b. Bombyx mori

One disadvantage of *Drosophila* is its relatively small size (Figure 1). The ring gland (RG) is the major endocrine tissue responsible for production of E during *Drosophila* larval development. The RG is less than $1/10^{th}$ of a millimeter and contains approximately 50 E-producing prothoracic gland (PG) cells (Figure 1). Dissection and collection of the *Drosophila* larval RG can pose technical difficulties when large amounts of tissue are needed for biochemical studies. To overcome this issue, we have harnessed the power of another insect model organism, *Bombyx mori,* commonly known as the silkworm. *Bombyx* is a large lepidopteran insect which has been used as a model organism for neuropeptide research [20,21]. *Bombyx* is the model insect for the order Lepidoptera and has been domesticated for over 5000 years [22,62]. The larval PGs of *Bombyx* are approximately 3 millimeters in length, about the size of a *Drosophila* larva. Although genetic tools in *Bombyx* are not as widely available as in *Drosophila*, the *Bombyx* genome has been sequenced since 2004 [22-24]. *Bombyx* has historically been used to study insect endocrinology; both ecdysone (E) and prothoracicotropic hormone (PTTH) were first isolated and characterized in

Bombyx [25,26]. Furthermore, *Bombyx* uses both neuronal and hormonal pathways to regulate ecdysteroidogenesis which makes it a good insect for studying how environmental and internal cues for development are related to PG activity [20].

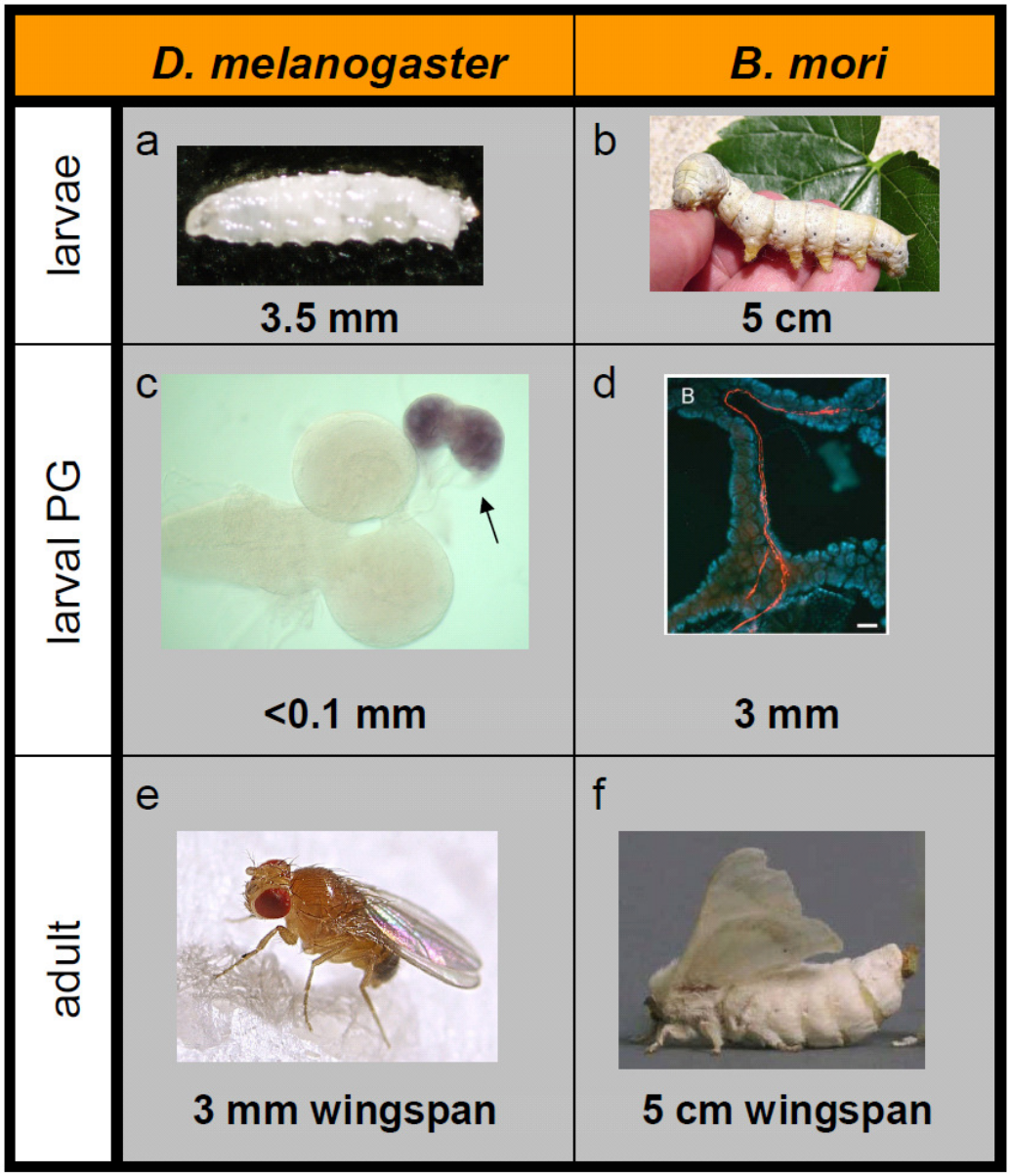

Figure 1: Relative sizes of *Drosophila melanogaster* and *Bombyx mori.*
The large size of the *Bombyx* PG make it a better model organism to collect large amounts of RNA. (a) a *D. melanogaster* third instar larva is approximately 3.5 mm in length; (b) a *B. mori* fifth instar larva is approximately 5 cm in length; image from http://www.suekayton.com/Silkworms/lifecycle.htm (c) a *D. melanogaster* PG (arrowhead) from a late third instar larva is <0.1 mm; (d) a *B. mori* PG from a mid-fifth instar larva is approximately 3 mm in length; image from Yamanaka et al. 2011 [20]; (e) the wingspan of an adult *D. melanogaster* fly is approximately 3 mm; © Max Westby (f) the wingspan of an adult *B. mori* is approximately 5 cm; image from http://www.blogspan.org/blogs/permalinks/10-2006/mate-attracting-chemicals-in-silk-worms.html

III. Control of ecdysteroid titers

a. E producing tissues

Biosynthesis of ecdysteroids (*i.e.* ecdysteroidogenesis) occurs predominantly in endocrine tissue located near the brain of larval insects and the ovaries of adult females [6]. In larvae of diptera, such as *Drosophila*, the PG cells are part of the RG endocrine complex and the PG are the cells that produce E (Figure 2). The RG also contains two other glandular tissues, the corpora allata (CA) and the corpora cardiaca (CC) [29][27]. In lepidopterians, like *Bombyx*, the CC, CA and PG are separate glands [28]. CA endocrine tissues produce a sesquiterpenoid insect hormone, called juvenile hormone (JH) which plays an essential role in development [29]. JH determines the nature of each larval molt, in the presence of JH a larval - larval molt occurs while in the absence of JH a metamorphic molt occurs [27]. The CC has been compared to the hypothalamus-pituitary axis in vertebrates and the main hormone produced by the CC is adipokinetic hormone (AKH), a peptide that acts on the fat body and mobilizes lipids and carbohydrates [30].

Ecdysteroids are also produced by epidermal and gonadal cells in some insects and the ovaries are important in producing the ecysteroids necessary for future embryonic development of the egg [6][27]. During larval stages, the PGs are the primary source of E which is hydroxylated to its active form, 20E, in peripheral

tissues [6,31]. The studies in this thesis pertain mainly to larval production of E in the larval PG.

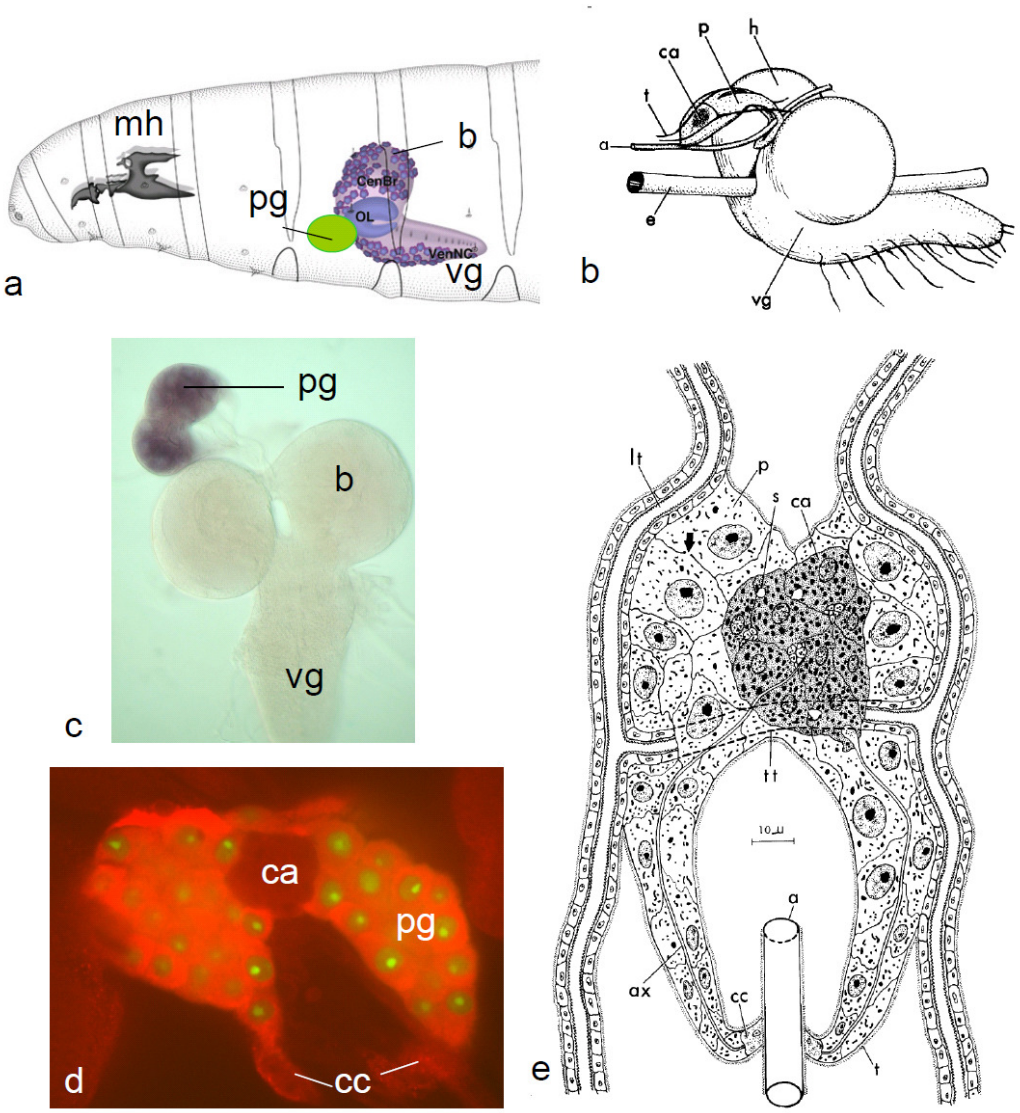

Figure 2: The ring gland in *Drosophila melanogaster*
(a) Illustration of the anterior portion of a third instar Drosophila larva, figure adopted from *Atlas of Drosophila Development* by Volker Hartenstein [32]. *mh* mouth hooks; *pg* prothoracic gland; *b* brain lobe; *vg* ventral ganglion. (b) Diagram of the central nervous system, ring gland, and portions of the circulatory and digestive systems of a third instar larva of *Drosophila melanogaster*,. *a* aorta; *ca* corpus allatum tissue of ring gland; *e* esophagus; *h* right brain hemisphere; *p* prothoracic gland tissue of ring gland; trachea; *vg* ventral ganglion. Image from King et al. 1966 [33]. (c) Image of the brain-ring gland complex from *Drosophila melanogaster*. *pg* prothoracic gland, stained by *in situ* hybridization with anti-MSBP probe; *b* brain lobe; *vg* ventral ganglion. (d) Image of a third instar *Drosophila* ring gland, stained by immunohistochemistry with

an anti-MSBP antibody. (e) Diagram of a transverse section through the ring gland of a third instar larva. *ca* corpus allatum cell; *cc* corpus cardiacum cell; *lt* left lateral trachea; *p* cell of prothoracic gland; *t* acellular tunica; *tt* transverse trachea. Image from King et al. 1966 [33].

c. Neuropeptide regulation of E biosynthesis

Many of the events that occur during insect development (including the morphological, physiological, biochemical, and molecular changes of molting and metamorphosis) are modulated by 20E [6]. In insects, the production and release of E from the PG is primarily regulated by a small neuropeptide called prothoracicotropic hormone (PTTH). Neuropeptide control of steroidogenesis is not unique to insects. In fact, the mechanisms that regulate steroidogenesis in vertebrates and insects are strikingly similar[1] [6,34-36]. Understanding PTTH regulation of E biosynthesis is key to understanding the mechanisms that regulate developmental timing in insects.

i. PTTH neurons

In insects, PTTH is a small neuropeptide produced by neurons that innervate the PG and stimulates up-regulation of E biosynthesis [37]. In *Drosophila* third instar larvae, PTTH is produced in the PG neurons by a pair of bilaterally symmetric central brain neurons whose axons terminate on the PG cells of the RG; these neurons are called the PG neurons or the PTTH neurons [28,37]. In *Bombyx* fifth instar larvae, PTTH is produced primarily in a pair of dorsolateral neurosecretory cells that terminate in the corpus allatum [38,39]. After being released from the

[1] In mammalian reproductive development, the neuropeptide, kisspeptin coordinates the timing of puberty with nutritional and metabolic inputs.

corpus allatum, PTTH then travels in the hemolymph where it targets the PG to trigger ecdysone release via activation of second messenger pathways [40-42]. The PTTH-neurons and mechanisms of PTTH release are divergent between lepidopteran and diptera, and it has been hypothesized that this reflects a difference in PTTH expression rather than a rewiring of PTTH neurons [37]. New evidence indicates that PTTH is also circulating in *Drosophila* as it is in *Bombyx* (N. Yamanaka and P. Léopold, unpublished communications).

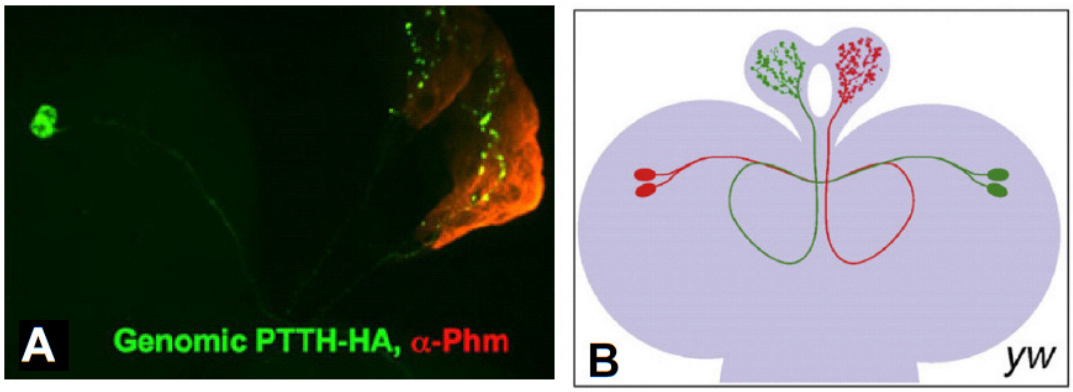

Figure 3: Diagram of PTTH neurons in a *Drosophila* third instar larva
In *Drosophila*, the PTTH neurons (sometimes called PG neurons) directly innervate the PG and induce production and secretion of ecdysone by releasing PTTH. (A) A pair of PTTH neurons, marked with GFP innervate the PG cells of the RG, shown in red. Figure courtesy of McBrayer et al. [37]. (B) Axon projections from PTTH neurons follow a well-defined path with the left lobe of the brain innervating the right PG and *vice versa.* Figure courtesy of Gosh et al. [43].

ii. PTTH molecule

Prothoracicotropic hormone (PTTH) is a diffusible neuropeptide hormone that has been purified, cloned, and characterized from a variety of Lepidoptera and Diptera, including *B. mori*, *M. sexta*, and *D. melanogaster* [6,38,44,45]. Comparison of the PTTH peptide sequences among Lepidopterans shows that PTTH sequences have diverged considerably resulting in the PTTH family of

proteins having species-specific action [6]. In Lepidopterans, PTTH is synthesized as a larger prohormone but is released as a shorter, glycosylated homodimeric molecule of approximately 25 to 30 kDa [6,53]. Each monomer has three intramolecular disulfide bridges and the seventh cystine forms a disulfide bond to facilitate dimerization of the monomers [6,56]. The intermonomer cystine-cystine bonds are essential for the activity of PTTH, whereas dimerization and glycosylation play a smaller role [56].

In *Drosophila*, the PTTH neuropeptide hormone is much larger than in Lepidopterans and *Drosophila* PTTH requires glycosylation for bioactivity [44]. *Drosophila* PTTH is 192 amino acids in length and is predicted to be 21.4 kDa [37]. When compared phylogenetcally, the *Drosophila* and Lepidopteran PTTH amino acid sequences are distantly related [37]. While purified PTTH from *Manduca* and *Bombyx* has been used to directly stimulate ecdysteroidgenesis of the PG, attempts to use recombinant *Drosophila* PTTH to directly stimulate ecdysteroidgenesis have been unsuccessful [37,46,47]. The inability of recombinant *Drosophila* PTTH (rPTTH) to stimulate PG activity may be due to the inability of *Drosophila* S2 cells to properly synthesize and process rPTTH into an active signaling molecule [37]. Alternatively, it could be that PTTH acts more like a neurotransmitter and needs to directly signal through the PG neurons [37].

iii. PTTH phenotype

In *Drosophila*, when the PTTH-producing PG neurons are ablated using the *ptth*>GAL4::UAS-*grim* system to specifically cause cell death in the PTTH-producing PG neurons, the result is a low level of 20E which results in developmental delay and a large body phenotype [37,43,46]. The large phenotype can be seen in both third instar larvae and pupae and the large body is a result of an extended period in larval feeding stages [37,43]. The larvae feed for a longer period of time because they are not exposed to a 20E peak that initiates prepupal development [37,43].

iv. PTTH receptor

Once PTTH is processed, it binds to a receptor called Torso on the surface of the PG [46]. Torso was originally identified for its role in anterior-posterior patterning in the early *Drosophila* embryo [48-50]. During early embryogenesis, the putative ligand for Torso is called Trunk [46]. Trunk and PTTH have many similarities: Trunk has a cysteine knot-motif near the C-terminus that is similar to PTTH; both PTTH and Trunk are proteolytically processed to generate an active signaling molecule. Once processed both proteins are of similar length; and the mature version of both proteins share similar structures [37,49,51,52]. Unlike PTTH, *trunk* expression is not detected in the third-instar wandering stage suggesting that the Torso receptor can recognize both the PTTH and Trunk ligands but that these proteins are expressed at different developmental times [46].

Torso is a receptor tyrosine kinase that functions in the mitogen-activated protein kinase (MAPK) pathway in the PG of *Drosophila* and *Bombyx* [40,41,46,53,54]. The canonical MAPK pathway includes: Ras (Ras85D), Raf (Draf), MAPK kinase (MEK), and extracellular signal-regulated kinase (ERK) [46,49]. Activation of Torso by PTTH in the larval PG stimulates ERK phosphorylation [46]. RNAi knockdown of Ras, Raf, or ERK in the PG gives a delayed pupariation phenotype, reminiscent of the delayed phenotype seen in ablated PTTH neuron and Torso-knockdown animals [37,46]. ERK knockdown in the PG also phenocopies the increase in pupal size seen in animals with ablated PTTH neurons and RNAi knockdown of Torso; this increase in pupal size can be rescued by 20E feeding [46].

During embryonic development, the Torso pathway specifies terminal cell fates by regulating target gene expression [49]. For example, the posterior expression of *tailless*, a nuclear hormone receptor, is mediated by the Torso pathway[49]. Similarly, the Torso pathway induces the expression of *huckebein*, a zinc-finger transcription factor [49]. Torso response elements have been identified in the *tailless* promoter, and mutation of the Torso response elements causes a change in reporter gene expression [49]. We hypothesize that in the PG, the PTTH-mediated Torso signaling pathway may be acting in a similar manner to regulate genes involved in E production. Identification of PTTH-responsive elements will

be important to understanding how PTTH signaling specifically elicits E production in the PG.

PTTH signaling induces a multifaceted response: it induces both gene transcription and translation, and also post-translational control of steroidogenic enzymes in the PGs of *Drosophila* and *Bombyx* [27]. For example, PTTH-stimulation specifically induces phosphorylation and translation of Spook in Bombyx [50]. Expression of several ecdysteriodogenic biosynthesis enzymes correlate with the fluctuation of the PTTH titer in *B. mori* [55]. PTTH stimulation also induces rapid translation of several proteins [56]. Phosphorylation events of steroidogensis enzymes have been detected in response to PTTH signaling [54]. PTTH influence of transcription, translation, and post-translational control of genes allows PTTH to influence both short- and long-term ecdysteroidogenic effects [27].

IV. Steroid hormone biosynthesis

In both humans and insects, steroid hormones are synthesized by a conserved mechanism. The basic four-ring structure of dietary cholesterol undergoes a step-by-step biosynthetic conversion of side chain groups to generate a specific signaling molecule[2]. Steroid hormone synthesis requires specific enzymes, usually cytochrome P450s, to catalyze the high-energy side chain reactions [2]. While humans have a large number of steroid hormone molecules, insects have one major signaling steroid hormone, 20-hydroxyecdysone (20E). Arthropods,

such as *D. melanogaster*, are sterol auxotrophs, meaning they require dietary sterols such as cholesterol (C) in their diet; unlike mammals, insects cannot synthesize sterols from precursor molecules, such as acetate or acetyl-CoA [6,57]. During post-embryonic development of Lepidoperan and Dipterian insects, E is synthesized from dietary cholesterol or phytosterols through a series of hydroxylation and oxidation steps [6].

a. Ecdysteroids

In insects, ecdysteroids function biologically to trigger developmental transitions, including: hatching, molting, and metamorphosis[2]. Chemically, the term ecdysteroids refers to a family of sterol derivatives that have common structural features: a cis (5β-H) junction of rings A and B, a 7-ene-6-one chromophore, and a trans (14α-OH or –H) junctions of rings C and D [58]. 20E is the major molting hormone in all arthropods, including insects [58]. E, the immediate precursor to 20E, is thought to play a minor role in most insect species [58]. 20E biosynthesis in *Bombyx* and *Drosophila* is the focus of this thesis.

Insects are unable to synthesize sterols *de novo* and therefore rely on dietary cholesterol and phytosterols as precursors to synthesize ecdysteroids [58]. Insects that are able to feed on an animal-derived food source can get cholesterol directly, while insects that feed exclusively on plants generally must dealkylate the phytosterols [58]. Phytosterol processing varies amongst different

[2] In early studies, “molting hormone” was the term used to describe the factor, now known as E, that was produced from the endocrine gland near the brain in *Bombyx mori*.

insect species; the different processing of sterols amongst insects is demonstrative of the ability of different insects to feed on different food sources [58]. Once cholesterol is made or ingested, it must travel from the gut to the steroidogenic cells (*e.g.* the PG in *Drosophila* and *Bombyx*) which occurs through the classical receptor-mediated low-density lipoporotein endocytic pathway that has been described in mammals [58]. Once cholesterol is delivered to the endosomes, intracellular trafficking must deliver cholesterol to the first enzyme involved in steroidogeneis; in the case of *Drosophila* and *Bombyx*, cholesterol must be delivered intracellularly to the endoplasmic reticulum (ER) for processing by Neverland (Nvd) [58]. During biosynthesis of E in the PG, sterol intermediates must be moved intracellularly because the various enzymes involved in steroidogenesis are localized in different compartments (*i.e.* the ER and mitochondria) [58]. Finally, E must be released to the hemolymph so that it can reach target cells and to be converted to the final signaling molecule 20E [58].

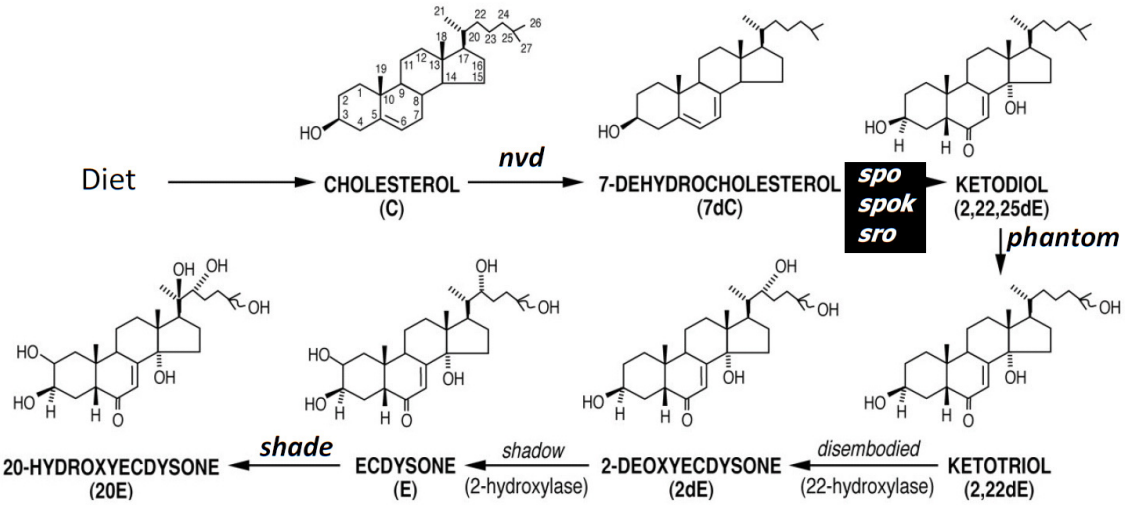

Figure 4: 20E Biosynthetic pathway.
In insects, 20 hydroxyecdysone (20E) is synthesized from dietary cholesterol through a cascade of sequential hydroxylations catalyzed by several enzymes, including: Neverland (Nvd), Spook (Spo), Spookier (Spok), Shroud (Sro), Phantom (Phm), Disembodied (Dib), Shadow (Sad), and Shade (Shd). Image courtesy of Warren et al. (2002) [5].

b. Ecdysteroidogenic genes

The ecdysteroidogenic biosynthetic pathway involves a cascade of sequential hydroxylations that are catalyzed by several enzymes, mainly cytochrome P450 monooxygenases (Figure 4) [58]. A number of these P450s belong to a group of genes termed the Halloween Genes. The so-called Halloween gene mutants were first identified in a large ethyl methane sulfonate (EMS) mutagenesis screen to identify mutations that affect the pattern of the larval cuticle [59-61]. The Halloween genes identified in the screen all shared a mid-embryonic lethality and a failure to form a differentiated first instar cuticle. They were given names such as phantom, disembodied, and spook to highlight the lack of differentiated cuticle phenotype [59-61]. Subsequent studies have shown that many of the Halloween mutants identified in the 1984 screen are deficient in 20E production in

Drosophila; their *Bombyx* homologues share a similar deficiency [5,31,62-65]. Some of the Halloween genes identified in the 1984 screen have a disrupted cuticle but are not thought to be involved in E biosynthesis (e.g. *haunted*, *mummy*, *ghost*) [63]. Additional genes involved in 20E biosynthesis have been identified since the 1984 screen; the known genes involved in 20E biosynthesis that are discussed in detail below include: *neverland* (*nvd*), *spook* (*spo; Cyp307a1*), *spookier* (*spok; Cyp307a2*)[3], *spookiest* (Cyp307B1)[4], *shroud* (*sro*), *phantom* (*phm; Cyp306a1*), *disembodied* (*dib; Cyp302A1*), *shadow* (*sad; Cyp315a1*), and *shade* (*shd; Cyp314a1*) [5,31,62-68]. The characterization of genes involved in ecdysteroidogenesis has been done largely using both the *Drosophila* and *Bombyx* systems; *Drosophila* has available powerful genetic tools and the advantage of *Bombyx* is its large PGs which makes it easier to dissect large amounts of tissue for biochemical analysis. The following section discusses what is known in *Drosophila* and *Bombyx* about each intermediate step in ecdysteriodogenesis, from cholesterol to 20E.

c. 20E Biosynthetic pathway

i. C → 7dC by Neverland

The first step of steroid hormone biosynthesis in arthropods is the conversion of dietary cholesterol (C) to 7-dehydrocholesterol (7dC) [6]. Nvd does not appear to be the rate-limiting enzyme in E biosynthesis [58]. Nvd was first identified in 2006 by Yoshiyama *et al*. and is essential for the first step of E biosynthesis:

[3] Spok has been identified only in *Drosophila.*
[4] *Spot* has been identified in mosquitoes, honey bees and red flour beetles but not *Drosophila*.

conversion of C to 7dC by 7,8-dehydrogenation [68]. *Nvd* is a Rieske-domain non-heme iron oxygenase protein that localizes in endoplasmic reticulum (ER) [68]. The *nvd* expression pattern in both *Bombyx* and *Drosophila* is consistent with its role in ecdysteroidogenesis. Temporally, *nvd* is expressed preceding molting and pupation in fourth and fifth instar *Bombyx* larvae, a result consistent with other ecdysteroidgenic genes [62,64,65,67]. In *Bombyx* fifth instar larvae, RT-PCR analysis shows *nvd* mRNA is expressed predominantly in the PG with weak expression in the brain and Malpighian tubules [68]. In *Drosophila*, *in situ* RNA hybridization shows specific *nvd* expression in the PG cells (but not the CA or CC) of the third instar larval RG, the primordial RG of the stage 14 embryo, and in the nurse cells of the adult female ovary [68].

The phenotype of a *Drosophila nvd* genetic mutant is yet to be determined because no *nvd* mutants have been isolated or created due to difficulties resulting from its location in heterochromatin [68]. The phenotypes of loss- and gain-of-function of *nvd* have been analyzed through the powerful *Drosophila* genetic tool, UAS/GAL4. Nvd overexpression in a variety of tissues shows no visible phenotypes [68]. GAL4/UAS-RNAi knock-down of *nvd* in the PG causes animals to arrest growth in their first instar larval stage and remain as first instar larvae[5][68]. This result is consistent with the phenotype of other ecdysteroidogenic genes knocked down by RNAi in the larval PG [62,67]. The

[5] The name "*neverland*" is a reference to the island in the play, *Peter Pan* by J. M. Barrie where children do not grow up.

larval arrest of *nvd*-RNAi knock down is due to a reduction in ecdysteroid titer and the larval arrest can be overcome by feeding with either E or 7dC, placing it in the first step of the 20E biosynthetic pathway [68,69]. The function of the Rieske oxygenase domain in Nvd as a 7,8-dehydrogenase is thought to be evolutionarily conserved in cholesterol metabolism throughout animal phyla [69].

ii. 7dC → → → Δ^4-diketol: The Black Box (spook, spookier, spookiest, and shroud)

Although the 20E biosynthetic pathway has been studied for over a decade, the critical steps that convert 7dC to Δ4-diketol (the so-called "Black Box") have remained elusive [70]. The "Black Box" terminology was adopted because during insect steroidogenesis, the intermediates immediately downstream from 7dC do not accumulate and have not been easily isolated [58]. It has been hypothesized that the lack of intermediates from the Black Box is because the first step after 7dC is a rate-limiting step and the intermediate steroidogenic compounds are unstable [58,71].

Drosophila spook (*spo;* Cyp307A1) is one of the Halloween mutants identified in the 1984 EMS screen; mutant *spo* alleles lack cuticle differentiation [60]. Like other *Drosophila* Halloween mutants, *spo* mutants develop normally until stage 14 of embryogenesis at which point head involution fails [62]. *Spo* encodes for a cytochrome P450 monooxygenase involved in the Black Box of embryonic E biosynthesis in Bombyx and Drosophila [62,72]. Spo contains an N-terminal sequence characteristic of microsomal P450s and has been shown to co-localize

with an ER marker but not a mitochondrial marker [62]. *Drosophila spo* is unique from the other Halloween genes involved in E biosynthesis, in that it is not expressed in the PG during embryonic or larval stages [62]. *spo* is expressed in the follicle cells of the adult ovaries and in the early embryonic yolk nuclei and amnioserosa [62].

Spookier (*spok;* Cyp307A2) is a cytochrome P450 that was identified and characterized by Ono et al. [62]. *Spok* shares 57% identity with *spo* and is believed to be a functionally redundant, stage-specific paralog, acting in the stage 17 embryonic ring gland and the larval PG but not in the early embryonic tissues or ovary [62]. Therefore, although *spo* and *spok* have different spatial and temporal expression, they likely share an equivalent biochemical role [51,62,72,73]. Indeed, *spo* expressed specifically in the PG (using a *phm*>GAL4/UAS-spo system) rescues $spok^{-/-}$ animals (unpublished observations from M.J. O'Connor). It is unknown if *spo* / *spok* gene have evolutionarily developed different subfunctionalities since the gene duplication event [73].

No *spok* mutants have been isolated or created but RNAi knockdown of *spok* in the PG using a *phm*-GAL4 driver results in first instar larval arrest [62]. The larval arrest of *spok*-RNAi knockdown animals can be rescued by feeding the larvae E or 20E but not 7dC, indicating that *spok* plays a role in the Black Box

[62]. Within the Black Box, recent feeding experiments indicate that Spok catalyzes a reaction upstream of Δ^4-diketol and diketol [71].

spo and *spok* have been placed in the Black Box reaction of 20E biosynthesis through genetic analysis and feeding-rescue experiments [62]. Curiously, when *spo* is transfected into the *Drosophila* S2 cell culture system and radiolabeled 7dC is added to the media, no further ecdysteroid intermediates have been detected, indicating that perhaps another co-factor is involved in this high energy reaction (unpublished observation, H. Ono). PTTH-stimulation specifically induces phosphorylation of *Bombyx* Spo and if phosphorylation is required to activate the enzymatic activity, this may also explain why radiolabeled intermediates have not been detected [50].

In insects, it appears that different numbers of *spo*-like sequences are found in different species. In *Bombyx* and *Manduca*, there is only one identified *spo*-like Cyp307A and it is expressed in the larval PG in addition to the embryonic PG and adult ovaries, indicating that the *spo*/*spok* gene duplication event may have been specific to Drosophilidae [62,72]. In mosquitoes, there are also two *spo*-like sequences; however, they are more divergent than *spok* and *spo* [62]. While *spok* and *spo* are part of the Cyp307A branch of P450s, the second *spo*-like in mosquitoes belongs to a more divergent Cyp307B branch and has been named

spookiest (*spot*) [62]. It is not known if *spot* plays a similar stage-specific role in E biosynthesis as *spo* and *spok* do in Drosophiladae.

The *Drosophila shroud* (*sro*) mutant was identified as a Halloween gene in the 1984 EMS screen; *sro* mutants displayed embryonic lethality due to a lack of cuticle differentiation [60]. *Drosophila sro* is an orthologue of the *Bombyx non-molting glossy* (*nm-g*). *nm-g*/*sro* is predominantly expressed in the E producing tissues, the PG and ovaries [67]. The cellular localization of *sro* has never been tested. *nm-g* mutants exhibit a reduced E titer and larval arrest in the first instar stage [67,74,75]. *sro* mutants do not exhibit a reduction in E titer but curiously the embryonic lethality of *sro* mutants can be rescued by treating animals with 20E midway through embryogenesis [67]. *sro*/*nm-g* encodes for a short-chain dehydrogenase/reductase that likely functions in the Black Box of 20E biosynthesis since *nm-g* mutants and *sro*-RNAi knockdown animals can be rescued by 20E feeding but not by feeding with 7dC [67].

The reactions of the Black Box have not been fully characterized and indeed it is not known if Sro works upstream or downstream from Spo and Spok. It has been hypothesized that Sro might play a role in the putative last step of the Black Box, either as a 5β-reductase that converts Δ^4-diketol to diketol or as a 3β-reductase [58]. Radiolabel-tracer experiments have identified Δ4-diketol and diketol as downstream intermediates [71,76-79]. It should be noted that the Δ^4-

diketol product has never been isolated from insects [62]. It is unknown what gene encodes for an enzyme with a 5ß(H)-reductase activity**.** Alternatively, it has been hypothesized that Sro works to catalyze the putative initial step in the Black Box by catalyzing the 3β-dehdrogenation of 7dC to 3-oxo-7dc (cholesta-5, 7-diene-3-one) [58].

iii. Ketodiol → Ketotriol by Phantom

The *phantom* (*phm*) mutant was first identified as a Halloween gene in the 1984 EMS screen; *phm* mutants have embryonic cuticles that are not well differentiated [61]. Phm (Cyp306a1) is a cytochrome P450 enzyme that functions as a C-25 hydroxylase to convert ketodiol to ketotriol in both *Bombyx* and *Drosophila* [64,80]. *In situ* experiments in *Drosophila* show that *phm* is expressed in the embryonic and larval PG and in the follicle cells of the adult ovary in *Drosophila* [64,80]. RT-PCR analysis shows that *phm* is expressed specifically in the *Bombyx* larval PG of and has a temporal expression pattern throughout development consistent with other ecdysteroidogenic genes [62-64,68,80]. Phm co-localizes with an ER marker in the PG of fifth instar larvae [64,80]. The enzymatic activity of Phm was confirmed in S2 cells where radiolabeled ketodiol was converted to ketotriol when S2 cells were transfected with *phm* but not in *gfp* controls [80].

iv. Ketotriol → 2dE by Disembodied

The *disembodied* (*di*b) mutant is another Halloween gene identified by the 1984 EMS screen that lacks an embryonic cuticle [60]. In addition, *Drosophila Dib* mutants also exhibit dorsal closure, head involution and gut morphogenesis defects due to a disruption in E biosynthesis [5,63]. Like most of the other Halloween genes, *dib* (Cyp302a1) codes for a cytochrome P450 that works as a 22-hydroxylase to catalyze the reaction of ketotriol to 2-deoxyecdysone (2dE) [5]. In *Drosophila* S2 cells, Dib co-localizes with mitochondrial markers [5].

The *Bombyx* homologue of *dib* is expressed primarily in the larval PG and the enzyme is thought to be a functional ortholog that works by the same 22-hydroxylase mechanism [65]. In fact, Dib was one of the first cytochrome P450 enzymes shown to be directly involved in E biosynthesis [5]. When *dib* is transiently transfected into S2 cell culture, Dib can catalyze the conversion of radiolabled ketotriol to 2dE [5].

Bombyx dib expression correlates with E levels in the hemolymph and *dib* expression has been shown to be induced by PTTH in *Bombyx* [5,65]. The *dib* expression pattern in *Drosophila* closely follows E production; higher levels of dib are detected just preceding larval molts and *dib* expression drops dramatically just after ecdysis [5].

v. 2dE → E by Shadow

Shadow (*sad*) was first identified in the 1984 EMS screen; *sad* mutants have no cuticle differentiation or head skeleton [60]. Sad (Cyp315a1) is a cytochrome P450 monooxygenase that catalyzes the reaction from 2dE to E [6]. Epitope-tagged Sad co-localizes with the mitochondria in S2 cells [5].

In situ hybridization shows that *sad* is expressed in the early embryo, the embryonic ring gland, the larval PG and in both the follicle cells and nurse cells of the ovary [5]. Just as with *dib*, the *sad* expression pattern in *Drosophila* closely follows E production; higher levels of *sad* are detected just preceding larval molts and *sad* expression drops dramatically just after ecdysis [5]. In S2 cells, when *sad* is co-transfected with *dib*, cells are able to catalyze the conversion of radiolabled ketotriol to E [5].

vi. E → 20E by Shade

The final step of 20E biosynthesis is catalyzed by Shade (Shd). *shd* mutants were first identified in the 1984 EMS screen because of the lack of cuticle differentiation and no head skeleton differentiation [60]. Like several of the other Halloween mutants, Shd is also a P450 cytochrome monooxygenase. In this case, it hydroxylates carbon 20 of E into the final molting hormone, 20E [31]. Unlike the other enzymes involved in insect steroidogenesis, *shd* is not expressed in the PG [31]. Instead, *in situ* hybridization experiments show that

larval expression of *shd* is in the peripheral target tissues (e.g. epidermis, midgut, Malphighian tubules and fat body) [31]. In the embryo, *shd* is not expressed in early stages; around stage 10 *shd* is expressed in the epidermis and *shd* expression decreases during embryogenesis [31]. In the ovaries, *shd* is expressed in both the follicle and nurse cells [31]. In transfected S2 cells, Shd co-localizes with mitochondrial markers and can convert radiolabeled E to 20E, indicating that *shd* catalyzes the final conversion of E to 20E [31].

V. A putative co-factor in E biosynthesis: Membrane Steroid Binding Protein (MSBP)

The Halloween cytochrome P450 enzymes are heme-dependent monoxygenases that synthesizes 20E from dietary cholesterol [6,58]. The so-called Black Box reactions of 20E biosynthesis have not been fully characterized. Spo and its functional paralog, Spok, are P450s known to be involved in the Black Box reaction [62]. However, when *Drosophila* S2 cells are transfected with *spo* and treated with radiolabeled precursors, no downstream radiolabled intermediates can be detected (H. Ono, unpublished data). One possibility is that a co-factor is needed to help catalyze the putative high-energy reaction of the Black Box [62].

In yeast, an enzyme called Dap1 has been shown to stimulate a P450-catalyzed step in sterol synthesis [81]. Dap1 is a homologue to the mammalian PGRMC1

(progesterone receptor membrane component 1) and *Drosophila* MSBP (membrane steroid binding protein) [82]. Both Dap1 and PGRMC1 bind to heme which is critical for its function [81]. Additionally, Dap1 mutants that have defective heme-binding abilities have inactive sterol synthesis abilities [81,83]. It has been hypothesized that Dap1 may be involved in intracellular heme trafficking and can stimulate a P450-catalyzed step in sterol synthesis [81].

The *Drosophila* MSBP was first identified and cloned by Fujii-Taira et al. who showed it to be a PGRMC homolog [84]. Western blot of whole body extracts shows that MSBP is expressed strongly during prepupa and early pupa stages and is expressed less strongly during third instar larval stage and late pupal stages [84]. There are some hints that in *Drosophila*, MSBP may play a role in E regulation. When the membrane fractions of S2 cells transfected with MSBP were exposed to radiolabeled E, it bound more 20E than a membrane fraction from an empty-vector transfected control [84]. Additionally, in a micro-array analysis of PTTH-responsive genes, MSBP expression increased in response to PTTH stimulation [85]. From these two initial studies, however, it is still unclear what role MSBP plays in E regulation. Neither study characterized the phenotype of MSBP gain- or loss-of-function in the ring gland.

VI. Project Aims

We have taken a three-pronged approach to better characterize the role of PTTH in regulation of E signaling. First, to gain an unbiased look at what genes are up and down regulated in response to PTTH stimulation, we have harnessed the power of Illumina Next Generation sequencing to determine what genes are differentially expressed after one and three hours of PTTH-stimulated *Bombyx* PGs. The transcriptome-wide analysis is an unbiased approach to find key players in E biosynthesis. Our experimental procedures and results are discussed in Chapter two.

Chapter three contains the second aim of my thesis, which is to find PTTH responsive elements in the enhancer regions of *dib*, *spok*, and *phm*. The expression of these three Halloween genes increases upon PTTH stimulation and we are interested in finding regulatory regions that transcription factors may bind to. The final chapter of my thesis discusses my third aim, which is to characterize the gene MSBP, a factor that we believe may be working as a co-factor in E biosynthesis. Finally, in the appendices are discussions of work that I contributed to two papers that are unrelated to PTTH signaling.

CHAPTER 2: TRANSCRIPTOME ANALYSIS OF PTTH-STIMULATED PGS IN *BOMBYX MORI*

a. Chapter Introduction and Aim

To better understand the global effects of PTTH signaling on gene transcriptional regulation in the PG, we used Illumina Next Generation sequencing to compare the transcriptome of PTTH-stimulated and –unstimulated PGs. This was used as an unbiased approach to determine what genes are up and down regulated in response to PTTH stimulation.

b. Materials and Methods

Bombyx mori and growth conditions

The *Bombyx mori* larvae used in this experiment were derived from a mixed-strain egg batch of domesticated silkworms (Mulberry Farms, LLC; www.mulberryfarms.com); the heterogenous population of *Bombyx* were grown at 25ºC under a 0L/24D photoperiod under semi-sterile conditions; the incubator and everything that came in contact with the *Bombyx* larvae were cleaned in a bath of 3.7% formaldehyde in distilled water (dH_2O) and rinsed with a 70% ethanol spray. *Bombyx* larvae were fed on an artificial diet of mulberry food made in small batches by combining a single half-pound package of powdered Silkworm Chow (Mulberry Farms, LLC) to 600-700 ml of dH_2O and autoclaved for twenty minutes in a liquid cycle. Autoclaved mulberry food was cut into ~0.5 cm

thick blocks and spread across semi-sterile glass containers and covered with plastic wrap. *Bombyx* larvae were placed on top of the food layer and were transferred to new food every 24 to 48 hours to prevent mold contamination. The excess mulberry food was stored at 4ºC for no more than one week before use. To stage fifth instar larvae, *Bombyx* in the fourth instar were screened daily for final ecdysis; pre-molt larvae were separated and kept in a starvation chamber overnight. The *Bombyx* larvae that underwent ecdysis (i.e. molted) in the overnight starvation chamber were characterized as fifth instar, day one (V_0) and placed on fresh mulberry food daily. Most *Bombyx* were dissected on V_4, however, several animals were monitored for the timing of their wandering behavior and pupation.

Dissection of Bombyx mori PGs and PTTH stimulation

Prothoracic glands (PGs) were dissected rapidly from 12-18 fifth instar *Bombyx* larvae (V_4) essentially as described in Yamanaka et al.[55]. The PGs were placed in a room temperature bath of 100 ul of Grace's Insect Medium (#11595; Gibco/Invitrogen; www.invitrogen.com) and allowed to pre-incubate in the media for 30 minutes. After pre-incubation, 10 nM PTTH (gift from Hiroshi Kataoka, University of Tokyo, Japan) was added to the appropriate samples. Samples were allowed to incubate at room temperature for either one or three hours. Several different types of Grace's Insect Medium were tested—both supplemented and unsupplemented and with or without bovine serum albumin

(BSA). Ultimately, PGs that were incubated in unsupplemented Grace's Insect Medium with BSA were used for future Illumina processing. As an internal control, the two PGs from each animal were separated in a manner so that one was added to the +PTTH bath and one was added to the corresponding –PTTH bath. Four sample types were generated: PGs incubated with no PTTH for one hour ($1h^{-PTTH}$), PGs incubated with PTTH for one hour ($1h^{+PTTH}$), PGs incubated with no PTTH for three hours ($3h^{-PTTH}$), and PGs incubated with PTTH for three hours ($3h^{+PTTH}$). Each of the four sample types was collected in biological duplicates. After incubation in the +/-PTTH bath, PGs were immediately placed at -80 ºC for no more than one week before RNA extraction. The Grace's Medium bath was preserved for ELISA analysis at -20ºC.

Sample quality control by ELISA

The enzyme-linked immunosorbant assay (ELISA) was performed essentially as described in Ou et al.[4] To perform the ELISA, 20-Hydroxyecdysone EIA Antiserum (#482202); 20E AchE tracer (#482200); Precoated Mouse anti-rabbit IgG EIA 96-well plates (#400007); and Ellman's reagent (#400050) were purchased from Cayman Chemical (www.caymanchem.com) and used according to manufacture's instructions.

Total RNA extraction from PGs

Total RNA extraction was optimized by using a combination of the TRIzol® Reagent and Qiagen RNeasy Kit protocols. 500 µL of TRIzol® Reagent (Invitrogen, www.invitrogen.com), was added to each sample, and the frozen PG tissue was homogenized at room temperature using a sterile 0.6 mm x 25.4 mm needle and sterile 1 ml (i.e. 1 cc) syringe. After homogenization in TRIzol, samples were stored at -80 ºC for no more than one week. After thawing, the homogenized samples were incubated at room temperature for five minutes before adding 350 µl of buffer RLT (QIAGEN RNeasy Mini Kit, www.qiagen.com) containing 1% ß-mercaptoethanol. Samples were vortexed and 100 µl of chlorophorm was added before spinning at 12,000 rpm for 15 minutes at 4ºC. The aqueous phase was removed and RNA was isolated according to manufacturer guidelines beginning with step five (QIAGEN, RNeasy Mini Handbook, November 2010, page 43). Total RNA was eluted from the column using 36 µl of RNase-free dH_2O and stored at -80 ºC. The concentration of RNA was measured using spectrometry.

Sample quality control by quantitative real time polymerase chain reaction (qrt-PCR)

To determine the developmental expression profiles of several genes, each total RNA sample was converted to cDNA. Single-stranded cDNA synthesis was performed using the SuperScript III First-Strand Synthesis Supermix with

oligo(dT) primers (Invitrogen, www.invitrogen.com). Each reaction was prepared in triplicate using the LightCycler 480 SYBR Green I Master Kit (Roche; www.roche.com) and transcripts were quantified using the LightCycler 480 Real-Time PCR Instrument (Roche, www.roche.com). After 1 minute at 95ºC, 45 cycles (95 ºC for 10 s; 68 ºC for 10 s and 72 ºC for 10 s) were carried out for the amplification of each gene. The primers used to amplify *Bm-RpL3*, *Bm-dib*, *Bm-MSBP*, *Bm-Cyp4G25*, *Bm-Bras1*, *Bm-IF-4Ebp* and *Bm-HpC19* are shown in Appendix C. *Bm-RpL3* was chosen as a reference and each gene was normalized to *Bm-RpL3* levels in the same sample. Analysis of relative gene expression was done using the 2-ΔΔCT method [86].

Illumina Library Preparation

To reach a total of 50 µL sample, with the highest concentration of RNA possible, the RNA biological duplicates were combined in a manner such that all remaining 32 µL of the higher concentrated sample was combined with 18 µL of the lower concentrated sample. The remaining 18 µl of the lower concentrated RNA biological duplicate was stored at -80ºC. Four RNA samples for library preparation were generated and submitted: $1h^{-PTTH}$, $1h^{+PTTH}$, $3h^{-PTTH}$, $3h^{+PTTH}$.

RNA sequencing libraries were prepared according to manufacturer specifications by the University of Minnesota's Biomedical Genomics Center (BMGC) using the Paired-end mRNA-Seq 8-Sample Prep Kit (Illumina;

www.illumina.com). The submitted samples contained approximately 12 micrograms of total RNA in 50 µL. As a quality control, the BMGC tested the total RNA concentration by RiboGreen RNA Quantitation Reagent and Kit (Molecular Probes; www.invitrogen.com). An Agilent 2100 Bioanalyzer using an RNA 6000 Nano Chip Kit was used to determine the RNA Integrity Number (Agilent; www.agilent.com).

Illumina Sequencing

This project was sequenced on a 100 bp paired end run on the Hiseq 2000 (Illumina; www.illumina.com). Four samples were analyzed: $1h^{-PTTH}$, $1h^{+PTTH}$, $3h^{-PTTH}$, $3h^{+PTTH}$. The one hour ($1h^{-PTTH}$ and $1h^{+PTTH}$) libraries were pooled and the three hour ($3h^{-PTTH}$ and $3h^{+PTTH}$) libraries were pooled. The one hour and three hour pools were each sequenced across two lanes, and two reads were performed for a total of eight lane reads. The data for both reads was trimmed to 50 bp because of low read quality after approximately cycle 65 in read 1. The average Qscore for the 50 bp trimmed data set met BMGC quality control requirements, with an average Qscore of over 30 for each lane. Approximately 50 million pass filter reads were achieved for all samples. The data was transferred to Minnesota Supercomputing Institute (MSI) and deposited in the Michal O'Connor laboratory account for analysis on Galaxy software; the data was additionally backed up on an external terabyte hard drive. The

bioinformatics data analysis is being performed on Galaxy software by C. Brakken-Thal at the time this thesis is being written.

c. Results

Bombyx animals were a heterogenous population and needed semi-sterile conditions to develop on time*. Bombyx* larvae were grown from eggs received from Mulberry Farms, LLC. The larvae appeared to be a heterogenous mix of strains with different body markings (data not shown). Despite the heterogenous mix, healthy *Bombyx* animals proceeded through development essentially as expected; fifth instar wandered on day 8 (V_7) and pupated on day 12 (V_{11}). The wandering and pupation occurred approximately one day later than previously reported [20,55]. Because of their intensive domestication, *Bombyx* can be vulnerable to disease, even in the laboratory [87,88]. We found that mold contamination and exposure to areas contaminated with baculovirus made the *Bombyx* sick and eventually caused lethality before or during the fifth instar stage. To avoid these complications, the following procedures were followed: *Bombyx* were grown in a room separated from areas contaminated with baculovirus and care was taken to avoid contamination; all food was sterilized by autoclaving; food was changed every 24 to 48 hours; *Bombyx* were kept in a 25ºC incubator where moisture levels were closely monitored; and all containers and tools were washed in a bath of 3.7% formaldehyde and wiped with a 70% ethanol spray before coming in contact with *Bombyx* or the food source. Once

these procedures were implemented, the *Bombyx* developed in a manner that was generally consistent with previous reports [55].

PTTH stimulation of PGs was most robust in unsupplemented medium with BSA. To determine what type of insect medium caused the most robust reaction to PTTH signaling, we tested *dib* expression in *Bombyx* PGs that were incubated in supplemented and unsupplemented Grace's Insect Medium, with or without BSA added. We found that *dib* expression increased most robustly when incubated the PGs for three hours in unsupplemented Grace's Insect Medium with BSA (Figure 5). To further verify our results, we measured the expression of three other genes, *Bm-msbp*, *Bm-If4ebp*, and *Bm-Hpc19*, in unsupplemented Grace's insect medium with BSA (Figure 6). As expected, *Bm-dib* and *Bm-mspb* expression increased in response to PTTH, while *Bm-If43bp* and *Bm-Hpc19* expression decreased.

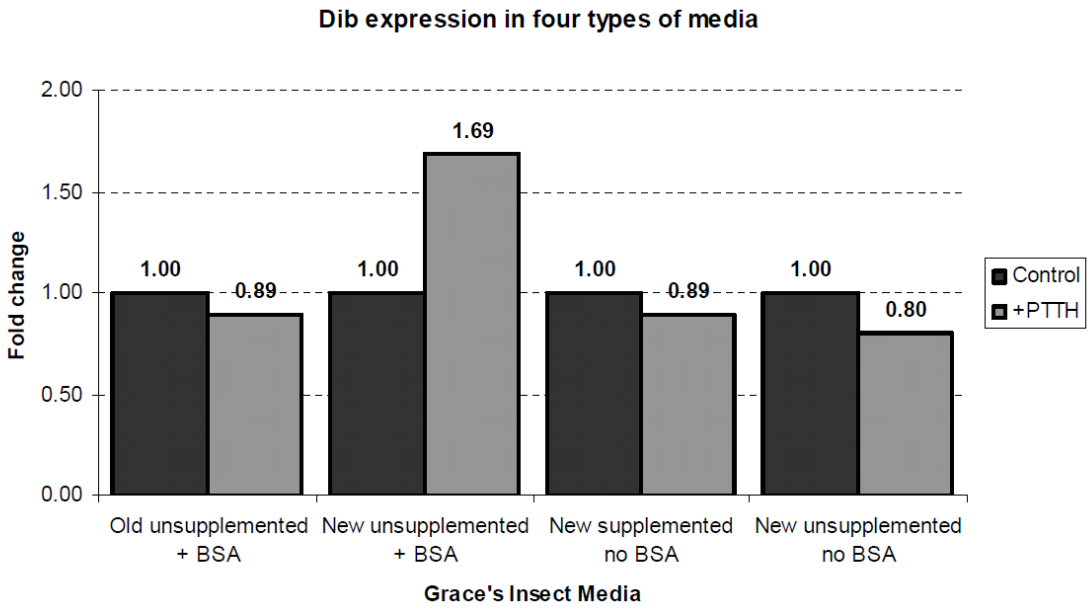

Figure 5: *dib* expression in several types of Grace's Insect Media
dib expression in four Grace's media types: old unsupplemented with BSA, new unsupplemented with BSA, new supplemented with no BSA and new unsupplemented with no BSA. There are no error bars because biological replicates were not performed.

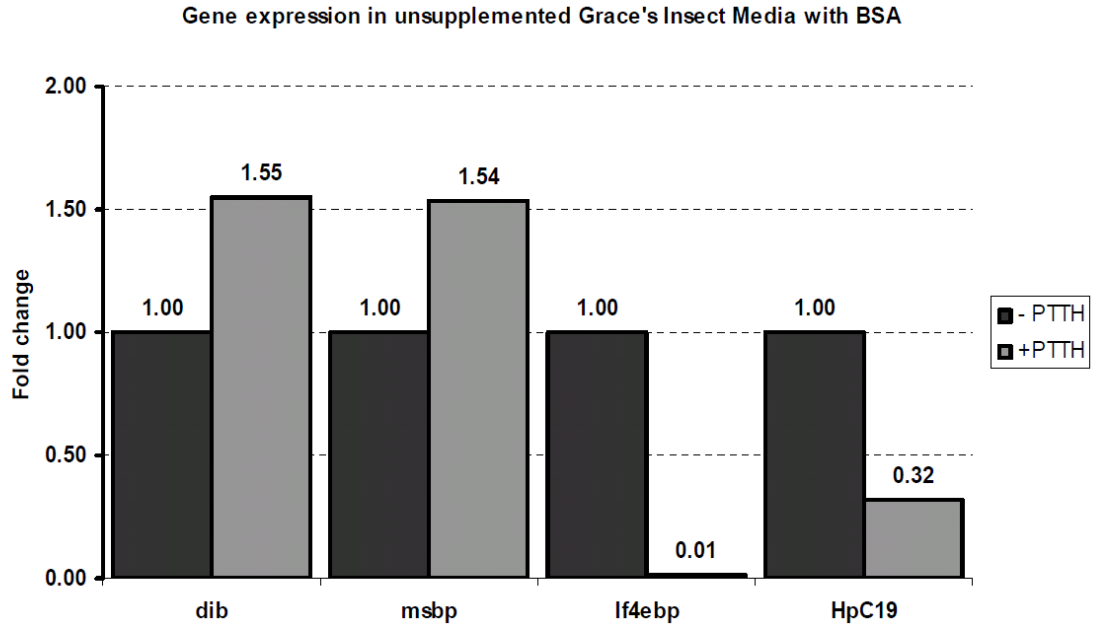

Figure 6: Gene expression changes in unsupplemented Grace's Insect Media

Gene expression in PGs incubated in new unsupplemented Grace's Insect Media with BSA. *Bm-dib* and *Bm-msbp* expression increases in response to PTTH stimulation while Bm-IF43bp and Bm-HpC19 expression decreases in response to PTTH stimulation. There are no error bars because biological replicates were not performed.

20E was released into the media after PTTH stimulation. To verify that PTTH stimulation of *Bombyx* PGs resulted in ecdysteroid release, as has been previously reported [55,89], we performed a 20E ELISA using the post-incubation medium. As expected, after one hour PTTH stimulated PGs released more ecdysteroid (0.66 ± 0.09 ng /gland) than the unstimulated control (0.15 ± 0.01 ng/gland). In the samples that were incubated for three hours, the effect was even more dramatic: PTTH-stimulated PGs released over 3.5 times more ecdysteroid than the unstimulated control (3.53 ± 0.06 ng/gland versus 0.26± 0.06 ng/gand) (Figure 7). The ecdysteroid released into the media was a bit lower than has been previously reported, however, this is likely due to the fact that the *Bombyx* animals were one day delayed in their wandering and pupation [55,89].

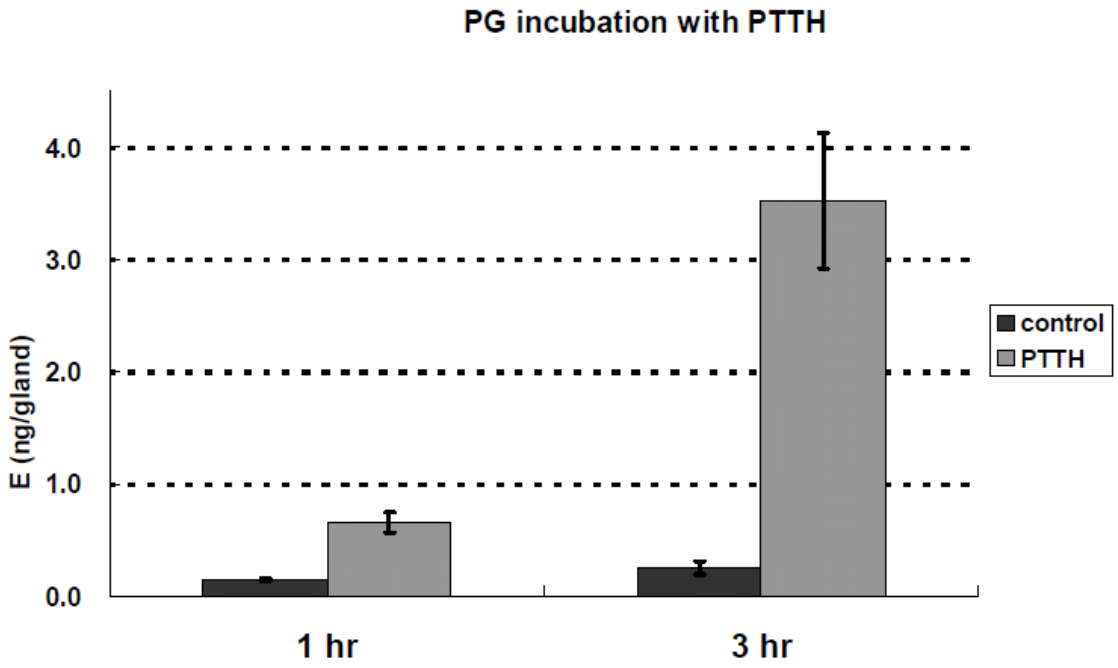

Figure 7: PTTH-stimulated PGs release more ecdysteroid than control PGs.
After one hour PTTH stimulated PGs released 0.66 ± 0.09 ng /gland while unstimulated controls released 0.15 ± 0.01 ng/gland. After three hours, PTTH-stimulated PGs released 3.53 ± 0.06 ng/gland whereas control glands released 0.26± 0.06 ng/gland. Data was collected by a standard 20E ELISA assay. Error bars indicate standard error of the mean.

PTTH stimulation causes an increase in Bm-dib and Bm-msbp expression and a decrease in Bm-IF43bp expression. Before submitting our samples for downstream Illumina processing, we wanted to verify that PTTH-responsive genes were, in fact, responding as expected to PTTH stimulation. To do this, we used qrt-PCR to look at expression of several genes. The expression of *Bm-dib*, *Bm- msbp, Bm-Cyp4G25* and *Bm-Bras1* increases in response to PTTH stimulation while *Bm-IF43bp* and *Bm-HpC19* expression decreases, as detected by qrt-PCR (personal communication with N. Yamanaka) [55]. Unfortunately, we

were unable to reliably amplify fragments of *Bm-cyp4G25*, *Bm-bras1*, or *Bm-HpC19* using the primers in Appendix C. However, we did find that both *Bm-dib* and *Bm-msbp* expression increased in response to PTTH stimulation while *Bm-IF43bp* expression decreased in response to PTTH stimulation (Figure 8).

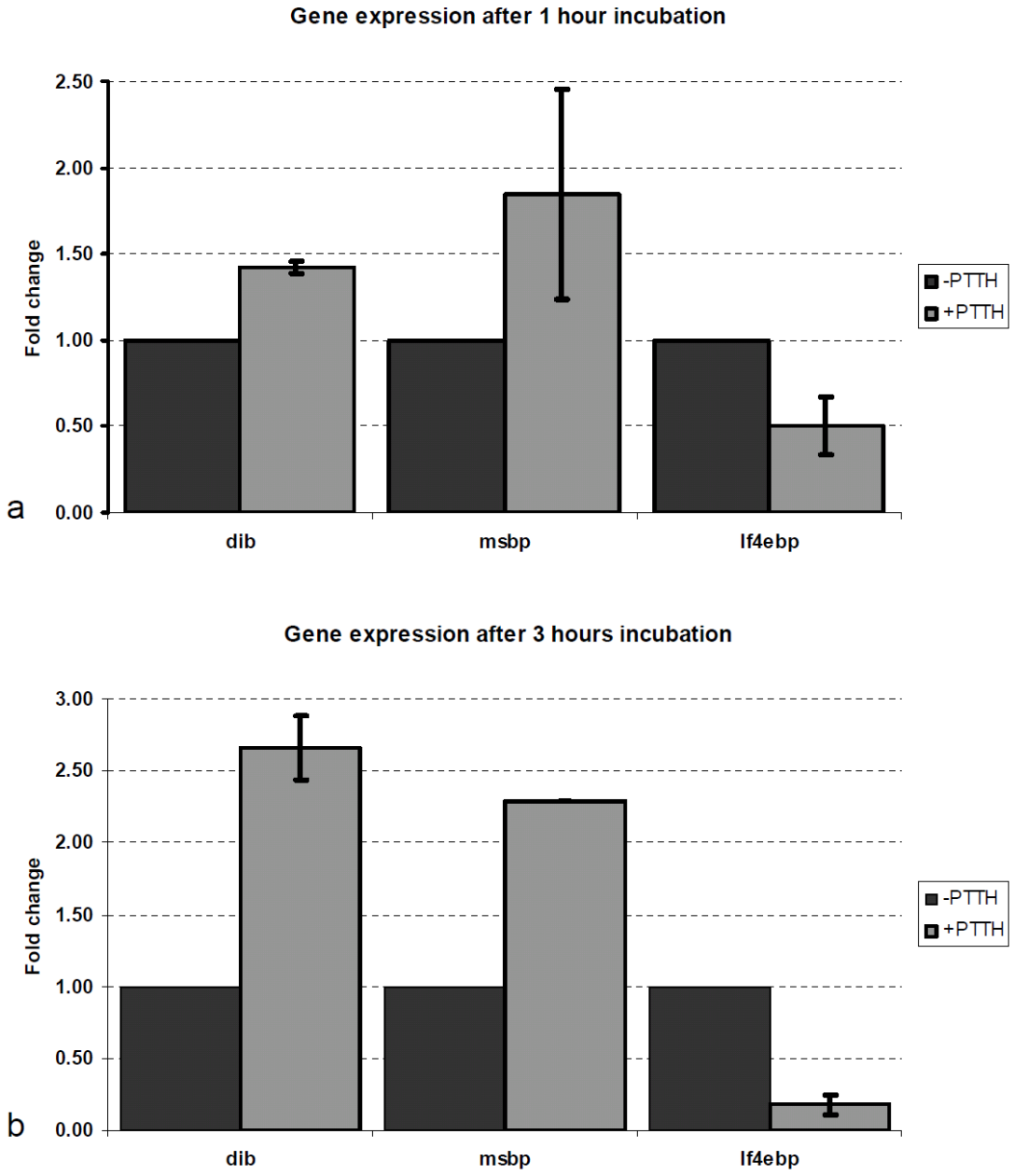

Figure 8. Gene expression changes in PTTH stimulated PG.
Bm-dib and *Bm-msbp* expression increases in response to PTTH stimulation while *Bm-IF43bp* expression decreases in response to PTTH stimulation, as detected by qrt-PCR. (a) Fold change of *dib*, msbp and If4ebp after one hour incubation with and without PTTH. (b) Fold change of dib, msbp, and *IF4Ebp* expression after three hours of incubation with and without PTTH. Error bars indicate standard error of the mean.

Electropherograms of Bombyx RNA show a signaling pattern characteristic of most insects.

To test the integrity of the RNA samples submitted for Illumina library preparation and sequencing, samples were analyzed on an Agilent 2100 Bioanalyzer using a Eukaryote Total RNA Nano assay to calculate a RNA Integrity Number (RIN). Typically, RNA electropherograms from heat-denatured eukaryotic rRNA samples display a signal profile that contains two clear peaks: one at 18S (~1900 nt) and one at 28S (~3800 nt) [90-93]. However, the electropherograms from all four of our submitted samples contained a unique profile: a doublet peak at the 18S rRNA area and an absence of a peak at the 28S rRNA area (Figure 9 and Table 1). The lack of a 28S peak resulted in low, and in one case, absent, RIN number. Low or absent RIN numbers generally indicate poor quality or degraded RNA [92,93]. Curiously, the electropherograms from our samples did not show a dramatic increase in baseline signal which is characteristic of samples that have undergone RNA degradation [90]. Interestingly, reports of a so-called “hidden break” in the 28S rRNA has been reported in numerous insect types, including Diptera, Lepidotera, and Hymenoptera [93-95]. The hidden break has been suggested to be introduced into the RNA chain during maturation and that the two 28S fragments are held together by non-covalent interactions, mainly through hydrogen bonds [93]. The heat denaturing conditions of the Agilent Eukaryote Total RNA Nano assay likely results in the separation of the two 28S fragments that co-migrate with the 18S band [93,96]. Therefore, the observed

rRNA profiles from the *Bombyx* samples and corresponding low RIN scores reflect the endogenous components of the insect rRNA after heat denaturation rather than being indicative of RNA degradation.

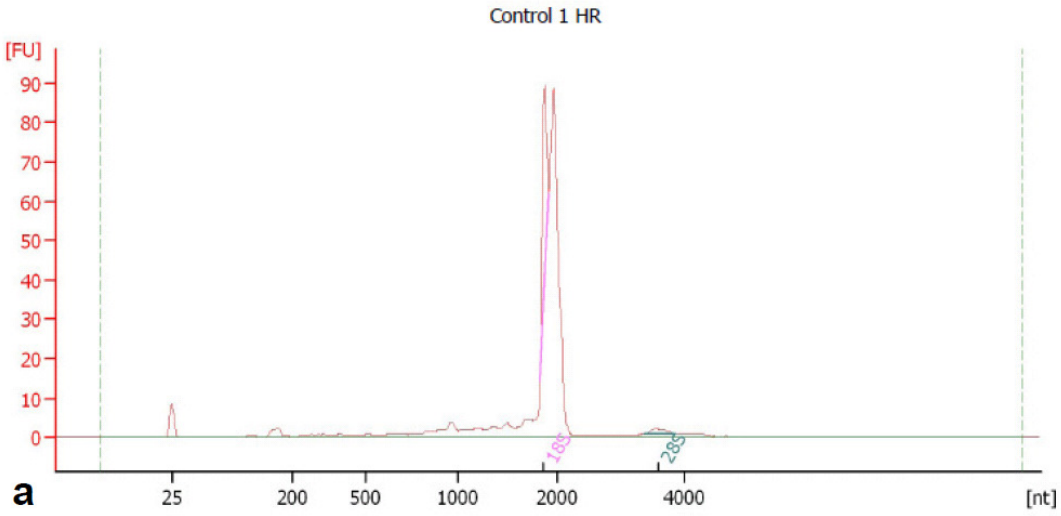
Control 1 HR
[FU]
90
80
70
60
50
40
30
20
10
0
18S
28S
25
200
500
1000
2000
4000
[nt]

a

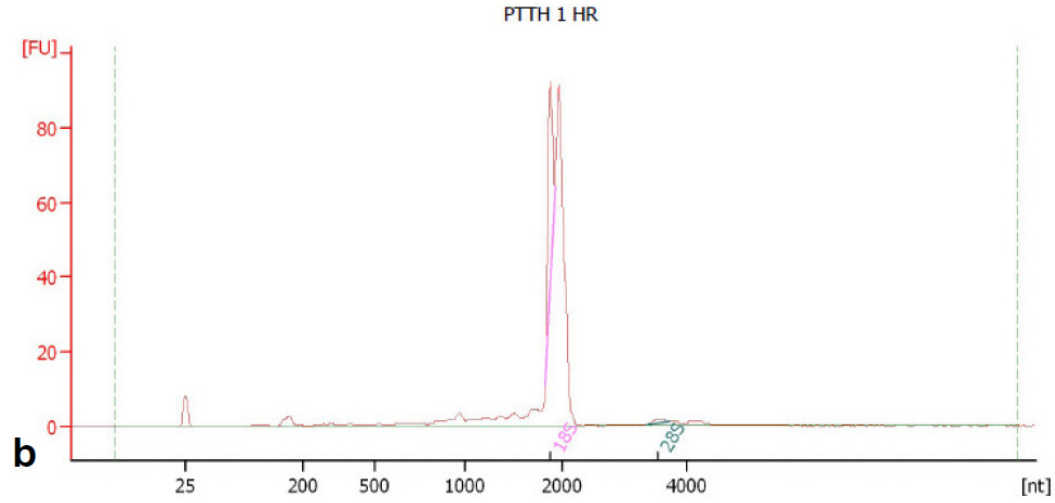
PTTH 1 HR
[FU]
80
60
40
20
0
18S
28S
25
200
500
1000
2000
4000
[nt]

b

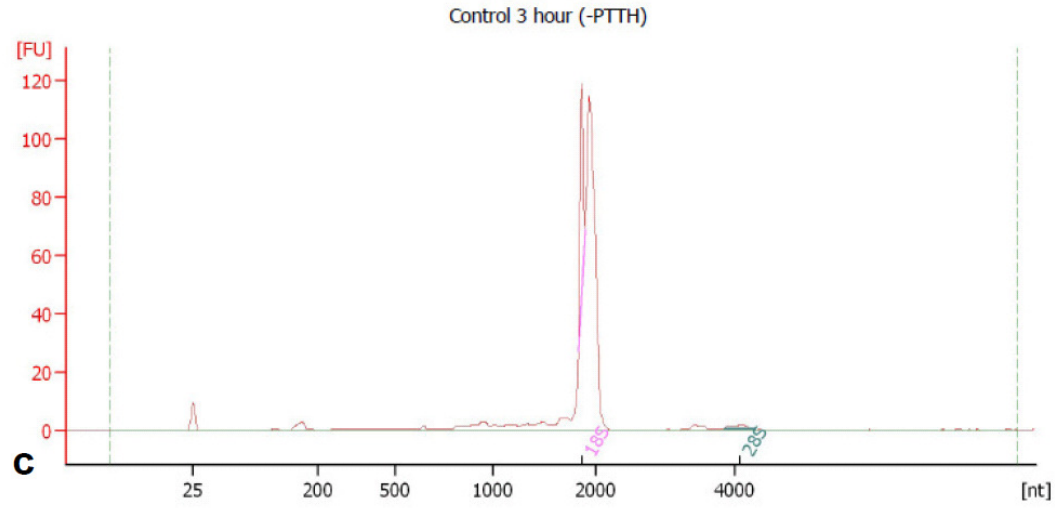
Control 3 hour (-PTTH)
[FU]
120
100
80
60
40
20
0
18S
28S
25
200
500
1000
2000
4000
[nt]

c

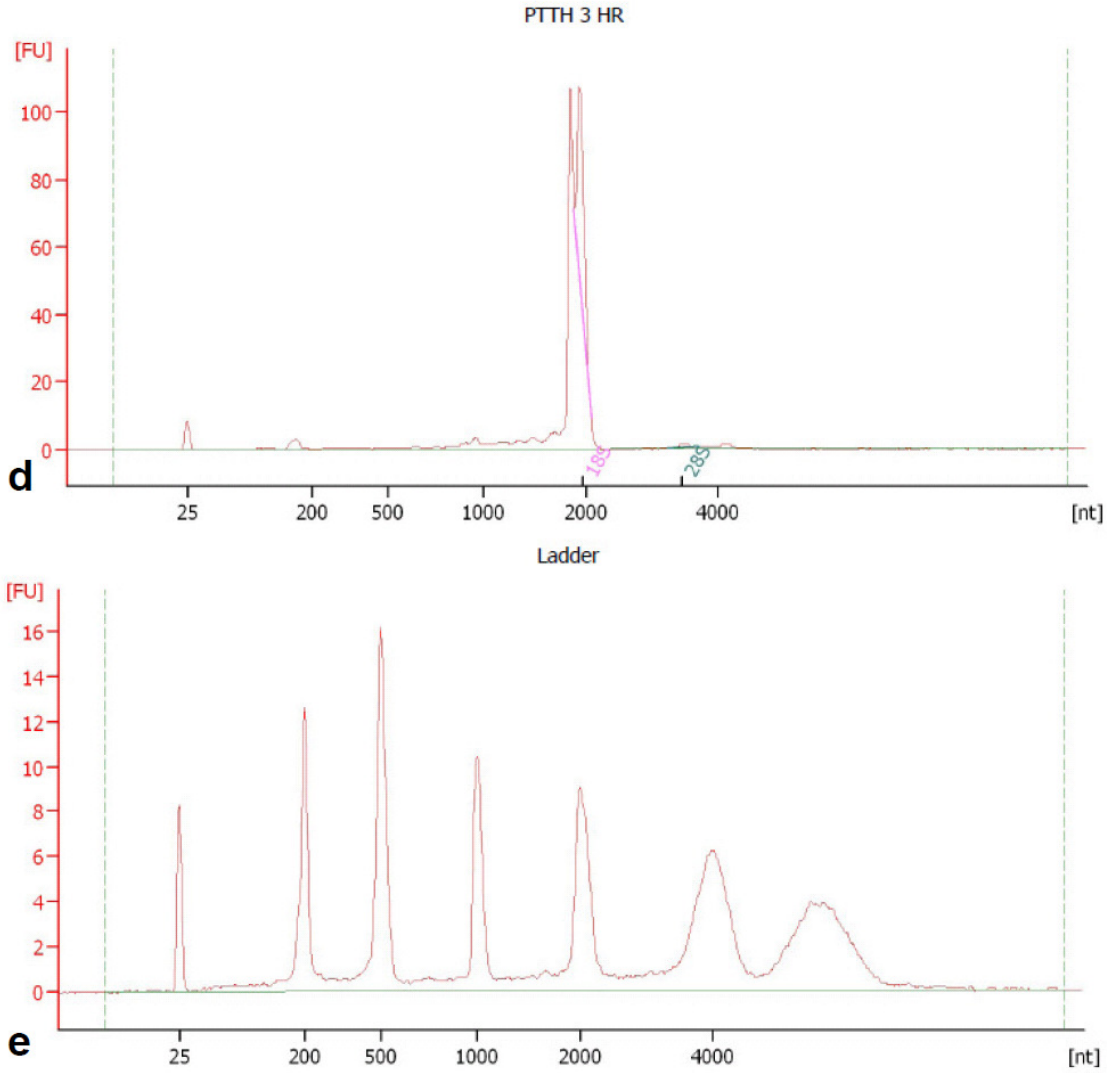

Figure 9: Analysis of RNA integrity from Illumina samples.
The RNA integrity of the four samples submitted for Illumina sequencing. (a) to (e) Electropherograms from the Agilent 2100 bioanalyzer showing the distribution of rRNA fragments from each sample. (f) An electropherogram of the ladder. The x-axis is nucleotides (nt) and the y-axis is fluorescent units (fu). The peaks for the eukaryotic 18S (red) and 28S (green) ribosomal subunits are indicated on each electropherogram. In lepidoptera, such as *Bombyx*, the 28S rRNA complex is comprised of two hydrogen-bonded fragments that, upon heat denaturation, separate and co-migrate with the 18S rRNA fragment. A doublet peak can be observed in each insect electropherogram at approximately 1900 nt.

sample	ng/μL	RIN
1h^{-PTTH}	230	4.7
1h^{+PTTH}	232	5.0
3h^{-PTTH}	464	5.0
3h^{+PTTH}	250	n/a

Table 1: Table indicating the RNA Integrity Number (RIN).
The concentration of RNA in each sample is indicated in ng/μL of total RNA of each sample and the corresponding RNA Integrity Number (RIN). The RIN values are low due to the absence of the 28S peak that is characteristic of most insects but is present in most other eukaryotes. RIN values sometimes cannot be computated if the computer software finds an unexpected peak or signal in certain regions; this happened in one sample and is indicated by n/a.

d. Discussion

Several reports have established that in lepidopteran and dipterian insects, PTTH signaling to the PG triggers ecdysone biosynthesis and release, which directly elicit molting and metamorphosis [6-8,37,46]. It has been previously shown that PTTH signals directly through the Torso/ERK pathway, however target genes of ERK signaling remain largely unidentified [4]. To fully understand the role of PTTH on ecdysteroid production in the PG, it is essential to identify what gene programs are up and down regulated in response to PTTH. In the present study, we used Illumina Next Generation sequencing to compare the whole transcriptome of PTTH-stimulated and unstimulated *Bombyx* PGs to find genes that are up and down regulated in response to PTTH.

A more in-depth discussion of the results will be possible after the bioinformatics portion of this project has been completed, currently that analysis is in progress by C. Brakken-Thal. However, below is a discussion outlining the framework in which we hope to discuss our results once the bioinformatics is complete.

First, we hope to quantify the sensitivity of our assay. This can be accomplished by identifying the number of total genes expressed in *Bombyx* larval PGs. This total gene number would include all genes expressed in the PG (i.e. both PTTH-responsive genes and housekeeping genes). Then, of this total number of genes we can identify the number of genes that show differential expression in response to PTTH. These differentially expressed genes could be further broken down into two categories: (1) genes down-regulated in response to PTTH and (2) genes upregulated in response to PTTH. Since the PTTH stimulation was carried out in two different time frames (i.e. one hour PTTH stimulation and 3 hours PTTH stimulation), we can further characterize genes as quick-response PTTH genes and slow-response PTTH genes.

Second, we can verify our results by comparing the genes we identify to genes we know are affected by PTTH-stimulation. For example, we know from previous reports and from our own qrt-PCR results that some genes have increased expression in response to PTTH-stimulation, these include genes such as: *dib*, *phm*, *msbp*, *Cyp4G25, bras1* and *Drosophila* Hormone Receptor 4 (DHR4) [4,55]. Additionally, we know some genes have decreased expression in

response to PTTH, including: *IF43bp*, *HpC19* and *Cyp6t3* [4,55]. Therefore, we would expect that these genes would be identified in the bioinformatics analysis as PTTH-responsive genes.

Third, and most important, we hope to uncover genes that have yet-to-be discovered as PTTH-responsive genes. These genes could be players in the PTTH-Torso MAP kinase pathway in the PG, genes involved in the Black Box reaction of ecdysone synthesis, transcription factors necessary for expression of PTTH-responsive elements, or other genes involved in PTTH signal transduction.

To further verify newly uncovered genes in *Bombyx* PTTH-signaling, we can compare our results with an unpublished microarray analysis performed by the King-Jones lab. In this microarray, they used *Drosophila melanogaster* with ablated PTTH neurons (PTTH knock-out animals) and compared to the gene expression to animals with intact PTTH neurons. We would expect that there would be overlap in the results. For example, we would predict that Halloween genes, such as *dib* and *phm* whose expression increases in response to PTTH stimulation will likely have no expression change in *Drosophila* with ablated PTTH neurons.

Finally, the limitations of our experimental design should be noted. First, we used a heterogenous silkworm population for experiments because the only sources for *Bombyx* in the United States have mixed populations. The

heterogeneity amongst the silkworms is likely to cause some variability in gene sequence and potentially in gene expression [97]. The variability was normalized as much as possible by preparing biological duplicates of each sample that contained ring glands from several animals, split between control and PTTH-stimulated samples.

The second limitation of our experimental design is the current annotation of the silkworm genome is not as advanced as other model organisms. The sequence of *Bombyx* genome is not currently available in a format that amends itself to bioinformatics analysis of Illumina data. This has resulted in a process that has taken longer than expected. C. Brakken-Thal is continuing to work on the bioinformatics of this project and once the bioinformatics is complete, more discussion of results will be possible.

CHAPTER 3: IDENTIFICATION AND CHARACTERIZATION OF ENHANCER ELEMENTS REGULATING INDUCTION OF ECDYSONE (EERIE) REGIONS OF *PHM*, *SPOK*, AND *DIB*

a. Chapter Introduction and Aim

Ecdysone (E) is synthesized in the prothoracic gland cells of the *Drosophila* ring gland[6]. A group of enzymes, mainly cytochrome P450 monoxygenases, catalyze the step-wise conversion of dietary cholesterol to E [6,62]. Several of the cytochrome P450s are members of the so-called Halloween gene group. The Halloween genes were identified in a 1984 mutagenesis screen and share a common "scary" phenotype: a mid-embryonic failure to form a differentiated cuticle [59-61]. Subsequently, several of the Halloween gene P450s were shown to be enzymes involved in the biosynthesis of dietary cholesterol to 20E.

Previously, it had been shown through RT-PCR analysis that some Halloween genes, including *spookier* (*spok*) and *phantom* (*phm*), fluctuate expression throughout larval development [62,80]. Furthermore, PTTH has been shown to directly regulate *disembodied* (*dib*), *spok*, and *phm* expression in *B. mori* [55]. This lead our lab to ask the question, is there a PTTH responsive element that is common among PTTH-stimulated genes?

To address this question, we performed a promoter-bashing experiment, whereby we chose putative Enhancer Element Regulating Induction of Ecdysone (EERIE) regions near *spok*, *phm*, and *dib* to see if they were sufficient to cause reporter gene expression *in vivo*. Using the reporter construct, pH-Stinger, we screened putative Halloween EERIE regions for GFP expression in third instar larvae.

Here, we report the identification of broad EERIE regions near *spok*, *phm*, and *dib*. Additionally, we have identified minimal EERIE regions for *spok*, *phm* and *dib*. Finally, we were able to identify specific, highly-conserved regions within the minimal EERIE region of *phm* that are necessary for reporter gene expression, indicating that these highly conserved regions may be important for a PTTH response *in vivo*.

b. Materials and Methods

Drosophila Genetics and growth conditions

All *Drosophila* crosses were carried out at 25ºC or at room temperature on standard media in vials. Transgenetic flies were obtained by standard transgenetic injection techniques performed either by Duke University Model System Genomics (www.biology.duke.edu/model-system/) or BestGene Inc. (www.thebestgene.com/).

For timing experiments, approximately 100 total male and female adult *Drosophila* were placed in small cages with apple juice-agar plates and yeast paste. The cages were kept at 25ºC and allowed to acclimate for at least 24 hours. Eggs were collected over a two hour time period (t = 0 AEL). Twenty four hours after egg lay (24 AEL), the animals hatched and approximately 50-100 first instar larvae were transferred to a bottle with standard food supplemented with dH_2O and yeast. Animals were collected at 76-78 AEL (two to four hours following the second to third instar molt) and at 120 AEL (immediately before pupariation). Animals were allowed to cool in an ice cold phosphate buffered saline (PBS) bath before dissection.

pH-Stinger reporter transgene construction

pH-Stinger, containing a nuclear eGFP reporter gene was used to screen for enhancer sequences [98]. DNA fragments spanning putative EERIE regions were PCR-amplified using the GoTaq Kit (Promega, www.promega.com). The template DNA was generated from single *y⁻w⁻ males* using standard techniques. Fresh PCR product of the amplified EERIE regions were directly subcloned into pCR®II-TOPO plasmid using the TOPO-TA Cloning kit (Invitrogen, www.invitrogen.com). Positive clones were screened for insert orientation by restriction digest and verified by Sanger sequencing at the University of Minnesota's Biomedical Genomics Center (BMGC).

Site-directed mutagenesis was performed on EERIE in pCR®II-TOPO using the QuikChange Site-Directed Mutagenesis Kit (Stratagene; www.stratagene.com).

To subclone from pCR®II-TOPO into pH-Stinger, the EERIE-pCR®II-TOPO was cut using: BamHI/XbaI (to preserve 5'→3' orientation); XhoI→KpnI (to reverse 3'→5' orientation); or, in rare cases, EcoRI (in the instance where the EERIE region contained one of the other restriction enzyme sites). EERIE fragments were gel-purified using the QIAquick Gel Extraction Kit (Qiagen, www.qiagen.com) and the fragments were ligated into similarly cut *pH-Stinger* vectors using standard techniques. Positive clones were digested and Sanger sequenced (BMGC) to confirm orientation and sequence.

GFP expression screening

Transgenetic *Drosophila* lines were screened for the presence of nuclear GFP in wandering third instar larvae using a fluorescent dissecting microscope. The number of independent transgenetic lines screened can be seen in Appendix D. Representative pictures of GFP expression were generated from unfixed samples mounted in 80% glycerol.

Quantitative analysis of eGFP expression

Brain-ring gland complexes were dissected from 76h AEL and 120h AEL animals on ice. Each sample contains the brain-ring gland complexes from 10 animals;

each time point was collected in biological triplicates. During dissection, brain-ring gland complexes were kept in ice cold PBS before being homogenized in 500 µl of TRIzol® Reagent using a sterile 0.6 mm x 25.4 mm needle and 1 cc syringe. After homogenization, collected samples were stored at -80ºC. After thawing, the homogenized samples were incubated at room temperature for five minutes before adding 350 µl of buffer RLT (Qiagen RNeasy Mini Kit, www.qiagen.com) containing 1% ß-mercaptoethanol. Samples were vortexed and 100 µl of chlorophorm was added before spinning at 12,000 rpm for 15 minutes at 4ºC. The aqueous phase was removed and RNA was isolated according to manufacturer guidelines beginning with step five (QIAGEN, RNeasy Mini Handbook, November 2010, page 43). Total RNA was eluted from the column using 50 µl of RNase-free dH_2O.

Single-stranded cDNA synthesis was performed using the SuperScript III First-Strand Synthesis Supermix with oligo(dT) primers (Invitrogen, www.invitrogen.com). Each reaction was prepared in triplicate using the LightCycler 480 SYBR Green I Master Kit (Roche; www.roche.com) and transcripts were quantified using the LightCycler 480 Real-Time PCR Instrument (Roche, www.roche.com). After 1 minute at 95ºC, 45 to 55 cycles (95º for 10 s; 65ºC for 10 s and 72ºC for 10 s) were carried out for amplification. The primers used were *Dm-Rpl3* and *eGFP* (Appendix C). *Dm-RpL3* was chosen as a reference gene and *eGFP* expression was normalized to *Dm-RpL3* in the same

sample. Analysis of relative gene expression was accomplished using the $2^{-\Delta\Delta CT}$ method [86].

c. Results

Characterization of three Halloween gene minimal EERIE region using pH-Stinger

To find the enhancer region for three of the Halloween genes, *phm*, *spok*, and *dib*, we made a number of putative enhancer region constructs of various sizes and cloned them into the reporter construct, *pH-Stinger,* to generate transgenic animals. Our strategy was to find a minimal enhancer region that was necessary and sufficient for PG-specific eGFP expression with the ultimate goal of uncovering a PTTH-responsive element contained within the sequence. The genomic regions we assayed included: the genomic region 5' upstream from the gene, the genomic region 3' downstream from the gene, and also intronic regions of the gene. We were able to find minimal enhancer regions for three of the Halloween genes: *phm*, *spok*, and *dib*.

Phantom (phm) EERIE region

To determine a putative *phm* enhancer region, several genomic sequences upstream from the *phm* transcriptional start sight were cloned into pH-Stinger, these genomic sequences ranged in size from 69 basepairs to 1.2 kb (Figure

10)[6]. After transgenic animals were generated, they were screened for reporter GFP expression in the PG. Eight of the eleven *phm* EERIE regions were found to be sufficient for reporter GFP expression, while three regions were not sufficient for GFP expression in the PG (Figure 10). The smallest region necessary and sufficient for reporter gene expression in the PG was a 69 bp region (F3.2-R4), called the minimal *phm* EERIE region (Figure 10).

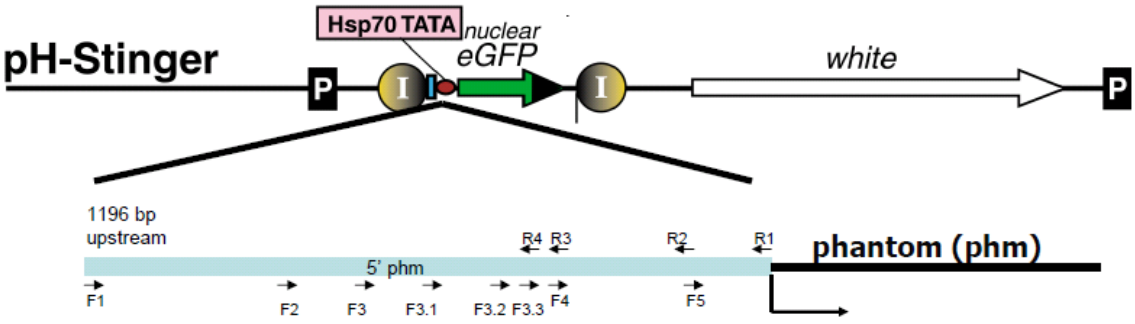

Construct name	GFP in PG
F1-R1	yes
F2-R1 (800 bp *phm* EERIE)	yes
F3-R1	yes
F3-R2	yes
F3.1-R1	yes
F3.2-R1	yes
F3.2-R3	yes
F3.2-R4 (minimal 69 bp *phm* EERIE)	yes
F3.3-R1	no
F4-R1	no
F5-R1	no

Figure 10: Analysis of *phm* EERIE constructs.
Eleven *phm* EERIE constructs were tested for their ability to drive GFP expression in the PG. Of the eleven constructs, eight were capable of driving GFP expression in the PG. Two of these constructs, F2-R1 (800 bp phm EERIE) and F3.2-R4 (minimal 69 bp phm EERIE) were used in subsequent experiments. These experiments were designed and conducted by M.J. O'Connor and K. Rewitz.

[6] Mary Jane O'Connor and Kim Rewitz performed the initial work identifying the *phm* EERIE regions and minimal *phm* EERIE region.

To further analyze what sequences within the minimal *phm* EERIE region are essential for PG expression, the *Drosophila melanogaster* minimal *phm* EERIE region sequence was compared to the analogous sequence from a closely related relative, *Drosophila pseudoobscura*. Five highly conserved motifs ("mot") were identified (mot1 to mot5) (Figure 11)[7].

To test if each of the five conserved *phm* EERIE motifs were necessary for GFP expression in the PG, mot1 through mot5 were each mutated. The resulting transgenic animals were screened for GFP expression in the PG. As a control, one region that was not conserved (NC) was also mutated and screened (Figure 11). As expected when the NC motif was mutated, GFP expression in the PG was maintained (Figure 11). This was also true for mot4, indicating that these mutated regions are not essential for PG-specific gene expression. However, when mot1, mot2, and mot3 were mutated, GFP expression in the PG was absent, indicating that these highly conserved motifs are essential for specific PG expression. Interestingly, when mot5 was mutated, GFP expression in the PG appeared to be much stronger than in the minimal *phm* EERIE region (Figure 11).

[7] Kim Rewitz compared and identified the conserved motifs and I performed the site directed mutagenesis and screen of the resulting transgenic animals.

Dm-phm^{EERIE} TGGGTGTAATGAATGTGCATACGATAAACGGGCAATTTCATTTTCAAATTTTACTTTCGCAC

Dp-phm^{EERIE} GGGTGTAATGTATGTGCATCTGATTTCCCAGCATTGATTTGATTTTCAAATTTTACTTTCGCT

EERIE construct	PG GFP	SG GFP	# of lines
Dm-phm^{EERIE}	yes	yes	1
mot1	no	yes	5
mot2	no	yes	6
NC	yes	yes	5
mot3	no	yes	2
mot4	yes	yes	3
mot5	yes	yes	2

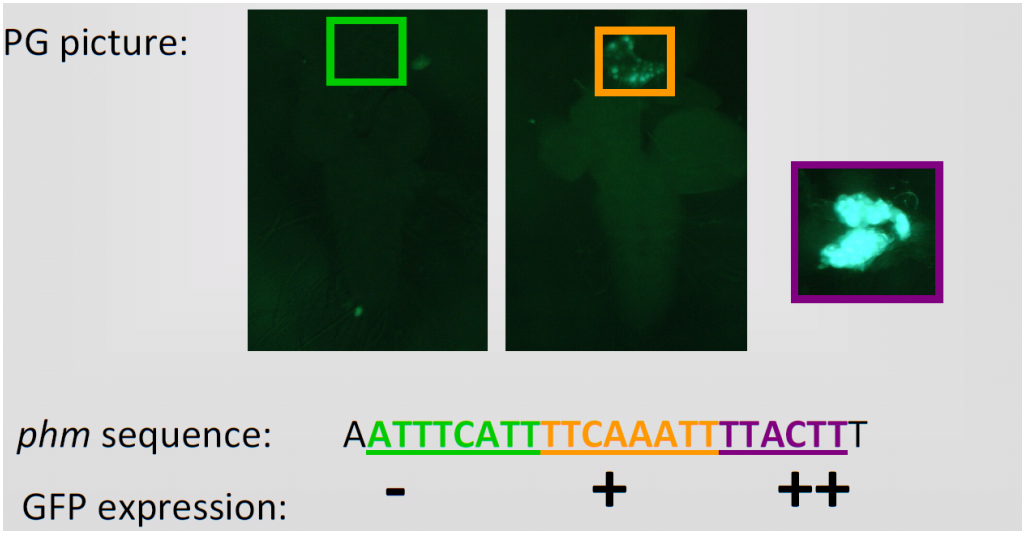

Figure 11: Analysis of minimal *phm* EERIE region.
Comparison of minimal *phm* EERIE region between *Drosophila melanogaster* (Dm) and *Drosophila pseudoobscura* (Dp). The highly conserved motifs are as follows (from left to right): mot1 (purple), mot2 (blue), mot3 (green), mot4 (orange), mot5 (dark purple). The not conserved (NC) motif is shown in red in the Dm *phm* EERIE region. Each of these motifs were mutated to see if it disrupted reporter GFP expression in the PG. The table displays the results. The minimal *Dm-phm* EERIE transgenic animals express GFP in both the prothoracic gland (PG) and the salivary gland (SG). All the phm EERIE constructs express GFP in the SG, due to background caused by using pH-Stinger as a vector. GFP expression in the PG was maintained

when the NC, mot4, and mot5 motifs were mutated. GFP expression was not detected in mot1, mot2, or mot3 transgenic animals, indicating that these motifs are necessary for specific expression in the PG. The far right column indicates the number of transgenic lines derived from independent insertion events. Brain-ring gland complexes from mot3, mot4, and mot5 are shown. Mutation of mot3 (green) resulted in no GFP expression in the PG. Mutation of mot4 (orange) resulted in maintenance of GFP in the ring gland. Mutation of mot5 (purple) resulted in stronger GFP expression in the ring gland. All photographs were taken at the same exposure time.

Spookier (spok) EERIE region

To determine a putative *spok* enhancer region, 1.45 kb upstream from the *spok* transcriptional start sight was cloned into pH-Stinger; transgenic animals were generated and screened for GFP expression in the PG. The 1.45 kb region was found to be sufficient for GFP expression (Figure 12)[8]. To identify smaller regions sufficient for PG expression, the 1.45 kb region was broken into eight genomic sequences (spok1 through spok8), these genomic sequences ranged in size from approximately 250 basepairs to 300 bp and each was cloned into pH-Stinger and transgenic animals were generated and screened for GFP expression (Figure 12). Of the eight regions, only the spok1 region was necessary and sufficient for GFP expression in the PG (Figure 12).

[8] Mary Jane O'Connor identified the 1.45 *spok* EERIE region.

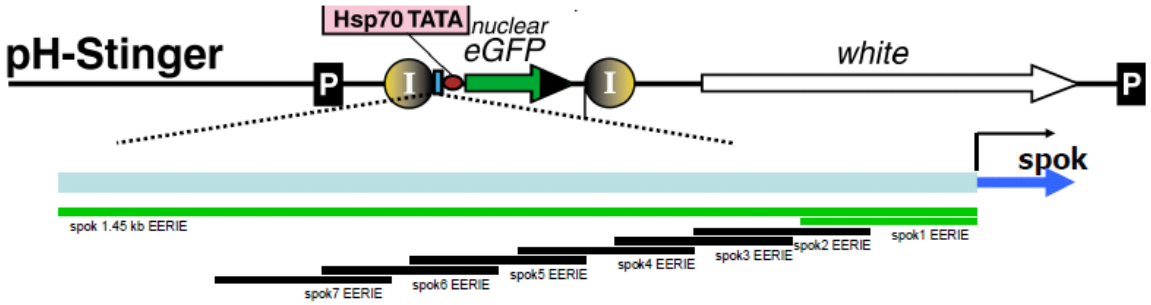

Construct name	GFP in PG
spok 1.45 kb EERIE	yes
spok1 EERIE	yes
spok2 EERIE	no
spok3 EERIE	no
spok4 EERIE	no
spok4 EERIE	no
spok6 EERIE	no
spok7 EERIE	no

Figure 12: Analysis of *spok* EERIE regions.
Eight *spok* EERIE constructs were tested for their ability to drive GFP expression in the PG. Of the eight constructs, only two were capable of driving GFP expression in the PG. Two of these constructs, spok 1.45 kb EERIE and spok1 minimal EERIE were used in subsequent experiments. The spok1.45 kb EERIE construct was designed and transgenic animals were made by MJ O'Connor; all other *spok* EERIE constructs and subsequent transgenic animals were made by RJH.

To further analyze if spok1 contains any motifs that are necessary for reporter gene expression in the PG, we attempted to compare the *Drosophila melanogaster* minimal *spok* EERIE region sequence to the analogous sequence from a closely related relative, *Drosophila pseudoobscura.* However, we were unsuccessful in identifying the analogous upstream region in *pseudoobscura* (data not shown). Instead, we used the four motifs identified in the *phm* EERIE region that, when mutated, resulted in altered GFP expression in the PG (mot1, mot2, mot3, and mot5) and found six similar sequences in the spok1 region

(spok1-M1 through spok1-M6) (Figure 13). These similar motifs were mutated using site-directed mutagenesis, cloned into pH-Stinger, and transgenic animals were generated and screened for GFP expression in the PG. Mutated motifs spok1-M3 through spok1-M6 did not display any change in GFP expression, indicating that these regions are not essential for specific gene expression in the PG.

Site-directed mutagenesis of two of the regions, spok1-M1 and spok1-M2, have yet to be completed. The motifs of spok1-M1 and spok1-M2 are located in an AT-rich region, making site-directed mutagenesis difficult. To overcome this technical obstacle, we used gene synthesis to obtain plasmids with the mutated regions.

Dm-ups-phm TGGGTGTAATGAATGTGCATACGATAAACGGGCAATTTCATTTTCAAATTTTACTTTCGCAC

spok1 EERIE

TCTTATATACAAAAACCCTTTCCAACAACAATAAAATTTCATAGGTCAAACGCATATTTAAAATAA
ATTCTATAAAAAAGAGAAGTAATTTTATTGTAGTCTTAAAACTTTAAGATGGTGCCTAAATAATAA
AGCTTATAACTATACCAAACAAGGCGAATATATTGGTAAGAATATATTAAAGAGTATACTAGATG
CTGGATGGTTTCCGATACCATTTATTTTATATATTCATGATCCGGATTACTTGTCGGGTCGATCT
AACCGTATCCATCTGTCTGCCCATCTGTACGTCTAGAT

Construct name	GFP in PG
spok1 EERIE	yes
spok1-M1 EERIE (red)	nd
spok1-M2 EERIE (blue)	nd
spok1-M3 EERIE (green)	yes
spok1-M4 EERIE (blue italics)	yes
spok1-M5 EERIE (purple)	yes
spok1-M6 EERIE (yellow)	yes

nd = no data available

Figure 13: Analysis of spok1 minimal EERIE region.
Comparison of minimal *phm* EERIE region with the spok EERIE region. Using the four highly conserved motifs found in *phm* EERIE that were necessary for GFP expression (shown in **BOLD UNDERLINE**) we identified five similar regions in the spok1 EERIE region. spok1-M1 (red), spok1-M2 (blue, unitalicized), spok1-M3 (green), spok1-M4 (blue italics), spok1-M5 (purple), and spok1-M6 (yellow). The similar nucleotides are highlighted in the same color in the phm EERIE sequence. spok1-M1 contains a sequence that was not conserved. Each of these motifs were mutated to see if it disrupted reporter GFP expression in the PG. The table displays the results; spok1-M3 through spok1-M6 expressed GFP in the PG, indicating that these regions are not essential for specific PG expression. There is no data yet available for spok1-M1 and spok1-M2.

Disembodied (Dib) EERIE region

Determination of the *dib* EERIE region was more difficult than for *phm* and *spok*. Previous attempts by our lab to isolate a *dib* EERIE region in the 5' region upstream of *dib* proved unsuccessful (MBO, personal communication). We then set out to determine if a necessary EERIE region was contained either

downstream of *dib* or within the *dib* gene[9] (Figure 14). We were able to identify a 420 bp region within *dib* that spanned the third and fourth introns that is sufficient for GFP expression in the PG (Figure 14). To further identify what area within the 420 bp *dib* EERIE region is necessary for GFP expression in the PG, we cloned a 190 bp fragment that spans the third but not the second intron. This 190 bp *dib* EERIE fragment is sufficient for weak GFP expression in the PG.

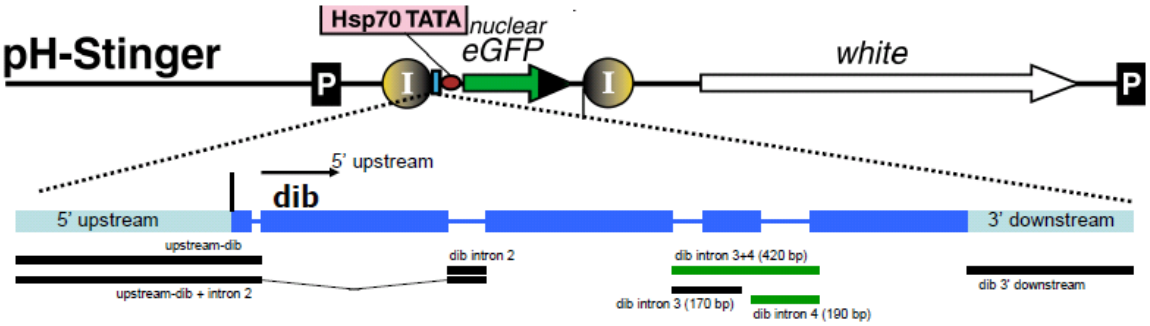

EERIE construct	GFP
upstream-dib	no
upstream-dib + intron 2	no
dib intron 2	no
dib intron 3 (170 bp)	no
dib introns 3 + 4 (420 bp)	yes
dib intron 4 190 bp	faint
dib 3' downstream	no

Figure 14: Analysis of putative *dib* EERIE regions.
Identification of the *dib* EERIE region. Several genomic regions around and within the *dib* gene were tested as putative EERIE elements. Of the seven constructs, only two were capable of driving GFP expression in the PG. dib intron 3+4 (420 bp) EERIE showed strong GFP expression in the PG while dib intron 4 (190 bp) had very faint GFP expression in the PG. The upstream-dib EERIE construct was tested by a previous O'Connor lab member. The upstream-dib + intron 2, intron 2, and dib 3' downstream EERIE elements were designed, cloned and tested by RJH and Abdi Ibraham. All other constructs were made and tested by RJH.

[9] Some of the *dib* EERIE cloning and screening was carried out by an undergraduate research assistant, Abdi Ibraham.

Quantification of EERIE GFP expression to find PTTH-responsive elements

To identify if a PTTH-responsive element is present in the minimal EERIE region of *phm* and *spok*, we wanted to determine if the level of the GFP reporter gene transcript changes during third instar. If PTTH is working to induce gene expression of Halloween genes, such as *dib* and *spok in vivo*, we hypothesized that expression of these genes would be low at the beginning of the third instar, after molting and high at the end of third instar state, in preparation for pupariation. In other words, we hypothesized that if the EERIE region did not contain a PTTH-responsive element, we would see no change in the level of GFP transcript in early and late third instar. However, if the EERIE region did contain a PTTH-responsive element, we would expect an increase in the level of GFP transcript at the end of third instar.

The data thus far are not conclusive because of the large amount of error present in our qrt-PCR samples (Figure 15). The 300 bp minimal *spok* EERIE region, spok1, trended towards a slight increase in gene expression between the 74 hour (early third instar) and the 120 hour (late third instar samples), however the data is not statistically significant (Figure 15). Interestingly, when the same experiment was performed using the full length 1.45 kb *spok* EERIE region, we observed a greater amount of GFP expression in our 74 hour (early third instar) samples compared to the 120 hour (late third instar) samples (Figure 15).

However, once again due to the large amount of error, this data is not statistically significant.

When a similar experiment was performed using an 800 bp *phm* EERIE element, comparing a 96 hour (mid-third instar larvae) with a 120 hour (late third instar larvae) we observed a trend towards an increase in *GFP* expression, however, once again, this data is not statistically significant.

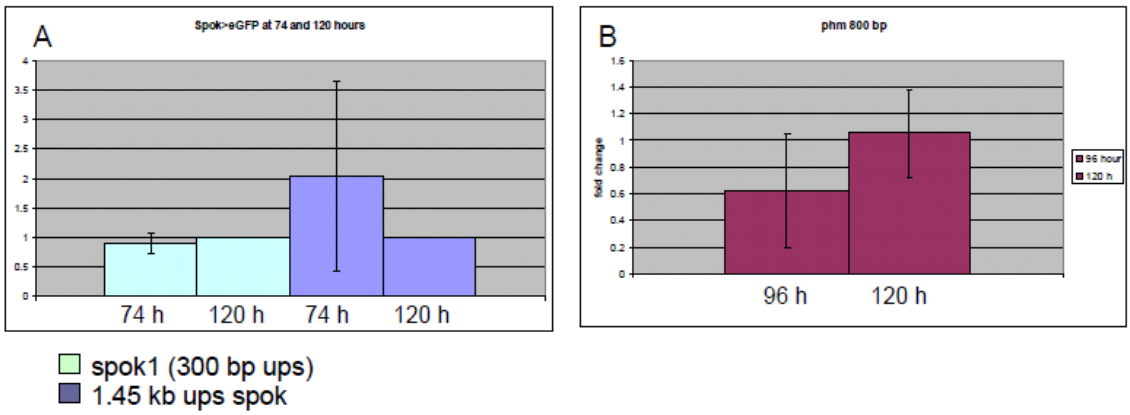

Figure 15: eGFP expression as detected by qRT-PCR from *phm* and *spok* EERIE samples. (A) qRT-PCR of eGFP from spok1 EERIE (light blue) and 1.45 kb ups spok (dark blue) EERIE samples. There is no statistically significant difference between the 74 hour and 120 hour larvae in either spok1 or 1.45 kb ups spok EERIE sample. (B) qRT-PCR of eGFP from the 800 bp phm EERIE sample. Although the trend is that eGFP is expressed at a higher level after 120 hours, the difference is not significant. Error bars represent standard error of the mean.

d. Discussion

We have successfully identified large and minimal EERIE regions for *phm*, *spok*, and *dib*. These regions are necessary and sufficient for specific GFP reporter gene expression in the PG and salivary glands of transgenic animals in late, wandering stages of the third instar stage. Although GFP is expressed in the salivary gland of these transgenic animals, we still conclude that the elements

identified are PG-specific because GFP expression in the salivary gland common background when using the pH-Stinger vector [99]. In fact, salivary gland expression of GFP has served as a positive control, in addition to eye color change, when determining if the pH-Stinger element was successfully cloned into each transgenic line.

In addition to finding a minimal *phm* EERIE element, we were able to identify four conserved motifs, that when mutated, altered GFP expression. Mutation of three of these motifs, mot1, mot2, and mot3, resulted in loss of GFP expression, indicating that these motifs are important for PG-specific GFP expression. Mutation of mot5 resulted in an increase of GFP expression in the PG, possibly indicating that this motif may be important for PG-expression. However, for these experiments, the level of GFP expression was not quantitative. The pictures of PGs from transgenic animals were taken at the same exposure time but this is not a quantitative measurement. Furthermore, variability exists between transgenic animal lines, due to the random insertion site of the P-element transposon from the pH-Stinger vector. Multiple transgenic lines of each sample type were generated and compared to ensure consistency. However, the strength of GFP expression varied amongst each sample type. Therefore, the increase in GFP expression in mot5 transgenic lines could simply be due to P-element insertion location, rather than the mutation of the mot5 motif.

Despite the variability of the GFP strength amongst transgenic lines of the same sample type, we believe the results of our EERIE screen are sound since we measured several transgenic lines of each sample type and the variability never resulted in total loss of GFP expression.

It is unclear if the EERIE elements we have isolated contained only PG-specific enhancer motif or if they also contain PTTH-responsive elements. We hypothesize that the PG-specific enhancer motifs would need to be present for specific expression in the PG and that loss or mutation of these elements would result in loss of *GFP* expression. In comparison, mutation or loss of a PTTH-responsive element may result in decreased or absent expression of *GFP* in late third instar larvae. Based on observation of *GFP* expression in the ring glands of early and late third instar we were unable to detect differences in *GFP* expression by eye. Therefore, we set out to quantify any differences of *GFP* transcript levels between early and late third instar larvae. We were unable to detect any statistically significant differences between early and late third instar larvae in either *spok* or *phm* EERIE samples. There are several reasons why we observed no significant difference.

First, there may be no difference in *GFP* reporter expression in either *spok* or *phm*. While plausible, based on our current data, it may not be a convincing answer without further study. Our data are not statistically significant and this is

due to a large amount of variability amongst biological replicates. One reason for the variability is that RNA needs to be extracted from an extremely small sample size. The PGs from ten larvae are needed to extract enough RNA for a qrt-PCR reaction. Even with ten animals, the amount of RNA is low. The number of animals used could be increased but the resulting increase in dissection time would likely result in increased RNA degradation, leading to another source of variability. A second reason for varying results may come from the technical difficulty in separating early third instar PG-brain complex from other tissues. It has been possible to ensure that no contaminating, *GFP*-expressing, salivary gland tissue is included, this would have resulted in an increase of GFP in the sample. However, even a small amount of contaminating tissue, such as the gut, would result in a larger tissue sample, leading to an increase in the amount of reference gene, Rpl23, leading to inaccurate results. These first two causes of variability may be overcome by skilled practice at dissection and isolation of samples. However, I was unable to achieve reliable results.

The third and final reason for variability may be that the amount of *GFP* expressed is so low that it is not reliably detected by qrt-PCR. This is a likely scenario based on the melting curves of samples. The melting curve generated from amplification of GFP from early third instar larvae occurs very late in the qrt-PCR cycle, sometimes only two to three cycles before amplification from negative control wells. This indicates that the small amount of *GFP* RNA in

samples isolated from early third instar may not be enough to reliably quantify the amount of gene expression.

One way to attempt to troubleshoot this problem may be to use the 420 bp *dib* EERIE region in a similar type of experiment. Dib exhibits a robust change in expression from early to late third instar in Bombyx, more-so than *phm* or *spok* [55]. Because of this more robust difference, changes in *GFP* gene expression may be more readily detectable in *dib* EERIE samples.

CHAPTER 4: CHARACTERIZATION OF THE PTTH-RESPONSIVE GENE, MEMBRANE STEROID BINDING PROTEIN (MSBP)

a. Chapter Introduction and Aim

The so-called Black Box reactions of 20E biosynthesis have not been fully characterized. Spo and its functional paralog, Spok, are P450s known to be involved in the Black Box reaction [62]. However, when *Drosophila* S2 cells are transfected with *spo* and treated with radiolabeled precursors, no downstream radiolabled intermediates can be detected (H. Ono, unpublished data). One possibility is that a co-factor is needed to help catalyze the putative high-energy reaction of the Black Box [62].

One possible co-factor is Membrane Steroid Binding Protein (MSBP, also called Pichb for PTTH inducible cytochrome P450-like heme binding protein). MSBP was first identified as a PTTH responsive gene in *Bombyx mori* [85]. The MSBP homologue in yeast, Dap1, has been shown to be involved as a P450 co-factor in sterol synthesis [100]. This project began with the goal of determining if MSBP played a role in ecdysone biosynthesis as a putative co-factor of Spo and Spok in the Black Box reaction.

b. Materials and Methods

Drosophila Genetics, stocks, and growth conditions

All *Drosophila* crosses were carried out at 25ºC or at room temperature on standard media in vials. The phm^{22}>GAL4 driver was used to drive expression of several UAS constructs in the larval PG. Five MSBP-RNAI stocks were obtained from the Vienna Drosophila RNAi Center: v5575, v45182, v45185, v45183, v45184 (VDRC, http://stockcenter.vdrc.at/control/main). The P-element line used for imprecise P-element excision was line #103825 (y- w- P[GawB]tayNP0941 / FM7c) obtained from the Drosophila Genetic Resource Center (DGRC, http://www.dgrc.kit.ac.jp/en/). P-element-mediated imprecise excision were made and mapped using standard techniques.

In situ hybridization

The RNA hybridization and detection were done according to standard protocols as described in [31,62,63]. To obtain the MSBP RNA sense and antisense probes, we used a cDNA vector containing MSBP in pBlueScriptSK- (cDNA AY061163; Berkeley Drosophila Genome Project; Drosophila Gene Collection Release 1; http://www.fruitfly.org/DGC/index.html). For the MSBP antisense probe, pBlueScriptSK-MSBP was linearized with NotI and transcribed with the SP6 promoter; for the MSBP sense probe, the same construct was linearized with SpeI and transcribed with the T& promoter.

Immunohistochemistry

Tissues from wandering third-instar larvae were fixed in 3.7% formaldehyde in PBS for 25 minutes, washed in PBS-Triton (0.1%), treated with primary antibody overnight at 4ºC overnight, exposed to secondary antibodies (Alexa Flour 488 or 555; 1:200) at room temperature for two to four hours. Samples were mounted in 80% glycerol before viewing on the CARV microscope.

Antibody generation

The anti-MSBP antibody was generated by OpenBiosystems (https://www.openbiosystems.com/) using the standard two guinea pig 80 day protocol using a 20 amino acid peptide sequence (ERKNLPKSKTETDDTKQEKE) located in the C-terminus of MSBP.

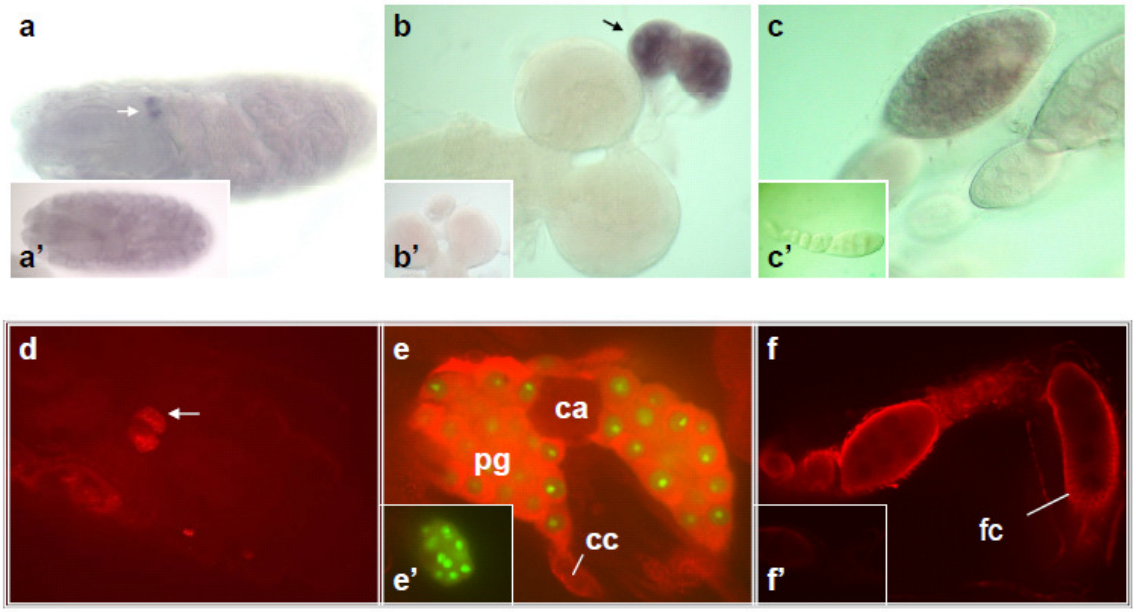

Figure 16: MSBP expression *in vivo*
(a-c) MSBP mRNA expression with sense and antisense digoxigenin-labeled MSBP ribo-probes. MSBP antisense riboprobe was detected in: (a) the ring gland (arrow) of a 20 h embryo; (b) PG cells of the 3rd instar larval ring gland (arrow); and (c) the adult female ovary. (a'), (b'), and (c') are MSBP sense riboprobe controls.(d-e) Immunodetection of MSBP protein using α-MSBP. MSBP was detected in: (d) the ring gland (arrow) and enocytes (arrow heads) of a 20 h embryo; (e) the prothoracic (pt) cells but not the corpora cardiaca (cc) or corporus allatum (ca) cells of the third instar larval ring gland (in *phm*-GAL4*; UAS*-GFP animals); and (f) the follicle cells (fc) of the adult female ovary. (e') and (f') are immuno controls using the prebleed serum from the guinea pigs used to generate α-MSBP.

c. Results

MSBP expression in ring gland, ovary and S2 cells

Using in situ hybridization and immunohistochemistry (IHC) techniques, we have found that MSBP mRNA and protein is expressed specifically in the prothoracic cells of the PG and in the adult ovary (Figure 16). In S2 cells transfected with tagged and untagged MSBP, MSBP can be detected by Western Blot and IHC. Mock transfected S2 cells express MSBP RNA. However, in these same cells

little or no MSBP protein can detected by Western Blot and IHC, indicating MSBP may be post-transcriptionally regulated (Figure 16).

Generation of an MSBP antibody

To detect MSBP *in vivo*, we generated an anti-MSBP antibody. The pre-injection sera from the guinea pig does not detect MSBP, whereas post-injection sera specifically detects MSBP by both Western blot and IHC (Figure 17).

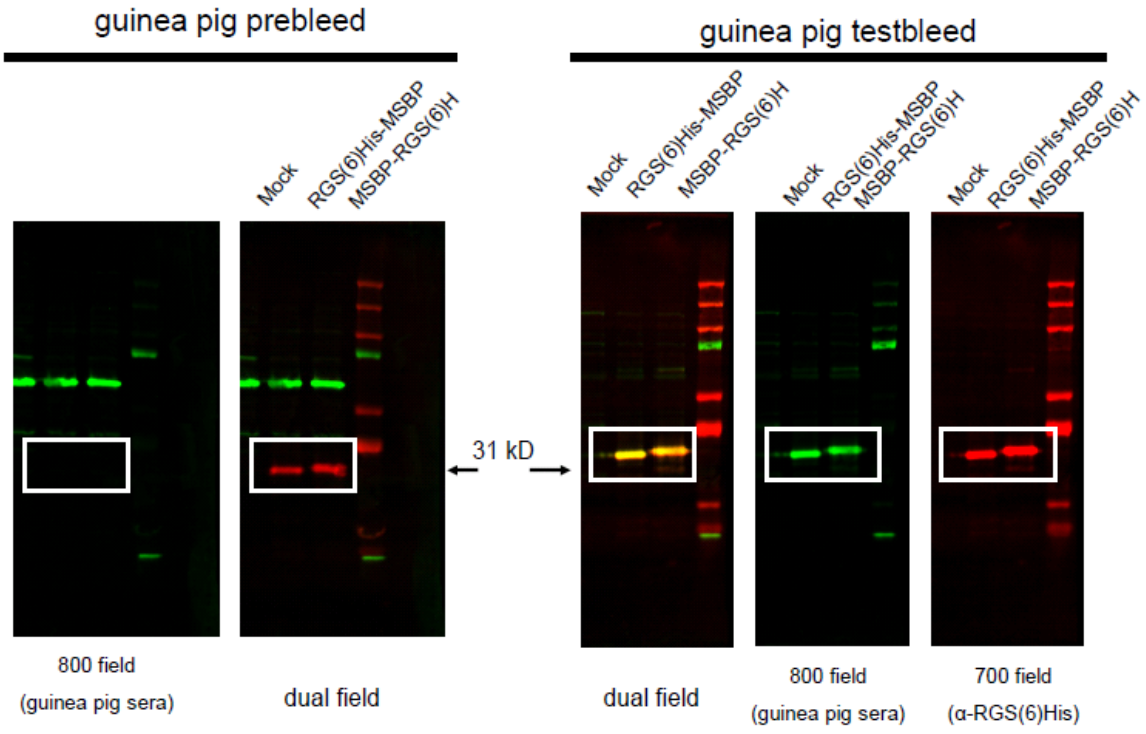

Figure 17: Test of the guinea pig α-MSBP antibody by Western blot
An α-MSBP antibody was generated by injecting an guinea pig with a 20 amino acid peptide sequence from the C-terminal end of MSBP. When S2 cells were transfected with RGS(6)His-tagged MSBP the guinea pig testbleed detected a band at 31 kD that overlapped with the RGS(6)His tag, indicating that the testbleed specifically detects MSBP. However, when the blot was probed with the guinea pig prebleed sera, no band was detected.

MSBP orientation

MSBP is a transmembrane protein with an N-terminal cytoplasmic domain. To test the membrane orientation of MSBP, S2 cells were transfected with MSBP or V5-MSBP-HA. Cells were fixed and either permeabilized or left unpermeabilized (Figure 18). Antibodies directed towards the C-terminal end of MSBP or V5-MSBP-HA could be detected under both cell permeable and unpermeable conditions, however, an antibody directed towards the N-terminal of HA-MSBP-V5 could not be detected in cell unpermeable conditions, indicating that the N-terminal of MSBP is cytosolic, while the C-terminal is extracellular (Figure 18).

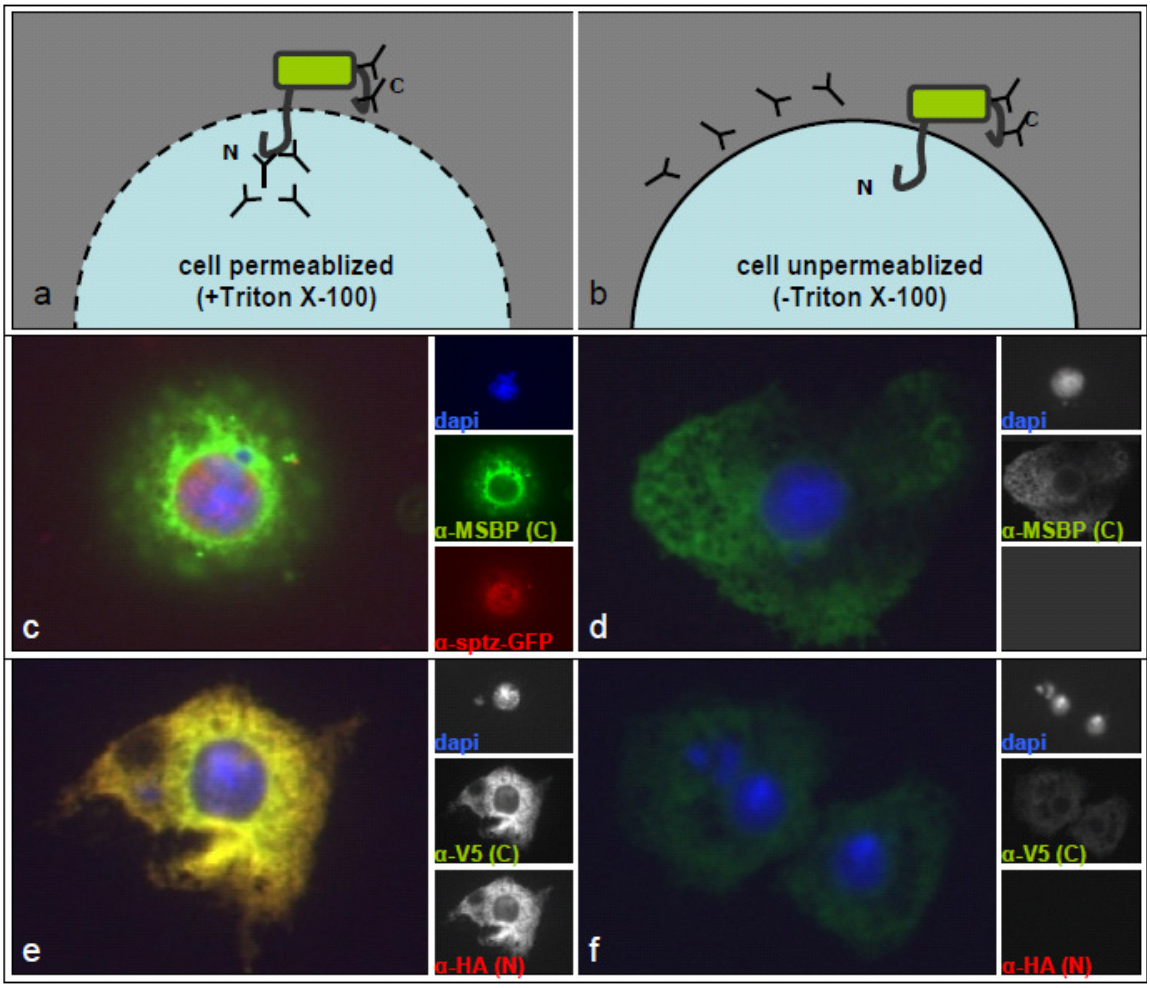

Figure 18: MSBP Orientation
The C-terminal region of MSBP is extracellular. (a)-(b) To test the orientation of MSBP, S2 cells were fixed and then permeablized or unpermeabilized. (c)-(d) S2 cells transfected with MSBP and stained with α-MSBP (which was generated using a peptide corresponding to 20 residues of the C-terminal end of MSBP); MSBP was detected in both (c) permeable and (d) unpermeable conditions. (e)-(f) S2 cells transfected with HA-MSBP-V5 and stained with α-HA and α-V5; (e) the C-terminal V5 tag could be detected under both conditions, (f) however the N-terminal tag could only be detected under permeable conditions.

MSBP RNAi knockdown animals arrest at 2nd instar

To study the phenotype of MSBP knockdown animals the Gal4/UAS system was used to specifically drive expression of MSBP-RNAi in the ring gland using the *phantom* (*phm*) promoter to drive GAL4 expression. 33% of *phm*>GAL4;UAS-

MSBP-RNAi (*phm*>MSBP-RNAi) animals were phenotypically normal, however 66% did not pupate. Some *phm*>MSBP-RNAi larvae arrested in the 2nd instar larval stage indefinitely (Figure 19).

Figure 19. MSBP-RNAi knockdown phenotype

To study the phenotype of MSBP mutants we took advantage of the GAL-4/UAS system in Drosophila to specifically drive expression of MSBP-RNAi in the ring gland. *phm*>GAL4 animals were crossed with UAS-MSBP-RNAi flies. 66% of *phm*>MSBP-RNAi animals died before reaching pupation. Some phm>pichb-RNAi larvae remained in the 2nd instar larval stage, even after 19 days. (a) 11 day old phm>MSBP-RNAi knockdown animal in 2nd instar larval stage. (b) yw control 3rd instar larva; (c) yw control 2nd instar larva. (d) 1st instar yw control larva. yw control animals all pupate by day 7, while some *phm*>*msbp*-RNAi animals remain as 2nd instar and cannot transition.

MSBP deletion mutants have no detectable phenotype

The $MSBP^{B22.1}$ mutant was generated by imprecise P-element excision. $MSBP^{B22.1}$ mutants exhibited a pupal lethal phenotype. Based on DNA sequence analysis, the imprecise excision deleted the entire MSBP coding region and also the neighboring upstream gene, CG15916. Therefore to confirm if the lethal phenotype was due to deletion of MSBP or CG15916, we generated transgenic animals with a BAC insertion that carried the genomic region surrounding MSBP but that had an premature stop codon in MSBP. Therefore the wildtype genomic region of CG15916 was present in the $MSBP^{stop}$-BAC line however, no MSBP protein would be present due to the premature stop codon. $MSBP^{B22.1}$, animals containing the $MSBP^{stop}$-BAC element rescue the $MSBP^{B22.1}$ phenotype, indicating that the pupal lethal phenotype we observed in the $MSBP^{B22.1}$ mutants was actually due to deletion of CG15916 and not MSBP. $MSBP^{stop}$-BAC in a $MSBP^{B22.1}$ background exhibits no observable phenotype, indicating that MSBP is not an essential gene.

d. Discussion

The expression pattern of MSBP in the PG and in the adult female ovary is consistent with its potential role in E production. The larval PG and the ovary are the two major locations for E production and where several other genes involved in E biosynthesis are expressed [6].

MSBP is a heme binding protein and it has been hypothesized that the heme binding domain may play a role as a co-factor with P450s to help mediate high-energy reactions [84]. The orientation of MSBP has been previously reported as having the C-terminal localized cytosolically in S2 cells [84]. However, when we repeated the experiment with several different tagged MSBP proteins and using a MSBP antibody, we found that the N-terminus was localized cytosolically in S2 cells. The discrepancy between our findings and this previous report are unknown, however, we performed a thorough analysis, including the use of a double-tagged HA-MSBP-V5 protein.

Deletion of MSBP causes no detectable phenotype which was surprising since when knocked down with RNAi specifically in the PG, some MSBP-RNAi knockdown animals displayed an arrested and delayed phenotype. However this larval arrest phenotype was not fully penetrant (Figure 14). Additionally, while one MSBP-RNAi line, Vienna stock line 45183, displayed a phenotype when knocked down specifically in the PG, other RNAi lines targeting MSBP did not display a phenotype. This could be due to off-target RNAi affects in the PG and not due to specific MSBP knockdown.

The pupal lethal phenotype observed in so-called $MSBP^{B22.1}$ mutants is actually a result of deletion of a neighboring gene, CG15916, not due to the deletion of

MSBP. CG15916 has not been studied extensively; however, InterPro sequence analysis suggests that CG15916 plays a role in rRNA processing (http://www.ebi.ac.uk/interpro/).

It may be that the MSBP phenotype is not immediately observable. To test this, we are currently studying whether $MSBP^{B22.1}$ CG15916-rescue animals have a disrupted developmental timing. It may be that MSBP mutants are viable but delayed, slightly. This type of phenotype would be consistent with a role in E biosynthesis.

We can also test the hypothesis that MSBP, while not essential for E biosynthesis, may enhance E synthesis under low cholesterol conditions. To test this, we are raising $MSBP^{B22.1}$ CG15916-rescue animals on a low-cholesterol diet to see if we can detect a more pronounced phenotype.

Finally, *Drosophila* contains two genes that share similar a similar sequence to MSBP; these are CG16957 and CG12056. Initially, we performed in situ hybridization to see where all three genes were expressed (*in situ* of CG16957 and CG12506 data not shown). However, of the three genes, only MSBP was expressed specifically in the PG. Although CG16957 and CG12506 do not seem to be PG-specific they may have enough expression in the PG to provide a redundant activity. To address this possibility, we would need to make

transgenic lines that either knock-out (by deletion) or knock-down (by RNAi) these genes to see if MSBP has a phenotype in the absence of CG16957 and CG12506.

REFERENCES

1. Moss E (2007) Heterochronic genes and the nature of developmental time. Current Biology 17: R425-R434.
2. Nussey S, Whitehead S (2001) Endocrinology: An Integrated Approach: Oxford: BIOS Scientific Publishers Limited.
3. Stavreva D, Wiench M, John S, Conway-Campbell B, McKenna M, et al. (2009) Ultradian hormone stimulation induces glucocorticoid receptor-mediated pulses of gene transcription. Nature Cell Biology 11: 1093-U1111.
4. Ou Q, Magico A, King-Jones K (2011) Nuclear Receptor DHR4 Controls the Timing of Steroid Hormone Pulses During Drosophila Development. Plos Biology 9.
5. Warren J, Petryk A, Marques G, Jarcho M, Parvy J, et al. (2002) Molecular and biochemical characterization of two P450 enzymes in the ecdysteroidogenic pathway of Drosophila melanogaster. Proceedings of the National Academy of Sciences of the United States of America 99: 11043-11048.
6. Gilbert L, Rybczynski R, Warren J (2002) Control and biochemical nature of the ecdysteroidogenic pathway. Annual Review of Entomology 47: 883-916.
7. Williams CM (1947) Physiology of insect diapause interaction between the pupal brain and prothoracic glands in the metamorphosis of the giant silkworm, Platysamia cecropia. Biol Bull 93: 89-98.
8. Ishizaki H, Suzuki A (1994) The brain secretory peptides that control molting and metamorphosis of the silkmoth, Bombyx mori. International Journal of Developmental Biology 38: 301-310.
9. Wilson TG (1988) Drosophila melanogaster (Diptera, Drosophilidae) - A model insect for insecticide resistance studies. Journal of Economic Entomology 81: 22-27.
10. Schneider D (2000) Using Drosophila as a model insect. Nat Rev Genet 1: 218-226.
11. Bonini NM (2001) Drosophila as a genetic approach to human neurodegenerative disease. Parkinsonism Relat Disord 7: 171-175.
12. Fortini ME, Bonini NM (2000) Modeling human neurodegenerative diseases in Drosophila: on a wing and a prayer. Trends Genet 16: 161-167.
13. Michno K, van de Hoef D, Wu H, Boulianne GL (2005) Modeling age-related diseases in Drosophila: can this fly? Curr Top Dev Biol 71: 199-223.
14. Bakhoum M, Jackson G, Chang K, Min K (2011) Demise of the Flies: Why Drosophila Models Still Matter. Progress in Molecular Biology and Translational Science: Animal Models of Human Disease, Vol 100 100: 483-498.
15. van Alphen B, van Swinderen B (2011) Drosophila strategies to study psychiatric disorders. Brain Res Bull.

16. Adams MD, Celniker SE, Holt RA, Evans CA, Gocayne JD, et al. (2000) The genome sequence of Drosophila melanogaster. Science 287: 2185-2195.
17. Myers EW, Sutton GG, Delcher AL, Dew IM, Fasulo DP, et al. (2000) A whole-genome assembly of Drosophila. Science 287: 2196-2204.
18. Bier E (2005) Drosophila, the golden bug, emerges as a tool for human genetics. Nat Rev Genet 6: 9-23.
19. Reiter LT, Potocki L, Chien S, Gribskov M, Bier E (2001) A systematic analysis of human disease-associated gene sequences in Drosophila melanogaster. Genome Res 11: 1114-1125.
20. Yamanaka N, Roller L, Zitňan D, Satake H, Mizoguchi A, et al. (2011) Bombyx orcokinins are brain-gut peptides involved in the neuronal regulation of ecdysteroidogenesis. J Comp Neurol 519: 238-246.
21. Yamanaka N, Yamamoto S, Zitnan D, Watanabe K, Kawada T, et al. (2008) Neuropeptide Receptor Transcriptome Reveals Unidentified Neuroendocrine Pathways. Plos One 3.
22. Consortium ISG (2008) The genome of a lepidopteran model insect, the silkworm Bombyx mori. Insect Biochem Mol Biol 38: 1036-1045.
23. Xia Q, Zhou Z, Lu C, Cheng D, Dai F, et al. (2004) A draft sequence for the genome of the domesticated silkworm (Bombyx mori). Science 306: 1937-1940.
24. Mita K, Kasahara M, Sasaki S, Nagayasu Y, Yamada T, et al. (2004) The genome sequence of silkworm, Bombyx mori. DNA Res 11: 27-35.
25. Karlson P (1996) The hormonal control of insect metamorphosis. A historical review. International Journal of Developmental Biology 40: 93-96.
26. Kataoka H, Nagasawa H, Isogai A, Ishizaki H, Suzuki A (1991) Prothoracicotropic hormone of the silkworm, Bombyx mori: amino acid sequence and dimeric structure. Agric Biol Chem 55: 73-86.
27. Marchal E, Vandersmissen HP, Badisco L, Van de Velde S, Verlinden H, et al. (2010) Control of ecdysteroidogenesis in prothoracic glands of insects: a review. Peptides 31: 506-519.
28. Siegmund T, Korge G (2001) Innervation of the ring gland of Drosophila melanogaster. Journal of Comparative Neurology 431: 481-491.
29. Weaver RJ, Audsley N (2009) Neuropeptide regulators of juvenile hormone synthesis: structures, functions, distribution, and unanswered questions. Ann N Y Acad Sci 1163: 316-329.
30. De Velasco B, Shen J, Go S, Hartenstein V (2004) Embryonic development of the Drosophila corpus cardiacum, a neuroendocrine gland with similarity to the vertebrate pituitary, is controlled by sine oculis and glass. Dev Biol 274: 280-294.
31. Petryk A, Warren J, Marques G, Jarcho M, Gilbert L, et al. (2003) Shade is the Drosophila P450 enzyme that mediates the hydroxylation of ecdysone to the steroid insect molting hormone 20-hydroxyecdysone. Proceedings of the National Academy of Sciences of the United States of America 100: 13773-13778.

32. Hartenstein V (1995) Atlas of Drosophila Development: Cold Spring Harbor Laboratory Press.
33. King RC, Aggarwal SK, Bodenstein D (1966) The comparative submicroscopic morphology of the ring gland of Drosophila melanogaster during the second and third larval instars. Z Zellforsch Mikrosk Anat 73: 272-285.
34. Fernandez-Fernandez R, Martini AC, Navarro VM, Castellano JM, Dieguez C, et al. (2006) Novel signals for the integration of energy balance and reproduction. Mol Cell Endocrinol 254-255: 127-132.
35. Navarro VM, Castellano JM, García-Galiano D, Tena-Sempere M (2007) Neuroendocrine factors in the initiation of puberty: the emergent role of kisspeptin. Rev Endocr Metab Disord 8: 11-20.
36. Smith JT, Clarke IJ (2007) Kisspeptin expression in the brain: catalyst for the initiation of puberty. Rev Endocr Metab Disord 8: 1-9.
37. McBrayer Z, Ono H, Shimell M, Parvy J, Beckstead R, et al. (2007) Prothoracicotropic hormone regulates developmental timing and body size in Drosophila. Developmental Cell 13: 857-871.
38. Kawakami A, Kataoka H, Oka T, Mizoguchi A, Kimurakawakami M, et al. (1990) Molecular cloning of the Bombyx mori prothoracicotropic hormone. Science 247: 1333-1335.
39. Mizoguchi A, Oka T, Kataoka H, Nagasawa H, Suzuki A, et al. (1990) Immunochistochemical localization of prothoracicotropic hormone-producing neurosecretory cells in teh brain of *Bombyx mori*. Development Growth & Differentiation 32: 591-598.
40. Rybczynski R, Bell SC, Gilbert LI (2001) Activation of an extracellular signal-regulated kinase (ERK) by the insect prothoracicotropic hormone. Mol Cell Endocrinol 184: 1-11.
41. Rybczynski R, Gilbert LI (2003) Prothoracicotropic hormone stimulated extracellular signal-regulated kinase (ERK) activity: the changing roles of Ca(2+)- and cAMP-dependent mechanisms in the insect prothoracic glands during metamorphosis. Mol Cell Endocrinol 205: 159-168.
42. Smith WA, Gilbert LI (1989) Early events in peptide-stimulated ecdysteroid secretion by the prothoracic glands of Manduca sexta. J Exp Zool 252: 264-270.
43. Ghosh A, McBrayer Z, O'Connor M (2010) The Drosophila gap gene giant regulates ecdysone production through specification of the PTTH-producing neurons. Developmental Biology 347: 271-278.
44. Kim AJ, Cha GH, Kim K, Gilbert LI, Lee CC (1997) Purification and characterization of the prothoracicotropic hormone of Drosophila melanogaster. Proc Natl Acad Sci U S A 94: 1130-1135.
45. Shionoya M, Matsubayashi H, Asahina M, Kuniyoshi H, Nagata S, et al. (2003) Molecular cloning of the prothoracicotropic hormone from the tobacco hornworm, Manduca sexta. Insect Biochem Mol Biol 33: 795-801.

46. Rewitz K, Yamanaka N, Gilbert L, O'Connor M (2009) The Insect Neuropeptide PTTH Activates Receptor Tyrosine Kinase Torso to Initiate Metamorphosis. Science 326: 1403-1405.
47. Gilbert LI, Rybczynski R, Song Q, Mizoguchi A, Morreale R, et al. (2000) Dynamic regulation of prothoracic gland ecdysteroidogenesis: Manduca sexta recombinant prothoracicotropic hormone and brain extracts have identical effects. Insect Biochem Mol Biol 30: 1079-1089.
48. Casanova J, Struhl G (1989) Localized surface activity of Torso, a receptor tyrosine kinase, specifies terminal body pattern in *Drosophila*. Genes & Development 3: 2025-2038.
49. Li WX (2005) Functions and mechanisms of receptor tyrosine kinase Torso signaling: lessons from Drosophila embryonic terminal development. Dev Dyn 232: 656-672.
50. Sprenger F, Stevens LM, Nüsslein-Volhard C (1989) The Drosophila gene torso encodes a putative receptor tyrosine kinase. Nature 338: 478-483.
51. Rewitz KF, O'Connor MB, Gilbert LI (2007) Molecular evolution of the insect Halloween family of cytochrome P450s: phylogeny, gene organization and functional conservation. Insect Biochem Mol Biol 37: 741-753.
52. Casali A, Casanova J (2001) The spatial control of Torso RTK activation: a C-terminal fragment of the Trunk protein acts as a signal for Torso receptor in the Drosophila embryo. Development 128: 1709-1715.
53. Lin JL, Gu SH (2007) In vitro and in vivo stimulation of extracellular signal-regulated kinase (ERK) by the prothoracicotropic hormone in prothoracic gland cells and its developmental regulation in the silkworm, Bombyx mori. J Insect Physiol 53: 622-631.
54. Rewitz KF, Larsen MR, Lobner-Olesen A, Rybczynski R, O'Connor MB, et al. (2009) A phosphoproteomics approach to elucidate neuropeptide signal transduction controlling insect metamorphosis. Insect Biochem Mol Biol 39: 475-483.
55. Yamanaka N, Honda N, Osato N, Niwa R, Mizoguchi A, et al. (2007) Differential regulation of ecdysteroidogenic P450 gene expression in the silkworm, Bombyx mori. Biosci Biotechnol Biochem 71: 2808-2814.
56. Keightley DA, Lou KJ, Smith WA (1990) Involvement of translation and transcription in insect steroidogenesis. Mol Cell Endocrinol 74: 229-237.
57. Espenshade PJ, Hughes AL (2007) Regulation of sterol synthesis in eukaryotes. Annual Review of Genetics 41: 401-427.
58. Lafont R, Dauphin-Villemant C, Warren J, Rees H (2012) Ecdysteroid Chemistry and Biochemistry. In: Gilbert L, editor. Insect Endocrinology. First ed. San Diego, CA: Academic Press. pp. 106-176.
59. Nusslein-Volhard C, Weischaus E, Kluding H (1984) Mutations affecting the pattern of the larval cuticle in *Drosophila melanogaster*. I. Zygotic loci on the second chromosome. Roux's Archive of Developmental Biology 193: 267-282.

60. Jurgens G, Wieschaus E, Nusslein-Volhard C, Kluding H (1984) Mutations affecting the pattern of the larval cuticle in Drosophila melanogaster II. Zygotic loci on the third chromosome. Roux's Archive of Developmental Biology 193: 283-295.
61. Wieschaus E, Nusslein-Volhard C, Jurgens G (1984) Mutations affecting the pattern of the larval cuticle in *Drosophila melanogaster*. III. Zygotic loci on the X-chromosome and 4th chromosome. Roux's Archive of Developmental Biology 195: 296-307.
62. Ono H, Rewitz K, Shinoda T, Itoyama K, Petryk A, et al. (2006) Spook and Spookier code for stage-specific components of the ecdysone biosynthetic pathway in Diptera. Developmental Biology 298: 555-570.
63. Chavez V, Marques G, Delbecque J, Kobayashi K, Hollingsworth M, et al. (2000) The Drosophila disembodied gene controls late embryonic morphogenesis and codes for a cytochrome P450 enzyme that regulates embryonic ecdysone levels. Development 127: 4115-4126.
64. Niwa R, Matsuda T, Yoshiyama T, Namiki T, Mita K, et al. (2004) CYP306A1, a cytochrome P450 enzyme, is essential for ecdysteroid biosynthesis in the prothoracic glands of Bombyx and Drosophila. Journal of Biological Chemistry 279: 35942-35949.
65. Niwa R, Sakudoh T, Namiki T, Saida K, Fujimoto Y, et al. (2005) The ecdysteroidogenic P450 Cyp302a1/disembodied from the silkworm, Bombyx mori, is transcriptionally regulated by prothoracicotropic hormone. Insect Molecular Biology 14: 563-571.
66. Christiaens O, Iga M, Velarde RA, Rougé P, Smagghe G (2010) Halloween genes and nuclear receptors in ecdysteroid biosynthesis and signalling in the pea aphid. Insect Mol Biol 19 Suppl 2: 187-200.
67. Niwa R, Namiki T, Ito K, Shimada-Niwa Y, Kiuchi M, et al. (2010) Non-molting glossy/shroud encodes a short-chain dehydrogenase/reductase that functions in the 'Black Box' of the ecdysteroid biosynthesis pathway. Development 137: 1991-1999.
68. Yoshiyama T, Namiki T, Mita K, Kataoka H, Niwa R (2006) Neverland is an evolutionally conserved Rieske-domain protein that is essential for ecdysone synthesis and insect growth. Development 133: 2565-2574.
69. Yoshiyama-Yanagawa T, Enya S, Shimada-Niwa Y, Yaguchi S, Haramoto Y, et al. (2011) The Conserved Rieske Oxygenase DAF-36/Neverland Is a Novel Cholesterol-metabolizing Enzyme. Journal of Biological Chemistry 286: 25756-25762.
70. Gilbert LI, Warren JT (2005) A molecular genetic approach to the biosynthesis of the insect steroid molting hormone. Vitam Horm 73: 31-57.
71. Ono H, Morita S, Asakura I, Nishida R (2012) Conversion of 3-oxo steroids into ecdysteroids triggers molting and expression of 20E-inducible genes in Drosophila melanogaster. Biochem Biophys Res Commun 421: 561-566.

72. Namiki T, Niwa R, Sakudoh T, Shirai K, Takeuchi H, et al. (2005) Cytochrome P450CYP307A1/spook: A regulator for ecdysone synthesis in insects. Biochemical and Biophysical Research Communications 337: 367-374.
73. Sztal T, Chung H, Gramzow L, Daborn P, Batterham P, et al. (2007) Two independent duplications forming the Cyp307a genes in Drosophila. Insect Biochemistry and Molecular Biology 37: 1044-1053.
74. Tanaka Y (1998) Induction of larval ecdysys by ecdysone in the non-molting glossy (nm-g) mutant larvae of Bombyx mori. Journal of Sericultural Science of Japan 67: 109-115.
75. Nagata M, Tsuchida K, Shimizu K, Yshitake N (1987) Physiological aspects of *nm-g* mutant: An ecdysteroid-deficient mutant of the silkworm, *Bombyx mori*. Journal of Insect Physiology 33: 723-727.
76. Blais C, Dauphin-Villemant C, Kovganko N, Girault JP, Descoins C, et al. (1996) Evidence for the involvement of 3-oxo-delta 4 intermediates in ecdysteroid biosynthesis. Biochem J 320 (Pt 2): 413-419.
77. Davies TG, Dinan LN, Lockley WJ, Rees HH, Goodwin TW (1981) Formation of the A/B cis ring junction of ecdysteroids in the locust, Schistocerca gregaria. Biochem J 194: 53-62.
78. Bocking D, Dauphin-Villemant C, Sedlmeier D, Blais C, Lafont R (1993) Ecdysteroid biosynthesis in moulting glands of the crayfish *Orconects Limosus*: evidence for the synthesis of 3-dehydroecdysone by in vitro synthesis and conversion studies. Insect Biochemistry and Molecular Biology 23: 57-63.
79. Dolle F, Hertru C, Roussel J, Rousseau B, Sobrio F, et al. (1991) Synthesis of a tritiated 3-dehydroecdysteroid putative precursor of ecdysteroid biosynthesis in Locusta migratoria. Tetrahedron 47: 7067-7080.
80. Warren JT, Petryk A, Marqués G, Parvy JP, Shinoda T, et al. (2004) Phantom encodes the 25-hydroxylase of Drosophila melanogaster and Bombyx mori: a P450 enzyme critical in ecdysone biosynthesis. Insect Biochem Mol Biol 34: 991-1010.
81. Craven RJ, Mallory JC, Hand RA (2007) Regulation of iron homeostasis mediated by the heme-binding protein Dap1 (damage resistance protein 1) via the p450 protein Erg11/Cyp51. Journal of Biological Chemistry 282: 36543-36551.
82. Ghosh K, Thompson AM, Goldbeck RA, Shi X, Whitman S, et al. (2005) Spectroscopic and biochemical characterization of heme binding to yeast Dap1p and mouse PGRMC1p. Biochemistry 44: 16729-16736.
83. Mallory JC, Crudden G, Johnson BL, Mo C, Pierson CA, et al. (2005) Dap1p, a heme-binding protein that regulates the cytochrome P450 protein Erg11p/Cyp51p in Saccharomyces cerevisiae. Mol Cell Biol 25: 1669-1679.

84. Fujii-Taira I, Yamaguchi S, Iijima R, Natori S, Homma KJ (2009) Suppression of the ecdysteroid-triggered growth arrest by a novel Drosophila membrane steroid binding protein. FEBS Lett 583: 655-660.
85. Kurokawa J (2007) Identification and analysis of a PTTH-inducible gene, Pichb. Tokyo, Japan: The University of Tokyo. 100 p.
86. Livak K, Schmittgen T (2001) Analysis of relative gene expression data using real-time quantitative PCR and the 2(T)(-Delta Delta C) method. Methods 25: 402-408.
87. Valentine J, Collins A (2000) The significance of moulting in Ecdysozoan evolution. Evolution & Development 2: 152-156.
88. Xia Q, Guo Y, Zhang Z, Li D, Xuan Z, et al. (2009) Complete resequencing of 40 genomes reveals domestication events and genes in silkworm (Bombyx). Science 326: 433-436.
89. Yamanaka N, Hua Y, Mizoguchi A, Watanabe K, Niwa R, et al. (2005) Identification of a novel prothoracicostatic hormone and its receptor in the silkworm Bombyx mori. Journal of Biological Chemistry 280: 14684-14690.
90. Mueller O, Lightfoot S, Schroeder A (2004) RNA Integrity Number (RIN) - Standardization of RNA Quality Control. Agilent Application Note, Publication Number 5989-1165EN. pp. 7.
91. Schroeder A, Mueller O, Stocker S, Salowsky R, Leiber M, et al. (2006) The RIN: an RNA integrity number for assigning integrity values to RNA measurements. BMC Mol Biol 7: 3.
92. Krupp G (2005) Stringent RNA quality control using the Agilent 2100 bioanalyzer. Agilent Application Note, Publication Number.
93. Winnebeck EC, Millar CD, Warman GR (2010) Why does insect RNA look degraded? J Insect Sci 10: 159.
94. Applebaum SW, Ebstein RP, Wyatt GR (1966) Dissociation of ribonucleic acid from silkmoth pupae by heat and dimethylsulfoxide: evidence for specific cleavage points. J Mol Biol 21: 29-41.
95. Greenberg JR (1969) Synthesis and properties of ribosomal RNA in Drosophila. J Mol Biol 46: 85-98.
96. Ishikawa H, Newburgh RW (1972) Studies of the thermal conversion of 28 S RNA of Galleria mellonella (L.) to an 18 S product. J Mol Biol 64: 135-144.
97. Sarup P, Sørensen JG, Kristensen TN, Hoffmann AA, Loeschcke V, et al. (2011) Candidate genes detected in transcriptome studies are strongly dependent on genetic background. PLoS One 6: e15644.
98. Barolo S, Carver LA, Posakony JW (2000) GFP and beta-galactosidase transformation vectors for promoter/enhancer analysis in Drosophila. Biotechniques 29: 726, 728, 730, 732.
99. Zhu Q, Halfon MS (2007) Vector-dependent gene expression driven by insulated P-element reporter vectors. Fly (Austin) 1: 55-56.
100. Hughes AL, Powell DW, Bard M, Eckstein J, Barbuch R, et al. (2007) Dap1/PGRMC1 binds and regulates cytochrome P450 enzymes. Cell Metabolism 5: 143-149.

101. Shi Y, Massagué J (2003) Mechanisms of TGF-beta signaling from cell membrane to the nucleus. Cell 113: 685-700.
102. Peterson AJ, Jensen PA, Shimell M, Stefancsik R, Wijayatonge R, et al. (2012) R-smad competition controls activin receptor output in Drosophila. PLoS One 7: e36548.
103. Söderström S, Bengtsson H, Ebendal T (1996) Expression of serine/threonine kinase receptors including the bone morphogenetic factor type II receptor in the developing and adult rat brain. Cell Tissue Res 286: 269-279.
104. Aberle H, Haghighi AP, Fetter RD, McCabe BD, Magalhães TR, et al. (2002) wishful thinking encodes a BMP type II receptor that regulates synaptic growth in Drosophila. Neuron 33: 545-558.
105. Baines RA (2004) Synaptic strengthening mediated by bone morphogenetic protein-dependent retrograde signaling in the Drosophila CNS. J Neurosci 24: 6904-6911.
106. Marqués G, Bao H, Haerry TE, Shimell MJ, Duchek P, et al. (2002) The Drosophila BMP type II receptor Wishful Thinking regulates neuromuscular synapse morphology and function. Neuron 33: 529-543.
107. McCabe BD, Marqués G, Haghighi AP, Fetter RD, Crotty ML, et al. (2003) The BMP homolog Gbb provides a retrograde signal that regulates synaptic growth at the Drosophila neuromuscular junction. Neuron 39: 241-254.
108. Rawson JM, Lee M, Kennedy EL, Selleck SB (2003) Drosophila neuromuscular synapse assembly and function require the TGF-beta type I receptor saxophone and the transcription factor Mad. J Neurobiol 55: 134-150.
109. Knox S, Ge H, Dimitroff BD, Ren Y, Howe KA, et al. (2007) Mechanisms of TSC-mediated control of synapse assembly and axon guidance. PLoS One 2: e375.
110. Sasai Y (2001) Regulation of neural determination by evolutionarily conserved signals: anti-BMP factors and what next? Curr Opin Neurobiol 11: 22-26.
111. Rhinn M, Picker A, Brand M (2006) Global and local mechanisms of forebrain and midbrain patterning. Curr Opin Neurobiol 16: 5-12.
112. Mehler MF, Mabie PC, Zhang D, Kessler JA (1997) Bone morphogenetic proteins in the nervous system. Trends Neurosci 20: 309-317.
113. Zhao GQ (2003) Consequences of knocking out BMP signaling in the mouse. Genesis 35: 43-56.
114. Sun M, Thomas MJ, Herder R, Bofenkamp ML, Selleck SB, et al. (2007) Presynaptic contributions of chordin to hippocampal plasticity and spatial learning. J Neurosci 27: 7740-7750.
115. Piccolo S, Sasai Y, Lu B, De Robertis EM (1996) Dorsoventral patterning in Xenopus: inhibition of ventral signals by direct binding of chordin to BMP-4. Cell 86: 589-598.

APPENDIX A: CHARACTERIZATION OF THE NULL DSMAD2^{F4} EXCISION MUTANT

In animals, Transforming Growth Factor β (TGF-β) superfamily signaling controls a large number of cellular activities throughout development [101]. The canonical TGF-β signaling pathway works in the following manner: extracellular ligands bind to and activate receptor complexes that in turn phosphorylate R-Smad transcription factors to regulate gene transcription [101]. The TGF-β superfamily contains two functional subfamilies, present in all metazoans: the TGF-β/Activin branch and the Bone Morphogenic Protein (BMP) branch (Huminiecki 2009). In *Drosophila,* dSmad2 works downstream of the TGF-β/Activin ligands to induce different transcriptional responses. The main difference between TGF-β/Activin and BMP pathways is that the receptor complexes activate different classes of R-Smads, leading to differential gene transcription. Genetic and molecular biology studies have shown that the two subfamilies activate different R-Smads, however, studies in mammalian cell culture have shown cross-talk activity between the two pathways (Goumans 2003).

To better understand if TGF-β/Activin and BMP cross-talk is present in *Drosophila*, we asked if the TGF-β/Activin Type I receptor, Baboon, could

activate the canonical BMP R-Smad, Mad, *in vivo*. We hypothesized that dSmad2, the canonical TGF-β/Activin R-Smad, and Mad were in direct competition to bind to Baboon[10].

To test this hypothesis *in vivo*, the level of Mad activation (P-Mad) needed to be tested in a dSmad2 protein null background. However, no protein null dSmad2 allele existed[11]. Therefore, a new *dSmad2* null allele was generated by imprecise P-element excision and confirmed by Southern blot[12]. The Southern Blot analysis was consistent with the $dSmad2^{F4}$ animals being protein null, however, the exact breakpoints of the P-element excision were unknown.

To determine the exact cytolocation of the 5' and 3' breakpoints of the $dSmad2^{F4}$ allele, I analyzed lethal chromosomes by PCR and sequencing to map the extent of the deletion[13]. The $dSmad2^{F4}$ deletion removed a portion of the 5' UTR (break point at nucleotide 457 of sequence AF101386) and the entire coding region (Figure 5A in [102], reprinted in full below). The 3' breakpoint was detected at 275 bp downstream of the dSmad2 transcript. No disruption of neighboring genes was detected; however several segments of the original P-element were

[10] AJP, PAJ, and MBO conceived and designed all experiments.
[11] One allele, $dSmad2^{MB388}$, generated through EMS mutagenesis was shown to be functionally inactive due to a point mutation resulting in a single amino acid change. However, a $dSmad2^{MB388}$ protein is still produced.
[12] RW, RS, and LAR performed the P-element excision and Northern Blot.
[13] MS assisted with primer design.

left behind. Deletion of the entire coding region makes *dSmad2*^{F4} unambiguously protein null.

In *dSmad2*^{F4} animals, p-Mad was elevated in a Baboon-dependent manner, indicating that cross-talk signaling was present *in vivo*. This observation, among others (described in detail in the paper below), led us to conclude that there is a cross-talk mechanism, in which Baboon signals through Mad. Mad and dSmad2 may compete in a manner that allows for a signal-switching mechanism but only when dSmad2 levels are low [102]. This indicates that BMP and TGF-β/Activin cross-talk does occur in *Drosophila in vivo*, but only when dSmad2 levels are limited. Additionally, Baboon activity can lower the level of dSmad2 protein, giving a regulatory possibility where the TGF-β/Activin signal can influence its own response. It is not clear how dSmad2 is being downregulated, however preliminary experiments indicate dSmad2 is rapidly degraded, possibly in a ubiquityation-proteosome manner in the presence. Additional studies are needed to further explore the different mechanisms by which dSmad2, Mad, and Baboon signaling works *in vivo*.

OPEN ACCESS Freely available online

PLoS one

R-Smad Competition Controls Activin Receptor Output in *Drosophila*

Aidan J. Peterson[1☯], Philip A. Jensen[1☯¤a], MaryJane Shimell[1], Ray Stefancsik[2¤b], Ranjula Wijayatonge[2¤c], Rachel Herder[1], Laurel A. Raftery[2,3], Michael B. O'Connor[1*]

1 Department of Genetics, Cell Biology, and Development, University of Minnesota, Minneapolis, Minnesota, United States of America, **2** Cutaneous Biology Research Center, Massachusetts General Hospital/Harvard Medical School, Charlestown, Massachusetts, United States of America, **3** School of Life Sciences, University of Nevada Las Vegas, Las Vegas, Nevada, United States of America

Abstract

Animals use TGF-β superfamily signal transduction pathways during development and tissue maintenance. The superfamily has traditionally been divided into TGF-β/Activin and BMP branches based on relationships between ligands, receptors, and R-Smads. Several previous reports have shown that, in cell culture systems, "BMP-specific" Smads can be phosphorylated in response to TGF-β/Activin pathway activation. Using *Drosophila* cell culture as well as *in vivo* assays, we find that Baboon, the *Drosophila* TGF-β/Activin-specific Type I receptor, can phosphorylate Mad, the BMP-specific R-Smad, in addition to its normal substrate, dSmad2. The Baboon-Mad activation appears direct because it occurs in the absence of canonical BMP Type I receptors. Wing phenotypes generated by Baboon gain-of-function require Mad, and are partially suppressed by over-expression of dSmad2. In the larval wing disc, activated Baboon cell-autonomously causes C-terminal Mad phosphorylation, but only when endogenous dSmad2 protein is depleted. The Baboon-Mad relationship is thus controlled by dSmad2 levels. Elevated P-Mad is seen in several tissues of dSmad2 protein-null mutant larvae, and these levels are normalized in *dSmad2*; *baboon* double mutants, indicating that the cross-talk reaction and Smad competition occur with endogenous levels of signaling components *in vivo*. In addition, we find that high levels of Activin signaling cause substantial turnover in dSmad2 protein, providing a potential cross-pathway signal-switching mechanism. We propose that the dual activity of TGF-β/Activin receptors is an ancient feature, and we discuss several ways this activity can modulate TGF-β signaling output.

Citation: Peterson AJ, Jensen PA, Shimell M, Stefancsik R, Wijayatonge R, et al. (2012) R-Smad Competition Controls Activin Receptor Output in *Drosophila*. PLoS ONE 7(5): e36548. doi:10.1371/journal.pone.0036548

Editor: Christian Bökel, Technische Universität Dresden, Germany

Received December 19, 2011; **Accepted** April 10, 2012; **Published** May 1, 2012

Funding: This work was supported by National Institutes of Health grants to MBO (R01 GM95746) and LAR (R01 GM060501). PAJ was supported in part by a National Institutes of Health Institutional Training Grant (T32 HD007430-11A1). The funders had no role in study design, data collection and analysis, decision to publish, or preparation of the manuscript.

Competing Interests: The authors have declared that no competing interests exist.

* E-mail: moconnor@umn.edu

☯ These authors contributed equally to this work.

¤a Current address: Department of Biology, Rocky Mountain College, Billings, Montana, United States of America
¤b Current address: FlyBase, University of Cambridge, Division of Genetics, Cambridge, United Kingdom
¤c Current address: Department of Neurobiology, Duke University Medical Center, Durham, North Carolina, United States of America

Introduction

TGF-β superfamily signaling controls a multitude of metazoan cellular behaviors. Much of the signaling activity can be explained by the canonical Smad pathway, wherein extracellular ligands direct formation of active receptor complexes that phosphorylate and activate R-Smad transcription factors [1]. Multiple levels of regulation are known, ranging from extracellular ligand processing to diverse post-translational modification of Smad proteins [2–3]. In addition, a number of Smad-independent signaling pathways have also been demonstrated for various receptors and in different cell types [4].

Two functional subfamilies in TGF-β signaling are generally recognized based on genetic phenotypes and molecular studies: the TGF-β/Activin branch and the BMP branch. Phylogenetic analysis indicates that the TGF-β and BMP branches are present in all metazoans [5], suggesting that a robust TGF-β signaling network is an ancient feature of multicellular animals. The key difference between the two branches is that they activate different classes of R-Smads and thus induce different transcriptional responses in target cells. The TGF-β/Activin ligands work through Smad2/3 (dSmad2 in *Drosophila*) and BMP ligands work through Smad1/5/8 (Mad in *Drosophila*). These selective outputs are orchestrated by the Type I receptors, which bind to specific extracellular ligands and phosphorylate specific subsets of R-Smads.

Although genetic and molecular biology studies have consistently indicated that TGF-β/Activin and BMP signals use different R-Smads, there have been several reports of activation of BMP R-Smads by TGF-β ligands. This cross-talk activity was observed in several types of mammalian cells, but conflicting mechanisms were put forth on how this is achieved. Goumans et al. [6] described phosphorylation of BMP R-Smads upon TGF-β ligand exposure in human endothelial cells, and they concluded that TGF-β and BMP Type I receptors are both required for the reaction. Another report suggested that TGF-β phosphorylation of BMP R-Smads in

human epithelial cells is accomplished by a BMP receptor [7]. In that model, the receptor signaling complex again includes two Type I receptors from different signaling branches: a TGF-β/Activin receptor that both acts as a scaffold for the ligand and phosphorylates TGF-β/Activin R-Smads, and a BMP receptor that phosphorylates BMP R-Smads. However, two other studies demonstrated that a human TGF-β/Activin receptor can phosphorylate BMP R-Smads directly, eliminating any role for a BMP receptor in some cell types [8–9]. Activin-to-BMP cross-talk in *Drosophila* cell culture has also been reported [10], but the receptor directly responsible for the Activin-stimulated phosphorylation of Mad, the mechanisms by which this phosphorylation are regulated, and whether such cross-pathway signaling occurs *in vivo* at endogenous levels of the various signaling components are not known.

In this report, we further explore these issues using both cell culture and *in vivo* methods. We conclude that phosphorylation of the *Drosophila* BMP R-Smad, Mad, by Baboon, encoded by the only Type I TGF-β/Activin family receptor, is direct and is an evolutionarily conserved signaling event. Furthermore, we find that competition between R-Smads has a profound influence on Baboon-to-Mad phosphorylation activity and that R-Smad pathway switching can be promoted by loss of dSmad2.

Results

Activation of Baboon by mutation or by ligand stimulation leads to phosphorylation of both Mad and dSmad2

In order to define the molecular nature of cross-talk, we employed a cell-based signaling assay that we have used to study other aspects of TGF-β signaling [11]. Expression of a constitutively active form of Baboon (Babo*) in *Drosophila* S2 cells resulted in phosphorylation of both the Activin and BMP R-Smads, dSmad2 and Mad (Figure 1A). To ensure that this phosphorylation of Mad is a property of the Baboon receptor itself and is not due to an artifact of the activating mutation in Babo*, we exposed S2 cells to the Activin-like ligand Dawdle (Daw), which signals through Baboon [12]. These cells, which express only endogenous Baboon, also responded to Daw by robustly phosphorylating both dSmad2 and Mad (Figure 1A). These results demonstrate that an Activin ligand can stimulate the BMP pathway in *Drosophila* S2 cells.

Mad phosphorylation by Baboon is independent of BMP Type I receptors

As described above, a key mechanistic question is whether Baboon can directly phosphorylate Mad or if the traditional BMP receptors are involved. We addressed this point by conducting the signaling assay in cells lacking specific TGF-β-family receptors due to experimental RNA interference (RNAi). Similar to data shown in Figure 1A, control cells whose receptors were not targeted by RNAi accumulated phosphorylated Mad in response to the BMP-type ligand Decapentaplegic (Dpp) or the Activin-type ligand Daw (Figure 1B). Reducing expression of Punt, the only Type II receptor expressed in S2 cells, by RNAi eliminated the response to both ligands (Figure 1B). Cells lacking Baboon due to RNAi depletion still phosphorylated Mad in response to Dpp, but not in response to Daw (Figure 1B). In contrast, cells with both BMP Type I receptors Saxophone and Thickveins knocked down by RNAi still phosphorylated Mad upon exposure to Daw, even though they had no response to Dpp (Figure 1B). The abolishment of one or both ligand responses in each condition demonstrates the effectiveness of the various RNAi treatments. Additionally, the

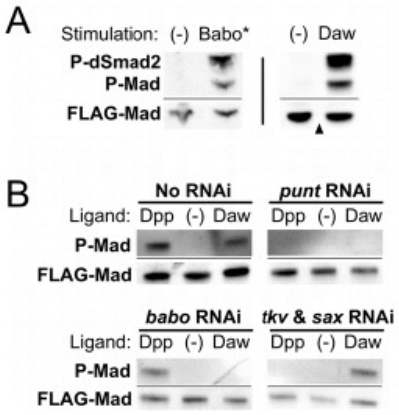

Figure 1. Stimulation of the Baboon receptor leads to phosphorylation of both R-Smads independently of BMP Type I receptors. S2 cells were transiently transfected with FLAG-tagged Smad expression constructs and analyzed by Western blot for C-terminal phosphorylation (P-dSmad2 and P-Mad). The FLAG-Mad band is shown as a loading control (FLAG-dSmad2 is not a useful loading control because of signaling-induced degradation as described later in the text). For all Western blot figures, a thin horizontal line indicates different infrared channels from the same blot. Co-expression of a constitutively active form of Baboon (Babo*) led to phosphorylation of dSmad2 and Mad (A, left blot). Exposure of cells expressing endogenous Baboon to the Dawdle ligand (Daw) had the same effect (A, right blot). RNAi treatment was used to determine receptor requirement for ligand activity (B). Controls confirmed that Dpp ligand treatment caused Mad phosphorylation independently of Baboon (B, left half). Dpp activity required the Punt Type II receptor and the Tkv and Sax BMP Type I receptors (B, right half). In contrast, Daw signaling to Mad required Baboon and Punt, but not Tkv and Sax.
doi:10.1371/journal.pone.0036548.g001

Saxophone and *Thickveins* RNAi treatments were validated for their ability to essentially eliminate expression of these proteins (see Figure S1). These results indicate that 1) BMP Type I receptors are neither necessary nor sufficient for Activin-induced phosphorylation of Mad in S2 cells, and 2) Baboon is the lone *Drosophila* Type I receptor that is necessary and sufficient for Activin-to-BMP cross-talk.

Cross-talk is a conserved property of TGF-β receptor intracellular domains

Recent work has uncovered functional differences among isoforms of the sole Activin receptor in *Drosophila*. The three isoforms have divergent extracellular domains and identical kinase domains, and only one isoform, $Babo_c$, is activated by the Daw ligand in S2 cells [12]. We wondered if the isoform differences might influence the ability to phosphorylate Mad, perhaps by directing different receptor complexes to form via extracellular interactions. We tested whether the other isoforms of Baboon, $Babo_a$ and $Babo_b$, were also able to stimulate cross-talk. When over-expressed in S2 cells, both of these isoforms displayed activity in the absence of exogenous ligand, and induced phosphorylation of both dSmad2 and Mad (Figure 2A). This result is consistent with studies suggesting that the kinase domain's L45 loop–a portion of the protein identical in Baboon isoforms–is primarily responsible for substrate recognition [13]. Extracellular differences among isoforms do not control cross-talk activity, supporting the

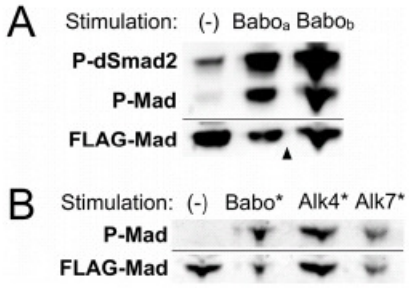

Figure 2. All isoforms of Baboon and mammalian Activin receptors can initiate cross-talk. (A) Overexpression of wildtype Babo$_a$ or Babo$_b$ in S2 cells led to phosphorylation of dSmad2 and Mad. In this experiment there was a detectable background level of P-dSmad2 well below the Babo-induced levels. Arrowhead indicates that the displayed image contains two portions of one blot. (B) Constitutively active versions of mammalian Activin receptors Alk4 and Alk7 (Alk4* and Alk7*), like Babo*, induce phosphorylation of *Drosophila* Mad in S2 cells.
doi:10.1371/journal.pone.0036548.g002

simplest model of direct interaction between Mad and the kinase domain of Baboon.

Many reports have demonstrated that members of the same TGF-β-family pathway are interchangeable across species. For example, expression of a human BMP ligand can rescue mutation of a *Drosophila* BMP ligand *in vivo* [14]. We were curious if trans-species cross-talk was also possible. We tested whether activated TGF-β/Activin Type I receptors from mammals could phosphorylate the *Drosophila* BMP R-Smad. When transfected into S2 cells, the constitutively active forms of mammalian Activin receptors Alk4 and Alk7, like Babo*, could induce phosphorylation of both dSmad2 and Mad (Figure 2B and not shown). This interaction highlights the strong evolutionary conservation of the described cross-talk phenomenon.

An *in vivo* Baboon gain-of-function phenotype is primarily mediated through Mad and not dSmad2

Given the demonstrated ability of Baboon to phosphorylate Mad and dSmad2 in cell culture, we looked for evidence that Baboon can signal through Mad *in vivo*. Previous studies have shown that moderate expression of Babo* in developing wings can generate enlarged but normally patterned wings [15]. We found that Babo* expression in the imaginal wing using the *tg*-GAL4 driver led to visible adult wing defects (Figure 3B, C). To determine whether activation of Mad or dSmad2 caused the phenotype, we used RNAi to remove one R-Smad at a time in wings expressing Babo*. *tg*-GAL4 driving *mad* RNAi alone produced a small, flat wing with missing veins (Figure 3E), whereas the effect of *dSmad2* RNAi knockdown alone was a moderately blistered wing (Figure 3F). When *mad* was removed in the presence of Babo*, the blistered and crumpled Babo* wing phenotype was suppressed (Figure 3H), and the resulting wings resembled those expressing *mad* RNAi alone. In contrast, removal of *dSmad2* by RNAi did not suppress the wrinkling phenotype induced by Babo*; in fact, the phenotype became more severe. The *dSmad2* RNAi, Babo* wings were more wrinkled and shrunken than wings where either construct was expressed alone (Figure 3I), suggesting that in the absence of dSmad2 more Mad is phosphorylated, perhaps because of less competition between dSmad2 and Mad for Baboon binding.

In support of this concept, we found that over-expression of dSmad2 suppressed the blistered wing phenotype of Babo* (Figure 3G), whereas dSmad2 over-expression alone did not affect wing size or vein formation (Figure 3D). This result rules out a general influence of dSmad2 on Mad activity and instead indicates that dSmad2 dosage specifically modifies the substrate choice of Baboon.

dSmad2 directly influences Baboon's phosphorylation of Mad

Competition between dSmad2 and Mad for interaction with Baboon is a straightforward model. We carried out additional tests in cell culture and *in vivo* to confirm that the dSmad2 protein concentration affects Mad activation. As one test of the model of competitive binding between R-Smads, we manipulated levels of dSmad2, Baboon's hypothetically preferred substrate, in the S2 cell signaling assay.

As noted above, Babo* expression or prolonged Daw stimulation led to phosphorylation of Mad in S2 cells. Steady-state levels of P-Mad or P-dSmad2 after prolonged Babo* expression were similar whether Mad or dSmad2 were expressed individually or together (data not shown). As a more sensitive assay, we performed time-course experiments using Daw ligand to observe the initial kinetics of substrate phosphorylation. When Flag-dSmad2 was overexpressed, P-dSmad2 accumulated steadily over a several hour exposure to Daw (Figure 4A, right lanes). Endogenous P-dSmad2 was also detected upon Daw treatment, but the accumulation was not linear. The rate of P-Mad accumulation varied with the expression level of dSmad2. When Flag-Mad was the only over-expressed substrate, P-Mad was detected after 1 hour and continued to rise during 3 hours of ligand exposure (Figure 4A, middle lanes). This accumulation was modestly enhanced when endogenous dSmad2 was eliminated by RNAi (Figure 4A, left lanes). In the other direction, over-expression of Flag-dSmad2 suppressed the accumulation of P-Mad such that it was not detectable above background after 3 hours of Daw exposure (Figure 4A, right lanes). Quantified P-Mad signals are plotted in Figure 4A. This result implicates dSmad2 protein in controlling the rate of Mad phosphorylation by Baboon in S2 cells.

We considered several possibilities for how this might occur. First, in vertebrate systems, the Activin/TGF-β R-Smads are assisted in their presentation to a receptor by SARA (Smad Anchor for Receptor Activation) [16], an endosome-associated protein that potentially could provide a competitive edge to dSmad2 over Mad for phosphorylation by Baboon. However, RNAi knockdown of SARA in S2 cells had no affect on the dSmad2/Mad phosphorylation ratio (see Figure S2A), suggesting that differential presentation of dSmad2 to Baboon by SARA is not a likely mechanism for substrate choice. Another possibility is that molecular motors contribute to substrate preference by discriminately presenting one Smad to the receptor. In *Xenopus*, one report suggests that efficient Smad2 phosphorylation requires kinesin motors, presumably to help traffic Smad2 to the receptor [17]. We treated cells with colcemid to depolymerize microtubules and block potential transport mechanisms, but we did not observe a change in the relative phosphorylation of dSmad2 and Mad (see Figure S2B).

Since we found no evidence for differential presentation to receptors, we decided to test more directly the direct-binding/competition model by altering the receptor interaction interface of dSmad2 to make it more similar to Mad. We reasoned that if there was direct competition between these two R-Smads for binding to Baboon, then Baboon would phosphorylate both substrates at similar rates if they had similar interaction interfaces. Previous

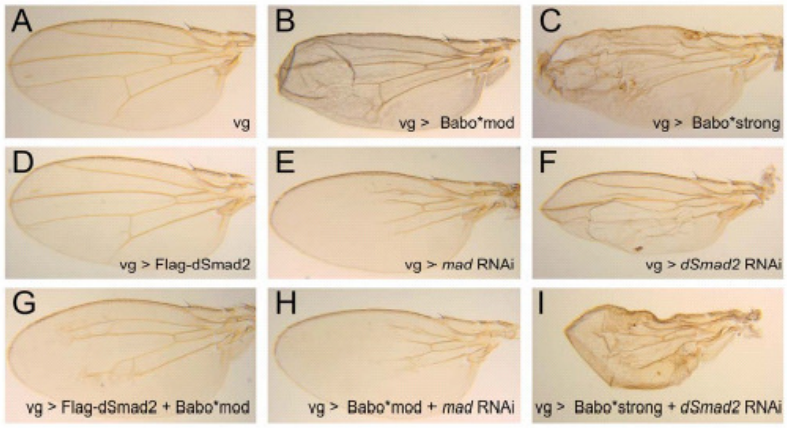

Figure 3. Excessive Baboon signaling perturbs wing development in a Mad-dependent manner. *vestigial*-GAL4 (*vg*) was used to express combinations of Baboon, dSmad2, and RNAi for *mad* and *dSmad2*. Normal wing development (A; one copy of *vg*-GAL4) was disrupted by Babo* expression (B, C; Babo*mod and Babo*strong are UAS insertions with varying activity as characterized in other assays). The Babo* phenotype was abrogated by simultaneous *mad* RNAi (H) and resembled *mad* RNAi alone (E). In contrast, the crumpling defect of Babo* wings was enhanced in conjunction with *dSmad2* RNAi (I) and was more severe than *dSmad2* RNAi alone (F). Overexpression of FLAG-dSmad2 did not affect wing formation (D), but partially rescued the Babo* overexpression phenotype, producing normal sized flat wings with residual peripheral vein defects (G). For each genotype, a representative wing is shown out of 4–7 wings photographed. Within a genotype there was only slight variation in appearance, except that 3/6 dSmad2 RNAi wings had vein defects and a blister (shown) and 3/6 had vein defects without a blister (not shown).
doi:10.1371/journal.pone.0036548.g003

studies comparing vertebrate TGF-β/Activin Smad2/3 and BMP Smad1/5/8 identified two residues in the L3 loop of the MH2 domain as key for targeting different Smads to the L45 loop of either TGF-β/Activin or BMP receptors [18]. We changed the R446 and T449 residues of dSmad2 to H and D, respectively, to give dSmad2 a Mad-like L3 loop. We also made a variant of dSmad2 that harbors the E300K substitution in the MH2 domain found in the $dSmad2^{MH388}$ allele [19].

We compared the relative phosphorylation levels of wildtype (WT) and mutant forms of dSmad2 versus Mad in response to Baboon. In the experiment shown in Figure 4B, the steady-state P-dSmad2(WT) signal was greater than the P-Mad signal, and the E300K and HD variants had reduced P-dSmad2. Importantly, the P-Mad signal increased as the P-dSmad2 signal decreased, which is consistent with the substrate competition model. This behavior was confirmed in a Daw time-course experiment for dSmad2(WT) and dSmad2(HD). During the first hours of signaling, phosphorylation of the HD variant was dramatically reduced compared to WT. P-Mad accumulation, modest over this time range when forced to compete with dSmad2(WT), was enhanced when pitted against the less effective dSmad2(HD) protein (Figure 4B).

dSmad2 restricts Baboon-Mad cross-talk activity *in vivo*

These signaling assays in S2 cells demonstrate that the Baboon kinase can use Mad as a substrate and that dSmad2 levels modulate the phosphorylation of Mad by Baboon. We next sought to determine if these two phenomena occur *in vivo*. We chose the wing disc as a platform to manipulate Baboon because the normal P-Mad pattern is well characterized and, as described below, seems to be independent of canonical dSmad2-Baboon signaling. Wing discs from third-instar larvae have a well-defined pattern of P-Mad that critically depends on the Dpp ligand and the BMP Type I and Type II receptors Tkv and Punt, respectively. *baboon* is expressed in the wing disc, but *baboon* mutants display a normal P-Mad pattern ([15] and Figure 4E). Similarly, *dSmad2* is expressed in discs, but removal of dSmad2 in the wing pouch by RNAi did not significantly alter the P-Mad pattern (Figure 4D, compare to 4C). The lack of an aberrant P-Mad pattern after reduction of either Baboon or dSmad2 is consistent with a lack of appreciable cross-talk activity in the larval wing disc at this developmental time under endogenous conditions.

Against this backdrop, we manipulated Baboon signaling in wing discs and used P-Mad staining patterns as an indicator of activity. When expressed in the L3 wing disc blade using a *tg*-GAL4 driver, constitutively active Babo* altered the P-Mad pattern. Curiously, the P-Mad signal was reduced in the wing blade, disrupting the normal gradient pattern (Figure 4F). This resembled a loss-of-function condition for Thickveins (compare to Figure 4I) that is likely caused by titration of Punt away from BMP signaling complexes. Indeed, when Punt was co-expressed with Babo*, P-Mad was detected throughout the *tg*-GAL4 pouch region (Figure 4H). The Punt expression line used for this experiment did not induce ectopic P-Mad in the wing pouch by itself (not shown). It is likely that Babo*-Punt complexes are active towards dSmad2, but we could not directly verify this because no P-dSmad2 immunohistochemistry (IHC) detection assay is available. However, we were able to show that dSmad2 impacts the output of Babo* by simultaneously expressing Babo* and knocking down endogenous *dSmad2*. This combination produced strong ectopic P-Mad throughout the *tg*-Gal4 expression domain (Figure 4G). Once again, we interpret these data as reflecting a competition between dSmad2 and Mad proteins for binding to and activation by Baboon. Reinforcing the result seen in S2 cells, this *in vivo* scenario implicates dSmad2 as the preferred substrate for Baboon since endogenous dSmad2 protein can prevent over-expressed Baboon from phosphorylating Mad.

We also tested if Babo* phosphorylation of Mad can occur independently of the relevant BMP Type I receptor in the wing disc. Simultaneous Babo* expression and *dSmad2* RNAi led to ectopic P-Mad even with effective knockdown of *tkv* (Figure 4K).

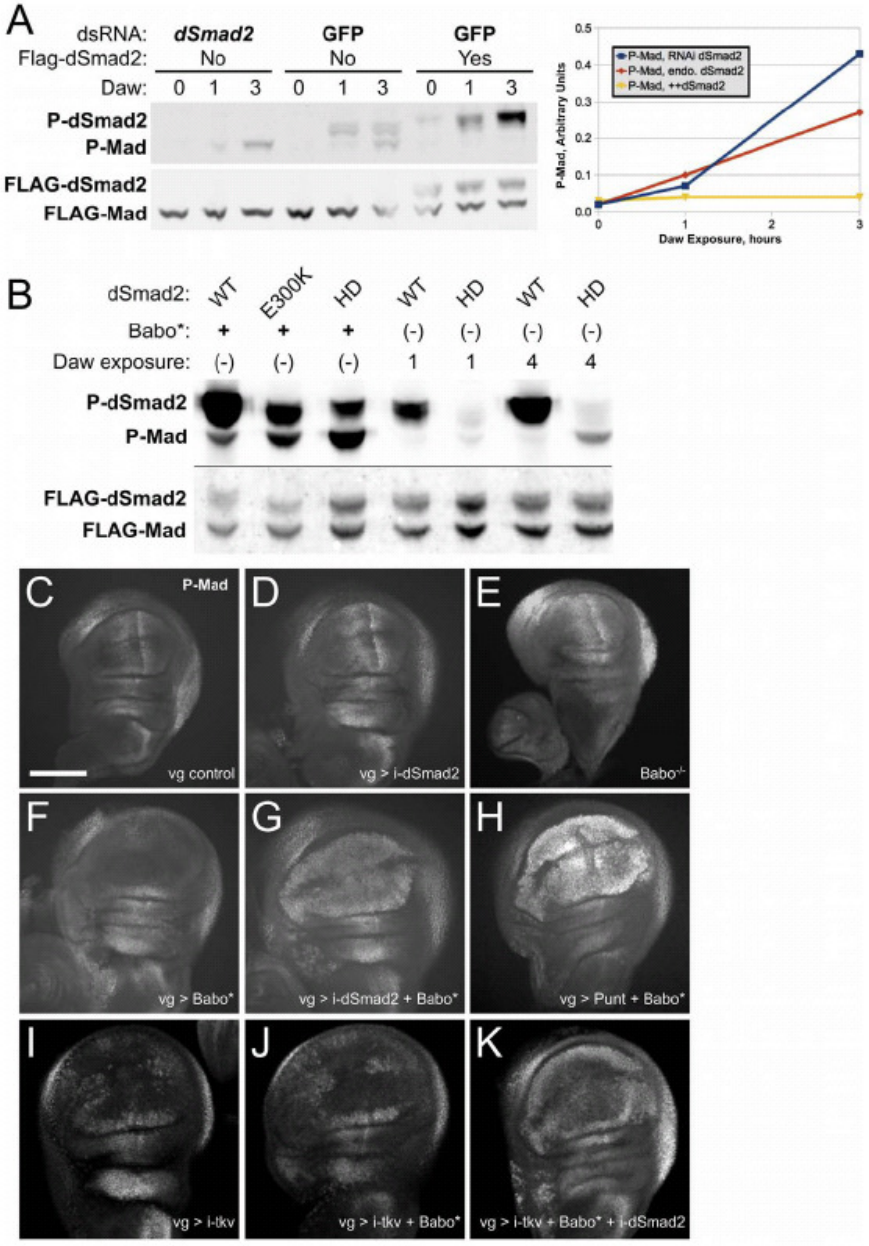

Figure 4. Baboon phosphorylation of Mad is inhibited by dSmad2. (A) Phospho-Smad accumulation upon exposure to Daw ligand. S2 cells transfected with Flag-Mad were treated with dsRNA for *dSmad2* or GFP, and transfected with Flag-dSmad2 as indicated. Phospho-Smad and Flag signals were assayed on samples before Daw exposure and after 1 and 3 hours of incubation. Note that there is a gel artifact affecting the appearance of the Flag bands in several lanes. Quantified P-Mad band intensities are plotted to illustrate that accumulation of P-Mad depends on the level of dSmad2. The experiment was repeated with several batches of reporter cells, and the relative signals for the 3 hour time point were always observed in the same order. The 1 hour time points were near background detection and are less reliable due to noise. (B) Mutated dSmad2 proteins with varying phosphorylation efficiency modulate the rate of P-Mad accumulation. Babo* stimulation revealed the steady-state levels of P-dSmad2 and P-Mad. Daw exposure for 1 or 4 hours showed the difference in response to short-term signaling between the WT and HD forms of dSmad2. In both conditions, P-Mad levels were inversely correlated to P-dSmad2 levels. (C–K) Wing imaginal discs from third instar larvae were stained to detect P-Mad

and imaged by confocal microscopy. For each condition at least three discs were imaged, and a representative Maximal Intensity Projection encompassing the wing blade is shown (6 sections @ 3 micron interval for C,D,F–H; all sections @ 3 micron interval for E; 5 sections @ 2 micron interval for I–K). Anterior is to the left and the scale bar shown in panel C applies to C–K. The normal P-Mad staining pattern is shown for *vg*-GAL4 alone (C; scale bar = 100 microns). Expression of a UAS-*dSmad2* RNAi construct did not alter the P-Mad pattern or the shape of the wing disc (D). Wing discs from $babo^{f04/f04}$ homozygotes showed nearly normal pMad gradient (E). Expression of Babo* altered P-Mad staining, obliterating the normal gradient in the pouch (F). Note the normal P-Mad staining outside of the pouch where *vg*-Gal4 is not expressed. Babo* and *dSmad2* RNAi together generated ectopic P-Mad in the entire wing pouch (G). Providing Babo* with additional Punt also produced ectopic P-Mad (H). *tkv* RNAi prevented P-Mad accumulation in the middle of the wing pouch (I), and addition of Babo* did not counteract this P-Mad pattern (J). Additional knockdown of *dSmad2* led to ectopic P-Mad (K), which paralleled the results without *tkv* RNAi. Data in panels C, D, F, and G were from the same experiment and were stained in parallel. Panel H is from a different experiment, but the pouch signals can be compared to the others because the endogenous P-Mad along the posterior margin has similar staining. Samples in panels I–K were stained and processed in parallel.
doi:10.1371/journal.pone.0036548.g004

In concordance with our cell culture studies, this result indicates direct Baboon to Mad cross-talk *in vivo*.

Dosage effects at endogenous levels: P-Mad levels increase in some tissues of dSmad2 protein-null animals

Given the observation that the presence of dSmad2 in the wing disc profoundly alters the activity of exogenous Babo*, we asked if a similar effect is observed with endogenous levels of TGF-β signaling components. To do this, we required a protein-null condition to preclude competition between Mad and dSmad2 binding to Baboon. The only available dSmad2 mutant allele, $dSmad2^{MB388}$, harbors a mis-sense mutation near the beginning of the MH2 domain. This mutation does not prevent interaction with Baboon, as the corresponding E300K protein was robustly phosphorylated in S2 cells by Babo* (Figure 4B). To generate a protein null allele, we excised P(G0348), a *white*-marked *P* element located approximately 400 nt downstream of the *dSmad2* transcriptional start, and screened for $white^{-}$ lethal progeny (see Materials and Methods). Among several candidates, one allele, $dSmad2^{F4}$, was a deletion of the entire coding sequence (Figure 5A). We next surveyed P-Mad levels by IHC in various tissues derived from *dSmad2* mutant larvae. We observed that many, but not all, tissues displayed greater P-Mad staining in the *dSmad2* mutant compared to control animals reared under the same conditions. For example, nuclear P-Mad in the fat body was weakly detected in control animals, but markedly elevated in $dSmad2^{F4}$ mutants (Figure 5B1 vs FB2). A similar increase was seen at various positions along the gut tract: P-Mad staining was elevated in the gastric caeca, the midgut/hindgut junction, and Malpighian tubules compared to equivalently stained control larvae (examples in Figure 5C and 5D, and summary in Figure S3).

We next tested the influence of the Baboon receptor on P-Mad levels in the fat body and gut. In contrast to *dSmad2* mutants, *baboon* mutant animals had normal P-Mad staining (Figure 5B3, 5C4 and 5D4). The low level of nuclear P-Mad seen in wildtype and *baboon*-mutant gut tissue is presumably due to canonical BMP-family signaling through Thickveins and Saxophone receptors. We next performed an epistasis test in which we assayed P-Mad levels in a *dSmad2*; *babo* double mutant. We reasoned that if the ectopic P-Mad in a dSmad2 protein-null mutant is due to enhanced phosphorylation of Mad by Baboon, then it should be suppressed in the double mutant. We observed this result in all tissues examined (Figure 5B4, 5C5 and 5D5, and Figure S3). Thus, Baboon function is required to produce the elevated P-Mad levels observed in dSmad2 deficient tissues. To explain this phenomenon we conclude simply that Baboon activity is directed towards Mad when dSmad2 is not present *in vivo*.

Baboon activation causes bulk degradation of dSmad2

During our experiments in S2 cells, we observed that over-expression of activated Baboon significantly lowered the level of co-over-expressed dSmad2 protein. In these experiments S2 cells were transfected with actin promoter expression constructs and were assayed several days later. Thus the dSmad2 protein level detected by Western blot represents the steady-state level, which reflects the production and degradation rates. Protein production rates should be constant in this system, so changes in the steady-state level of dSmad2 can be interpreted as changes in the degradation rate. By this measure, the degradation rate of dSmad2 increased about 5- to10-fold when Babo* was present (Figure 6A).

We next tested this behavior in several *in vivo* situations to determine the generality of the bulk degradation of dSmad2 upon Baboon activation. Western blot detection of dSmad2 from embryo extracts showed that co-expression of Babo* lowered the dSmad2 level about 5-fold, compared to dSmad2 expression alone (Figure 6B). A similar reduction of exogenously expressed dSmad2 was seen in the wing blade upon expression of Babo* (compare Figure 6D to 6C). These results confirm that Baboon stimulation lowers dSmad2 stability *in vivo*. Below we consider how such degradation could alter the output of Baboon signaling in the context of cross-talk.

Discussion

Comparison with cross-pathway signaling in other systems

In this report we present experimental results showing that the Baboon receptor can directly phosphorylate Mad in cell culture and *in vivo*, and that this cross-talk activity is tightly controlled by the availability of dSmad2. These findings extend the initial report describing canonical signaling between Baboon and dSmad2 where dSmad2, but not Mad, was shown to be a substrate of Baboon in mammalian cells [15]. There are several possible reasons why Baboon-Mad activity is observed in *Drosophila* cells but was missed in the initial report. First, it is possible that Mad binding to Baboon may be too weak or transient to be detected by immunoprecipitation. Alternatively, endogenous Smad2/3 may have blocked the interaction in heterologous cell systems, or species-specific co-factors may facilitate Mad-Baboon binding.

The strong functional conservation of TGF-β superfamily proteins prompts a comparison of our results in *Drosophila* with studies describing cross-pathway signaling in mammalian systems. The limited number of pathway members and the efficacy of RNAi in *Drosophila* enabled us to distinguish between competing models presented for mammalian epithelial cells. With regard to the key mechanistic question of whether TGF-β Type I receptors can directly phosphorylate the BMP R-Smads, our observation of Mad phosphorylation in the absence of BMP Type I receptors (Figure 1) is inconsistent with the model of heteromeric TGF-β/BMP Type I receptor complexes proposed by Daly et al. [7], but is consistent with the model of direct phosphorylation of BMP R-Smads by TGF-β/Activin receptors proposed by Liu et al. [8]. It is possible that both types of mechanisms exist, but are differentially utilized depending on the ligands and receptors present in the

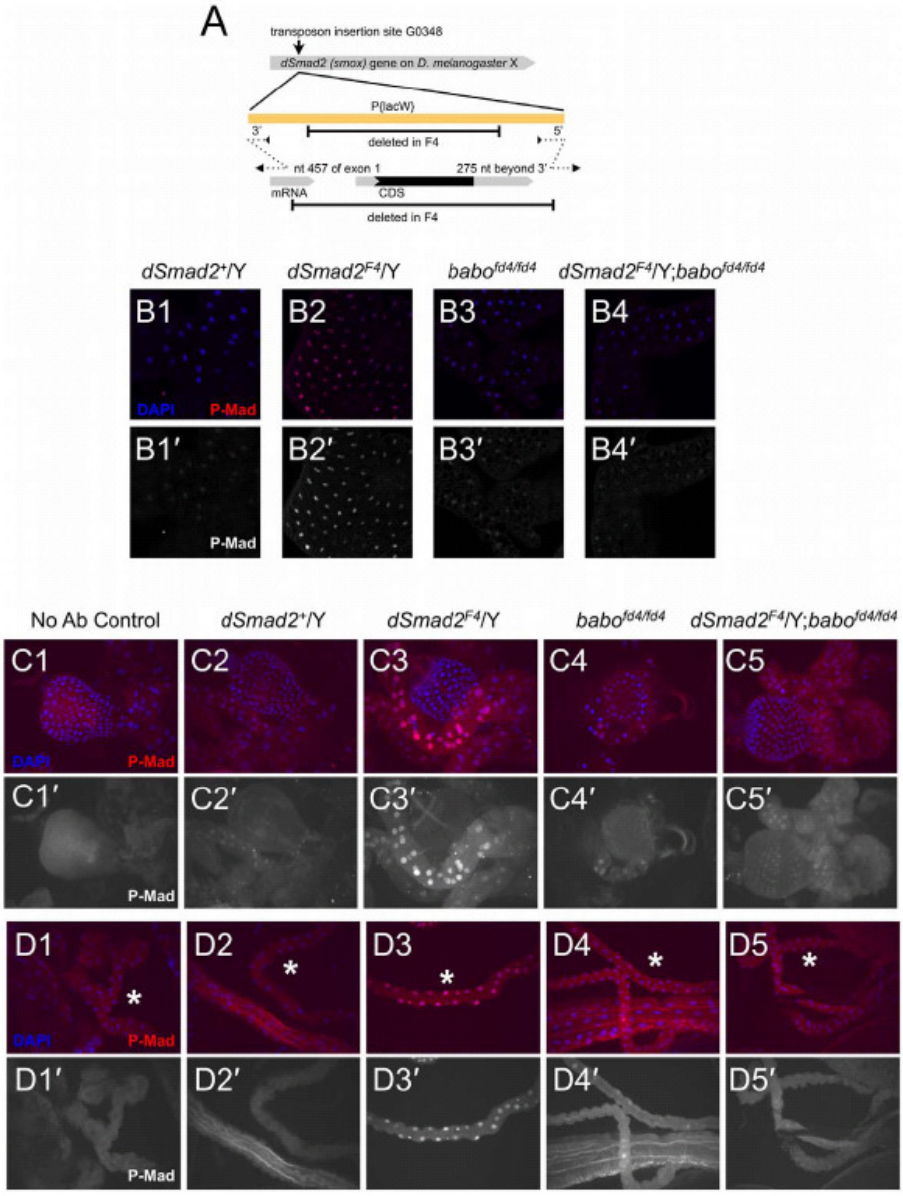

Figure 5. P-Mad elevation in *dSmad2* null mutant tissues depends on *baboon*. The schematic depicts the location of the l(X)G0348 *P* element insertion in relation to the *dSmad2* locus (A). The F4 excision product removed the entire coding region of *dSmad2* and portions of the *P*-element. The genomic breakpoints are indicated above the *dSmad2* mRNA; they were determined by sequencing PCR products, indicated by dotted lines. (B–D) P-Mad was detected by IHC of fixed larval tissues from several genotypes. For each image, a merged DAPI (blue) and P-Mad (red) panel is displayed above the isolated P-Mad channel. (B) Single confocal sections of P-Mad staining in the fat body. Under the staining conditions employed, endogenous nuclear P-Mad in a control fat body was barely detected (B1), but was increased in a *dSmad2* null mutant animal (B2). *Baboon* single mutants and *dSmad2*; *baboon* double mutants had normal P-Mad staining (B3,4). (C, D) P-Mad staining at two representative positions along the digestive tract. Images are Maximal Intensity Projections of 3 micron interval confocal sections through the entire sample. The P-Mad primary antibody was omitted from "No Ab Control" samples to convey any background staining and auto-fluorescence in the red channel. (C) In the gastric caeca near the proventriculus, *dSmad2* mutants showed elevated P-Mad (C3) compared to wildtype control males (C2). *baboon* single mutants and *dSmad2*; *baboon* double mutants showed wildtype levels (C4 and C5). Distal Malpighian tubule staining (lumpy tubes marked with asterisks) showed the same pattern, with the *dSmad2* mutant displaying the strongest P-Mad staining (D3 compared to D2, D4 and D5).
doi:10.1371/journal.pone.0036548.g005

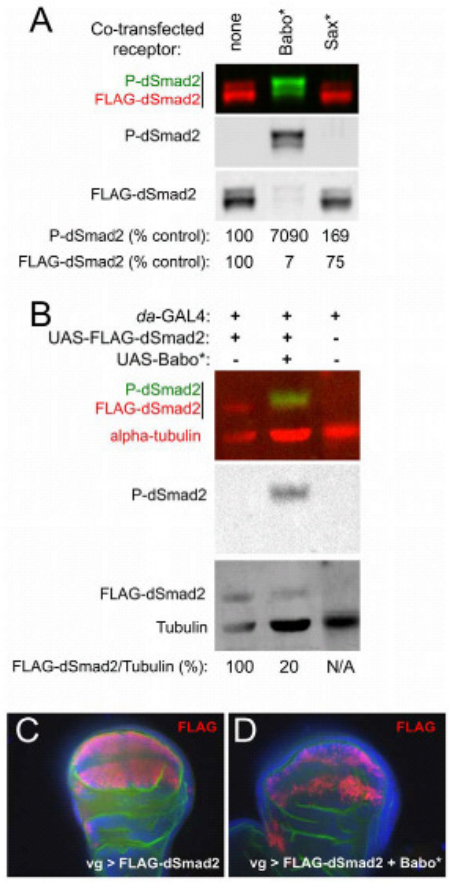

Figure 6. Hyperactive Baboon signaling leads to dSmad2 destabilization. The steady-state level of transfected dSmad2 in S2 cells was significantly reduced when Babo* was co-expressed (A). Quantified band intensities are displayed as a percentage of the control for each channel. Note that the P-dSmad2 level was greatly increased but the total dSmad2 level was reduced in the presence of Babo*, causing a greater than 1000-fold increase in the ratio of P-dSmad2 to total Flag-dSmad2. This effect was specific to Babo*, as inclusion of activated Saxophone (Sax*) neither stimulated P-dSmad2 nor significantly decreased the FLAG-dSmad2 signal (A, right lane). FLAG-dSmad2 was expressed in embryos using the *da*-GAL4 driver, either alone or with Babo* (B). Total exogenous dSmad2 and P-dSmad2 was detected by Western blot and the amount of FLAG-dSmad2 was normalized to endogenous alpha-tubulin. (C, D) *vg*-GAL4 was used to express Flag-dSmad2 alone (C) or with Babo* (D) in the wing disc. FLAG antibody IHC was used to gauge dSmad2 levels (red), and DAPI (blue) and aPKC IHC (green) are shown as counter-stains. Each image is a single confocal plane through the wing blade, and represents at least three discs stained per genotype.
doi:10.1371/journal.pone.0036548.g006

particular tissue being examined. Even in *Drosophila*, we note that direct action of Baboon on Mad does not preclude the possibility that mixed receptors form active signaling complexes in some situations. Mixed receptor complexes have been detected in *Drosophila* cell culture under over-expression conditions, but their functionality is unknown [20]. A similar point can be made regarding mixed Smad oligomers detected in mammalian epithelial cells by Daly et al. [7]. In our adult wing assay, we found that the Babo* phenotype depended primarily on Mad and that dSmad2 was not required. If the wing development defect was caused by the activity of a complex containing both P-Mad and P-dSmad2, then removal of either one should have blocked the Babo* phenotype. Again, this observation does not argue against the formation or activity of mixed R-Smads complexes in some contexts, but shows that productive signaling by cross-pathway phosphorylation can take place independently of such complexes.

One key observation in this report concerning the mechanism of cross-pathway signal regulation is that the degree to which it occurs, both in cell culture and *in vivo*, appears to be regulated by competition between the R-Smads, likely for receptor binding. Further work is required to determine how general this mechanism might be. Epithelial cell culture models showed that cross-talk is important for the TGF-β-induced migratory switch [8]. Our results in the larval wing disc and gut represent the first examples of cross-talk *in vivo*, and we expect that additional examples will be found in various animals and tissues. With regard to developmental studies, other systems should be evaluated to see if loss-of-function mutations of Smad2/3 orthologs lead to increased signaling through BMP R-Smads. Additionally, several human diseases have been attributed to mutations in TGF-β components [21]. A cautionary implication of our work is that mutations in the TGF-β branch may have unanticipated loss- or gain-of-function influences on the BMP branch.

Curiously, TGF-β/Activin Type I receptors appear to have gained or retained cross-phosphorylation activity throughout evolution, but BMP Type I receptors do not appear to have reciprocal activity. We have never seen phosphorylation of dSmad2 by activated *Drosophila* Type I BMP receptors (Figure 6A and data not shown), or in response to various ligands. Likewise, no phosphorylation of Smad2/3 by BMP receptors has been reported in vertebrate cells. Why is there this distinction? The growing number of complete genome sequences has allowed phylogenetic reconstruction of the evolution of TGF-β signaling [5]. Apparently all metazoans, even the simple placazoan [22], have a complex TGF-β network containing both TGF-β/Activin and BMP subfamilies. It is tempting to speculate that a single receptor with dual Smad targets could have played a transitional role in the expansion of the signaling network. The all-or-none nature of the TGF-β-superfamily network (both BMPs and TGF-β/Activins present, or none) in extant organisms, however, does not provide support for this idea. What it does support is the possibility that relationships between core pathway proteins stabilized hundreds of millions of years ago. If the dual-kinase activity of Baboon orthologs has been available to all metazoans during the radiation of animal forms, we would expect this activity to be deployed by different animals and different cell types in diverse ways. We are currently investigating several phenotypes that differ between *baboon* and *dSmad2* mutants to determine which depend on Babo-Mad cross-talk and which might depend on other forms of Smad-independent signaling [23].

Smad2 degradation as a signaling switch

The different responses of adult wings and larval imaginal tissue upon Baboon activation (Figures 3 and 4) illustrate that TGF-β pathway wiring and output can vary with developmental context. Given the relationship between Babo and dSmad2, the cross-talk activity can be viewed two ways. From one perspective, the response to loss of dSmad2 depends on the level of Baboon signaling: only cells with Baboon activity can produce P-Mad by cross-talk. From the other perspective, the response of wildtype

cells to Baboon stimulation depends on dSmad2 levels: efficient cross-talk will only occur in the absence of dSmad2.

Given the dominant control that dSmad2 exerts on the ability of Baboon to phosphorylate Mad, the simplest model is that output of TGF-β ligand stimulus in a given cell depends on the expression level of dSmad2 (Figure 7A). Although dSmad2 is widely expressed, as are Smad2/3 proteins in other animals, different subsets of cells might express different ratios of R-Smads that could influence the signaling output.

Our observation that Baboon activity can lower the overall level of dSmad2 protein offers an additional regulatory possibility, where the TGF-β/Activin signal itself can influence its response. In the substrate-switch model, a cell exposed to a prolonged Activin signal would eventually degrade enough of its dSmad2 pool to allow Baboon signaling through Mad (Figure 7B). It is not known which tissues, if any, require Baboon-to-Mad signaling in normal developmental contexts. We have observed that in some cases, dSmad2 over-expression leads to *mad* loss-of-function phenotypes, which could represent disruption of a sensor incorporating dSmad2 concentration as an input and Mad activity as an output (unpublished observations). Proteosomal degradation of activated Smad proteins is a well documented mechanism of signal attenuation [24], but the current observation of bulk degradation adds a new dimension because it can redirect receptor signaling. The mechanism of signal-dependent bulk dSmad2 degradation is unknown, and preliminary experiments do not

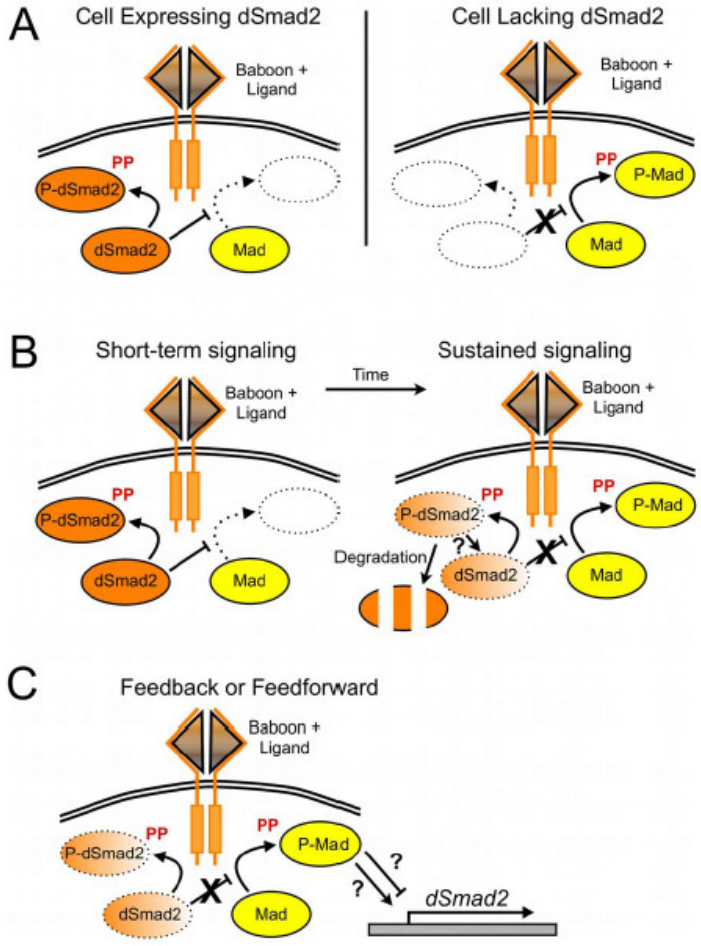

Figure 7. Models of signaling outputs generated by dual kinase activity of the Baboon receptor. Given the potential of Baboon to phosphorylate and activate dSmad2 and Mad, we present several configurations of Baboon, dSmad2 and Mad interaction that would generate different signaling outputs. In each schematic, only the most relevant pathway components are drawn. The first model represents a logic gate, where the ability of Baboon to phosphorylate Mad is strictly controlled by the expression of dSmad2 in that cell (A). Another model incorporates the observed degradation of dSmad2 in response to Baboon signaling (B). The final model (C) incorporates feed-back or feed-forward of Mad activity through *dSmad2* regulation. If P-Mad positively regulated *dSmad2* this would prevent the complete loss of dSmad2. Conversely, if P-Mad negatively regulated *dSmad2* expression, this would enforce the switch from Baboon signaling through dSmad2 towards Mad.
doi:10.1371/journal.pone.0036548.g007

support a simple ubiquitylation-proteosomal pathway (unpublished observations). Regardless of the molecular details, the observed reduction of total dSmad2 available for receptor competition is the key parameter in our competition model. Since activated R-Smad proteins can also be dephosphorylated to rejoin the pool of would-be substrates, the relative rates of recycling and bulk degradation would be predicted to influence the substrate switch to Mad.

What could be gained by the substrate switch? A general answer is that multiple interactions permit diverse regulatory schemes. For example, cross-talk would permit Mad signaling in a cell that is not exposed to BMP ligands or is otherwise not competent to transduce such signals. Other modes of signal integration are intriguing, such as the conditional formation of mixed R-Smad complexes observed by Daly et al. [7]. Another type of regulatory link that could contribute to the evolutionary maintenance of an integrated dSmad2-Babo-Mad triad is depicted in Figure 7C. If *dSmad2* transcription were a target for P-Mad, this would affect the substrate switch. In once case, Baboon signaling to Mad would be triggered by dSmad2 depletion and serve to up-regulate Smad2 to return balance to the system. On the other hand, if dSmad2 were down-regulated by P-Mad, this would stabilize the switch to the Baboon-Mad interaction. Additional studies are required to explore these intriguing possibilities.

Materials and Methods

Signaling assays in S2 cells

The S2 signaling assay has been described [12]. Briefly, conditioned media was collected from cells that expressed a construct encoding Dawdle. This media was mixed 1:1 with cells that had been transfected with a combination of Smads [11] and resuspended in their own media. Conditioned media from cells that were mock transfected was used as a negative control; recombinant Dpp (R&D Systems) was added to conditioned media at a final concentration of 20 nM for BMP stimulation. Mutated forms of dSmad2 (E300K and HD = R446H+T449D) were generated by site-directed mutagenesis and the changes were verified by sequencing. Constructs encoding different isoforms of Baboon are described by Jensen et al. [12]. Expression vectors for Babo* and Sax* are described by Gesualdi and Haerry [10]. Mammalian Alk4* and Alk7* [25,26] were cloned into the pAcPA vector for S2 cell expression.

RNAi treatment of S2 cells was as described [12], except that for Figure 4A dsRNA was added only once after transfection. Primers used to make PCR products for T7 transcription templates against *tkv*, *sax*, and *punt* are described by Shimmi and O'Connor [27] and GFP dsRNA was used as a negative control [28]. Additional primers for RNAi are as follows:

dSmad2 forward–TAATACGACTCACTATAGGGAGAGGGCAAGTGGTCAGAGAA;

dSmad2 reverse–TAATACGACTCACTATAGGGATGCCCACACTAAGCACACTC;

babo forward–TAATACGACTCACTATAGGGACCTGCGCTCCGGCTAATCTTCC;

babo reverse–TAATACGACTCACTATAGGGACGGATGATAGCCACAAACTCCC;

dSARA forward–TAATACGACTCACTATAGGGGTATCGTCCTCCGAATCGCTGAC;

dSARA reverse–TAATACGACTCACTATAGGGGATTTAGGGTTTGTGGTCGCTGGGG.

Cells for microtubule disruption tests were exposed to a final concentration of 2 µg/mL colcemid in their own media for 2 hours prior to signaling assays. Control samples were treated similarly, but without drug pre-treatment. After the signaling assay, cells were pelleted, resuspended in 1× sample buffer, and boiled. Samples were resolved on NuPAGE 4–12% Bis-Tris gels (Invitrogen) and transferred to PVDF or nitrocellulose (Figure 4A only) membrane after electrophoresis. Membranes were probed with primary antibodies against C-terminally phosphorylated Mad (1:1000, gift from E. Leof), phosphorylated dSmad2 (1:1000, Cell Signaling #3108), the FLAG epitope (1:2000, Sigma (M2)), or Saxophone (1:1000, Fabgennix). Membranes were exposed to secondary antibodies (Rockland (IRDye)) and imaged on the Odyssey Infrared Imaging system. To obtain fold change of degradation rates of FLAG-dSmad2 under steady-state conditions, we quantified the bands and calculated the ratio of unstimulated to Babo*-stimulated FLAG-dSmad2. This simple formula applies if production is constant and degradation is assumed to be a first order reaction.

Fly lines

The *tg*-GAL4 driver (Bloomington stock #8229) was used to drive expression of several UAS constructs in the developing wing, and *da*-GAL4 (Bloomington stock #5460) was used to drive expression in the embryo. UAS-Babo* lines have been reported previously [15], as has the UAS-FLAG-dSmad2 overexpression line [29]. $dSmad2^{MB388}$ and $babo^{\Delta 4}$ are described in Zheng et al. [19]. UAS-punt is described in Marqués et al. [30].

New RNAi lines were made using the pUAST-R57 vector (National Institute of Genetics, Japan) and included gene-specific sequences spanning bases 1264–1700 of the *mad* transcript (U10328; insertion line 6C3), 1469–1928 of the *dSmad2* transcript (AF101386; insertion line 25A3 or 3B3), and 926–1461 of the *tkv* transcript (NM_175975; recombinant line 38D2, 1A2). *P*-element-mediated insertions were made and mapped using standard techniques.

Larval IHC and tissue handling

Tissues from wandering third-instar larvae were fixed in 3.7% formaldehyde in PBS for 25 minutes, washed in PBS-Triton (0.1%), treated with primary antibody overnight at 4°C, exposed to secondary antibodies (Alexa Fluor 488 or 568; 1:200) at room temperature for two hours, and counterstained with DAPI. The P-Mad antibody (gift from E. Leof) was affinity purified against a peptide corresponding to the di-phosphorylated C-terminus of Mad. M2 monoclonal antibody (Sigma) was used to detect FLAG-tagged proteins. Anti-PKCζ (rabbit polyclonal, Santa Cruz) was used to visualize cell membranes for Figure 6. Confocal images were collected using a Zeiss Axiovert microscope with a CARV attachment, or with a Zeiss LSM710. The images in Figure 4C–H and 6C,D were collected using a 20×/0.75NA objective (CARV). The images in Figure 5C,D were collected using a 10×/0.45NA objective (CARV). The images in Figure 4I–K and Figure 5B were collected using a 20×/0.80 NA objective (LSM). Where indicated in Figure Legends, Maximum Intensity Projections were generated using Axiovision (CARV images) or ImageJ (LSM images) software.

Wings from adult females were dissected in ethanol and mounted in 1:1 Canada balsam:wintergreen oil under a coverslip for light microscopy using a 4×/0.16NA objective. All flies for wing and wing disc studies were reared on standard cornmeal medium at 25°C. Larvae for whole-animal P-Mad IHC were grown on yeast paste agar plates, and mutant animals were identified by the absence of GFP balancers. Embryo extracts were

made by boiling dechorionated 6–20 hour old embryos in 2× reducing sample buffer, and the soluble fraction was used for Western blot analysis.

Generation of a null *dSmad2* mutant

A new *dSmad2* allele was generated by imprecise excision of a *P* element from stock l(X)G0348 (Flybase allele $smax^{G0348}$), which is located in the *dSmad2* 5′ UTR. *P*-element males carrying a duplication (Tp1;2 sn+ 72d) to provide viability were outcrossed, and male progeny lacking the visible eye color marker were recovered and tested for lethality. Lethal chromosomes were analyzed by PCR and sequencing to map the extent of deletion. The $dSmad2^{F4}$ deletion removed a portion of the 5′ UTR (break point at nucleotide 457 of sequence AF101386) and the entire coding region. The 3′ breakpoint was found to be 275 bp downstream of the *dSmad2* transcript and the deletion does not disrupt the neighboring gene. Several segments of the original *P* element were left behind (see Figure 5A). Hemizygous $dSmad2^{F4}$ males died as larvae or pupae. The $dSmad2^{F4}$ allele was fully rescued to viability and fertility by one copy of a small duplication covering *dSmad2* (either Dp(1;3)DC185 or Dp(1;3)DC186). An independent excision allele was generated in parallel from a *yellow*-marked *P*-element insertion (Flybase allele $smax^{GG01120}$), using a slightly different strategy (details available upon request to LAR). The $dSmad2^{C15}$ allele from this screen was found to be an internal deletion of the transposable element. Like $dSmad2^{F4}$, hemizygous $dSmad2^{C15}$ males died as larvae or pupae and were fully rescued by duplications overlapping *dSmad2*. We chose the *F4* allele for our mutant analysis because it is an unambiguous protein null.

Supporting Information

Figure S1 Efficient knockdown of *sax* and *tkv* in S2 cells. (A) Cells were transfected with a Sax over-expression (O/E) construct with or without *sax* RNAi treatment. Western blotting for Sax showed that the RNAi treatment rendered Sax undetectable. (B) A similar test for Tkv showed approximately 98% reduction of overexpressed Tkv-FLAG upon RNAi as detected by FLAG Western blot. In both panels, the loading control is a FLAG cross-reactive band from the same gel lanes. Note that endogenous Sax and Tkv are not detected under these conditions.
(TIF)

Figure S2 Relative phosphorylation of dSmad2 and Mad are unaffected by knockdown of *SARA* or disruption of microtubules. (A) Smad phosphorylation upon Daw treatment in S2 cells without or with *dSARA* RNAi. As judged by the FLAG bands (red in merged image, and isolated in bottom slat), the RNAi samples had less Smad per lane, but the relative P-dSmad2 versus P-Mad ratios were similar between control and *dSARA* RNAi samples. (B) Colcemid treatment did not affect the preferential activation of dSmad2 by Baboon. In this particular experiment pMad stimulation by Daw was weak, but P-Mad was not increased in cells pre-treated with colcemid to depolymerize microtubules. This is in contrast to the increase in P-Mad caused by knockdown of dSmad2. Together these suggests that dSmad2 delivery to Baboon is not compromised upon microtubule disruption. In both panels, rDpp was included as a control for the ability of the cells to produce P-Mad.
(TIF)

Figure S3 P-Mad elevation in *dSmad2* mutants requires *baboon*, and occurs in tissues that express a *dSmad2* reporter. (A) A chart summarizing P-Mad IHC staining results in a panel of larval tissues. At least six animals were examined for control and *dSmad2* mutants, and three animals were examined for *babo* and *dSmad2*; *babo* mutants. Some gut sections were lost during staining; n.d. indicates that the tissue was not photographed for that genotype. (B) LacZ staining in G0348 heterozygous female larvae was used as a proxy for *dSmad2* expression because the *P*-element insertion into the *dSmad2* 5′ UTR contains a LacZ reporter. Control animals are shown to indicate very low nuclear background staining. LacZ was readily detected in several alimentary tissues and in the fat body. Staining was weak in the salivary gland, which is a tissue where pMad does not increase in the *dSmad2* null mutant. Displayed images are Maximum Intensity Projections of confocal sections collected at 3 micron intervals, and were processed in parallel.
(TIF)

Acknowledgments

We thank Ed Leof, Caroline Hill & Liangjun Wang for reagents, the Bloomington Stock Center for several fly lines, Nzovu Ulenga for $dSmad2^{GG01120}$ excision screening, and Melissa Ritter for characterization of RNAi and mutant fly lines.

Author Contributions

Conceived and designed the experiments: AJP PAJ MBO. Performed the experiments: AJP PAJ MS. Analyzed the data: AJP PAJ MS MBO. Contributed reagents/materials/analysis tools: RS RW RH LAR. Wrote the paper: AJP PAJ MBO.

References

1. Shi Y, Massagué J (2003) Mechanisms of TGF-β signaling from cell membrane to the nucleus. Cell 113: 685–700.
2. Shimmi O, Umulis D, Othmer H, O'Connor MB (2005) Facilitated transport of a Dpp/Scw heterodimer by Sog/Tsg leads to robust patterning of the Drosophila blastoderm embryo. Cell 120: 873–886.
3. Sapkota G, Alarcón C, Spagnoli FM, Brivanlou AH, Massagué J (2007) Balancing BMP signaling through integrated inputs into the Smad1 linker. Mol Cell 25: 441–454.
4. Zhang YE (2009) Non-Smad pathways in TGF-β signaling. Cell Res 19: 128–139.
5. Huminiecki L, Goldovsky L, Freilich S, Moustakas A, Ouzounis C, et al. (2009) Emergence, development and diversification of the TGF-β signalling pathway within the animal kingdom. BMC Evol Biol 9: 28.
6. Goumans MJ, Valdimarsdottir G, Itoh S, Lebrin F, Larsson J, et al. (2003) Activin receptor-like kinase (ALK)1 is an antagonistic mediator of lateral TGFβ/ALK5 signaling. Mol Cell 12: 817–828.
7. Daly AC, Randall RA, Hill CS (2008) Transforming growth factor β-induced Smad1/5 phosphorylation in epithelial cells is mediated by novel receptor complexes and is essential for anchorage-independent growth. Mol Cell Biol 28: 6889–6902.
8. Liu IM, Schilling SH, Knouse KA, Choy L, Derynck R, et al. (2009) TGFβ-stimulated Smad1/5 phosphorylation requires the ALK5 L45 loop and mediates the pro-migratory TGFβ switch. EMBO J 28: 88–98.
9. Wrighton KH, Lin X, Yu PB, Feng XH (2009) Transforming Growth Factor β Can Stimulate Smad1 Phosphorylation Independently of Bone Morphogenic Protein Receptors. J Biol Chem 284: 9755–9763.
10. Gesualdi SC, Haerry TE (2007) Distinct signaling of Drosophila Activin/TGF-β family members. Fly (Austin) 1: 212–221.
11. Ross JJ, Shimmi O, Vilmos P, Petryk A, Kim H, et al. (2001) Twisted gastrulation is a conserved extracellular BMP antagonist. Nature 410: 479–483.
12. Jensen PA, Zheng X, Lee T, O'Connor MB (2009) The Drosophila Activin-like ligand Dawdle signals preferentially through one isoform of the Type-I receptor Baboon. Mech Dev 126: 950–957.
13. Feng XH, Derynck R (1997) A kinase subdomain of transforming growth factor-β (TGF-β) type I receptor determines the TGF-β intracellular signaling specificity. EMBO J 16: 3912–3923.
14. Padgett RW, Wozney JM, Gelbart WM (1993) Human BMP sequences can confer normal dorsal-ventral patterning in the Drosophila embryo. Proc Natl Acad Sci U S A 90: 2905–2909.

15. Brummel T, Abdollah S, Haerry TE, Shimell MJ, Merriam J, et al. (1999) The Drosophila activin receptor baboon signals through dSmad2 and controls cell proliferation but not patterning during larval development. Genes Dev 13: 98–111.
16. Tsukazaki T, Chiang TA, Davison AF, Attisano L, Wrana JL (1998) SARA, a FYVE domain protein that recruits Smad2 to the TGFβ receptor. Cell 95: 779–791.
17. Batut J, Howell M, Hill CS (2007) Kinesin-mediated transport of Smad2 is required for signaling in response to TGF-β ligands. Dev Cell 12: 261–274.
18. Chen YG, Massagué J (1999) Smad1 recognition and activation by the ALK1 group of transforming growth factor-β family receptors. J Biol Chem 274: 3672–3677.
19. Zheng X, Wang J, Haerry TE, Wu AY, Martin J, et al. (2003) TGF-β signaling activates steroid hormone receptor expression during neuronal remodeling in the Drosophila brain. Cell 112: 303–315.
20. Haerry TE (2010) The interaction between two TGF-β type I receptors plays important roles in ligand binding, SMAD activation, and gradient formation. Mech Dev 127: 358–370.
21. Wu MY, Hill CS (2009) Tgf-β superfamily signaling in embryonic development and homeostasis. Dev Cell 16: 329–343.
22. Srivastava M, Begovic E, Chapman J, Putnam NH, Hellsten U, et al. (2008) The Trichoplax genome and the nature of placozoans. Nature 454: 955–960.
23. Ng J (2008) TGF-β signals regulate axonal development through distinct Smad-independent mechanisms. Development 135: 4025–4035.
24. Alarcón C, Zaromytidou AI, Xi Q, Gao S, Yu J, et al. (2009) Nuclear CDKs drive Smad transcriptional activation and turnover in BMP and TGF-β pathways. Cell 139: 757–769.
25. Nakao A, Imamura T, Souchelnytskyi S, Kawabata M, Ishisaki A, et al. (1997) TGF-β receptor-mediated signalling through Smad2, Smad3 and Smad4. EMBO J 16: 5353–5362.
26. Jörnvall H, Blokzijl A, ten Dijke P, Ibáñez CF (2001) The orphan receptor serine/threonine kinase ALK7 signals arrest of proliferation and morphological differentiation in a neuronal cell line. J Biol Chem 276: 5140–5146.
27. Shimmi O, O'Connor MB (2003) Physical properties of Tld, Sog, Tsg and Dpp protein interactions are predicted to help create a sharp boundary in Bmp signals during dorsoventral patterning of the Drosophila embryo. Development 130: 4673–4682.
28. Wang L, Brown JL, Cao R, Zhang Y, Kassis JA, et al. (2004) Hierarchical recruitment of polycomb group silencing complexes. Mol Cell 14: 637–646.
29. Ting CY, Herman T, Yonekura S, Gao S, Wang J, et al. (2007) Tiling of r7 axons in the Drosophila visual system is mediated both by transduction of an activin signal to the nucleus and by mutual repulsion. Neuron 56: 793–806.
30. Marqués G, Bao H, Haerry TE, Shimell MJ, Duchek P, et al. (2002) The Drosophila BMP type II receptor Wishful Thinking regulates neuromuscular synapse morphology and function. Neuron 33: 529–543.

APPENDIX B: ULTRASTRUCTURAL CHANGE OF HIPPOCAMPAL SYNAPSES IN CHORDIN$^{-/-}$ MICE

Mu Sun, Mark Thomas, ***Rachel Herder****, M. Lisa Bofenkamp, Scott B. Selleck, and Michael B. O'Connor. (2007). Presynaptic Contributions of Chordin to Hippocampal Plasticity and Spatial Learning. The Journal of Neuroscience, 27(29):7740-7750.*[14]

The hippocampus is the center for spatial learning and memory in the adult mammalian brain. Components of the bone morphogenic protein (BMP) signaling pathway are expressed in the mammalian adult hippocampus [103]. BMP signaling pathway components have been shown to be important for synaptic homeostasis and regulation of synaptic transmission in *Drosophila* [104-109]. In addition, BMP signals regulate a number of developmental, physiological, and homeostatic processes in mice, including neural induction and neuronal lineage determination [101,110-112]. This led us to hypothesize that the BMP pathway plays a role in regulating synaptic function in the mouse hippocampus.

When key components of the BMP signaling pathway are eliminated, including ligands, receptors, and Smads, mice die in early embryonic stages [113]. Therefore, we chose to examine if loss of chordin (Chrd), a BMP ligand antagonist, alters hippocampal physiology, learning, memory, or behavior [114]. Chrd$^{-/-}$ animals do not die in early embryonic stages but Chrd is expressed in the

[14] RJH contributed to data shown in Table 1 and Figure 4 from the Sun et al.; MS and MBO conceived and designed all experiments and hypotheses.

mouse hippocampus, making it ideal to study the effect of enhancing BMP signaling in the mouse hippocampus [114].

Chrd is a secreted factor that is an extracellular antagonist of BMP signaling [115]. It is thought to function by binding to BMP ligands and prevent them from receptor interaction [115]. Chrd is expressed in the hippocampus and loss of Chrd results in a presynaptic transmitter release defect that increases both short and long term synaptic plasticity [114][15]. Mice also have altered cognitive abilities, as measured by Y-maze, open-field/ novel object recognition, and Morris water maze tests [114].

Because $Chrd^{-/-}$ mutants showed altered transmitter release in electrophysiology experiments, we wanted to determine if the animals exhibited a change in synapse morphology at the ultrastructural level[16]. To address this question, we used transmission electron microscopy (TEM) to examine the CA1 region of hippocampal synapses from $Chrd^{-/-}$ mice. The CA1 region is the portion of the hippocampus thought to be involved in long-term potentiation (i.e. memory and learning). We used a double-blind study to compare hippocampal synapses from $Chrd^{-/-}$ mice with their littermate controls ($Chrd^{+/+}$) (Sun et. al Figure 4A and B). The ultrastructural parameters we measured included: the total number of

[15] MS designed and performed all electrophysiology and Y-maze, open field, and Morris water maze tests.
[16] MS designed the experiment. I performed the electron microscopy of samples and the double-blind analysis of samples, including fixation protocols, ultramicrotome sectioning, and analysis of TEM micrographs.

vesicles per bouton; the number of docked vesicles per synapse; the length of the active zone; the number of docked vesicles per activezone length; and the width of the synaptic cleft.

While Chrd$^{-/-}$ animals had normal gross anatomy of the hippocampus, we found that Chrd$^{-/-}$ axon terminals showed a significantly higher number of docked vesicles per active zone length (Sun et al. Table 1). We also found that the width of the synaptic cleft in Chrd$^{-/-}$ mice was decreased compared to their littermate controls. These statistically significant ultrastructural changes in morphology may play a role in the altered transmitter release that was observed in electrical physiology experiments.

Chrd is a BMP antagonist, therefore knockout of Chrd putatively results in increased BMP signaling in the hippocampus. Chrd-/- mice show improved learning in the watermaze test and a decreased amount of curiosity in the Y-maze and open field/novel object recognition tests [114]. The decreased curiosity could result from: a decreased baseline of curiosity or from the Chrd$^{-/-}$ mice learning faster [114]. Additional studies will be required to determine which of the two possibilities is more likely and if the altered hippocampal morphology and electrophysiology profile of Chrd$^{-/-}$ mice a result or a cause of the different behavior.

Cellular/Molecular

Presynaptic Contributions of Chordin to Hippocampal Plasticity and Spatial Learning

Mu Sun,[1,2] Mark J. Thomas,[3,4] Rachel Herder,[2] M. Lisa Bofenkamp,[1,2] Scott B. Selleck,[2,5] and Michael B. O'Connor[1,2]
[1]Howard Hughes Medical Institute and Departments of [2]Genetics, Cell Biology, and Development, [3]Neuroscience, [4]Psychology, and [5]Pediatrics, University of Minnesota, Minneapolis, Minnesota 55455

Recently, several evolutionary conserved signaling pathways that play prominent roles in regulating early neurodevelopment have been found to regulate synaptic remodeling in the adult. To test whether adult neuronal expression of bone morphogenic protein (BMP) signaling components also plays a postnatal role in regulating neuronal plasticity, we modulated BMP signaling in mice both *in vivo* and *in vitro* by genetic removal of the BMP inhibitor chordin or by perfusing recombinant BMP signaling pathway components onto acute hippocampal slices. Chordin null mice exhibited a significant increase in presynaptic transmitter release from hippocampal neurons, resulting in enhanced paired-pulse facilitation and long-term potentiation. These mice also showed a decreased acquisition time in a water maze test along with less exploratory activity during Y-maze and open-field tests. Perfusion of BMP ligands onto hippocampal slices replicated the presynaptic phenotype of chordin null slices, but bath application of Noggin, another antagonist of BMP signaling pathway, significantly decrease the frequency of miniature EPSCs. These results demonstrate that the BMP signaling pathway contributes to synaptic plasticity and learning likely through a presynaptic mechanism.

Key words: **BMP; chordin; hippocampus; synaptic plasticity; learning and memory; neurotransmission**

Introduction

Many components of the bone morphogenic protein (BMP) signaling pathway, a distinct subfamily within the TGF-βs, are expressed in different parts of the mammalian adult brain, including the hippocampus (Soderstrom et al., 1996; Pappano et al., 1998; Scott et al., 2000). Despite this strong expression in the adult brain, their potential role in regulating postnatal neuronal plasticity in vertebrates has not been investigated. All members of the TGF-β superfamily bind to and activate transmembrane serine/threonine receptors, which, during canonical signaling, transduce transcriptional regulatory signals to the nucleus via phosphorylation and nuclear import of Smad (Sma and Mad-related protein) transcription factors (Shi and Massague, 2003). Noncanonical pathways that signal through mitogen-activated protein kinase (MAPK), LIM (Lin-11/Isl-1/Mec-3 gene products) kinase, PKCα, and small GTPases have also been identified (Derynck and Zhang, 2003; Moustakas and Heldin, 2005).

BMP signals regulate numerous developmental, physiological, and homeostatic processes, including, but not limited to, early embryonic patterning, organ development, apoptotic responses, and bone remodeling (Shi and Massague, 2003). From a neurodevelopment point of view, BMPs are critical for neural induction (Sasai, 2001; Rhinn et al., 2006) and neuronal lineage determination (Mehler et al., 1997). In addition to these neurodevelopment roles, BMPs have also been found recently to regulate synaptic homeostasis at the *Drosophila* neuromuscular junction (NMJ) by a retrograde mechanism (Aberle et al., 2002; Marques et al., 2002; McCabe et al., 2003; Rawson et al., 2003). BMP signals also regulate synaptic transmission between motor neurons and interneurons in the CNS of *Drosophila*, suggesting that BMP signaling likely integrates the development and function of the central motor circuitry to help coordinate larval movements (Baines, 2004).

The importance of BMP signaling in regulating synaptic function in *Drosophila*, coupled with the high level expression of BMP signaling components in the mammalian hippocampus, prompted us to examine whether modulation of BMP signaling alters hippocampal function. According to the Allen Brain Atlas, there are numerous BMPs expressed in hippocampus, including BMP2, BMP4–BMP7, and BMP10. Because elimination of most BMP signaling components results in early embryonic lethality (Zhao, 2003), we chose to examine whether loss of chordin alters hippocampal physiology, learning, memory, or other behavior. Chordin is a secreted extracellular antagonist of BMP signaling whose only known function is to bind BMP ligands and prevent them from interacting with their receptors (Piccolo et al., 1996). Chordin is expressed in many tissues throughout development, including the hippocampus (Pappano et al., 1998; Scott et al., 2000). We find that loss of chordin results in a presynaptic transmitter release defect that enhances short- and long-term synaptic plasticity in slice preparations. In addition, these mice exhibit altered cognitive behaviors in Y-maze and open-field tests as well as a significantly enhanced learning rate in Morris water maze

Received April 10, 2007; revised June 2, 2007; accepted June 6, 2007.
M.B.O. is an investigator of Howard Hughes Medical Institute. We are grateful to Drs. Anna Petryk and Lorene M. Lanier for advice on mouse genetics and hippocampal neuronal culture. We thank Dr. Bob Hafner and Alice Ressler of the EM Characterization Facility at University of Minnesota for technical help in preparing and analyzing EM sections. We thank Dr. John Klingensmith for supplying us with the chordin knock-out mice.
Correspondence should be addressed to Michael B. O'Connor, Department of Genetics, Cell Biology, and Development, 6-160 Jackson Hall, University of Minnesota, Minneapolis, MN 55455. E-mail: moconnor@mail.med.umn.edu.
DOI:10.1523/JNEUROSCI.1604-07.2007
 0270-6474/07/277740-11$15.00/0

tests. Because acute application of BMP6, but not BMP2, to hippocampal slices could also increase transmitter release probability and paired-pulse facilitation (PPF) similar to that seen in chordin knock-out mice, we suggest that BMP signaling can regulate synaptic plasticity and learning behavior through a presynaptic mechanism.

Materials and Methods

Animals. Two- to 3-month-old chordin $Chrd^{-/-}$ and $Chrd^{+/+}$ male mice (Bachiller et al., 2000) were used in this study following protocols approved by the Research Animal Resources committee at the University of Minnesota.

Preparation of hippocampal slices. Mice were decapitated after anesthesia, and hippocampal slices (350 μm thick) were cut in ice-cold artificial CSF (ACSF) containing the following (in mM): 250 sucrose, 25 $NaHCO_3$, 25 glucose, 2.5 KCl, 1.25 NaH_2PO_4, 2 $CaCl_2$, and 1.5 $MgCl_2$, pH 7.3 (320 mOsm). The slices were recovered in a submerged chamber at room temperature (24–25°C) in carbogen-bubbled ACSF, containing 125 mM NaCl in place of 250 mM sucrose, for at least 2 h before the start of recordings.

Extracellular field EPSP recordings, PPF, and long-term potentiation (field). Recordings were made in a standard interface chamber or submerged chamber and held at 30°C [Fine Science Tools (Foster City, CA) and Warner Instruments (Hamden, CT)] with 1–2 ml/min perfusion speed. A test pulse is given by a custom-designed platinum bipolar electrode (MX21CEPMS1; FHC, Bowdoinham, ME) for stimulating Schaffer collaterals at 0.05 ms duration and every 20 s. Field EPSP (fEPSP) was recorded by 1–2 MΩ glass recording in the stratum radiatum of CA1 in the hippocampal slice. Data were acquired through Axoclamp B and pClamp 8 software (Molecular Devices, Palo Alto, CA).

PPF was examined at 25, 50, 100, and 200 ms interstimulus intervals (ISIs) with stimulation strength correlated to 30% of the maximal fEPSP. Stimuli intensity correlated to 50% maximal fEPSP slope was used for baseline and induction of LTP. Induction protocol is single train, 100 Hz, 1 s or theta burst stimulation (TBS) that entailed four trains of 10 bursts of four stimuli with 20 s, 200 ms, and 10 ms intervals between trains, burst, and stimuli, respectively (Law et al., 2003). For late-phase long-term potentiation (LTP), 30% maximal fEPSP was set as basal synaptic transmission and four trains of 100 Hz for 1 s duration with 5 min interval induced at least 3 h LTP. To analyze the depolarization envelope during induction of LTP, the negative area of each depolarization trace was normalized by correlated baseline slope of fEPSP.

Whole-cell patch-clamp, miniature EPSC recordings and pairing protocol induced LTP. Pyramidal neurons in CA1 were identified by infrared differential interference contrast microscope under a submerged recording chamber; data were acquired by Multipatch (Molecular Devices) and customized Igor software (WaveMetrics, Lake Oswego, OR). Patch electrodes (3–5 MΩ) contained the following (in mM): 117 cesium gluconate or potassium gluconate, 2.8 NaCl, 20 HEPES, 0.4 EGTA, 5 tetraethylammonium-Cl, 2.5 MgATP, and 0.25 MgGTP, pH 7.2–7.4 (285–295 mOsm). Miniature EPSCs (mEPSCs) of pyramidal neurons were recorded voltage clamped at −60 mV with 1 μM TTX and 20 μM bicuculline. Human recombinant BMP6, BMP2, and Noggin (R&D Systems, Minneapolis, MN) were perfused at 200 ng/ml concentration and at a flow rate of 2 ml/min for 5 min. mEPSCs were detected by Mini Analysis Program (Synaptosoft, Decatur, GA) from continuous recordings of every 3 min.

Evoked EPSCs were recorded by patch pipettes (3–5 MΩ) filled with the intracellular solution containing the following (in mM): 5 KCl, 135 K-gluconate, 10 HEPES, 0.2 EGTA, 2.5 Mg-ATP, 0.25 Na-GTP, 10 glucose, and 5 QX-314 [*N*-(2,6-dimethylphenylcarbamoyl methyl)triethylammonium chloride], pH 7.2–7.25 (290–300 mOsm). Cells were held at −60 mV. LTP was induced by pairing of stimulation of Schaffer collaterals at 1 Hz for 100 ms by glass stimulating electrode with depolarization of the postsynaptic cell to 0 mV. Care was taken to avoid "washout" of LTP, by inducing LTP within 15 min after disruption of the cell plasma membrane. Serial resistance in whole-cell configuration was ~25–40 MΩ. Cells were discarded when either input or serial resistance changed >25% after baseline recording. Resting potentials normally were from −60 to −65 mV.

Immunocytochemistry and staining. Twenty micrometer cryosections from adult mice were incubated with primary antibodies at 1:200, 4°C overnight. After incubation with fluorescently labeled secondary antibodies for 1 h at room temperature, *Z*-stack images were captured and processed using a Zeiss (Oberkochen, Germany) Axioplan 2 microscope equipped with a Carve spinning disk (Atto Instruments, Rockville, MD) and Axiovision software (Zeiss). Anti-phosphorylated Smad (pSmad) antibodies were either purchased from Upstate Biotechnology (Lake Placid, NY) and Cell Signaling Technology (Beverly, MA) or were a gift from Dr. Carl-Henrick Heldin (Ludwig Center for Cancer Research, Uppsala, Sweden). Anti-chordin and BMP receptor type II (BMPRII) antibodies were purchased from R&D Systems. Anti-microtubule-associated protein 2 (Map2) and synapsin I were obtained from Chemicon (Temecula, CA).

Hippocampal and glial cultures were prepared from embryonic day 16 and postnatal 0 mice, respectively, following a published protocol (Strasser et al., 2004). Approximately 1×10^4 hippocampal cells were plated on each 12 mm coverslip inside 35 mm culture dishes. On day 4, 3 μM AraC was put into the culture to maintain pure primary neuronal culture. Staining of BMPRII (1:10; R&D Systems), synapsin I (1:100; Chemicon), and Map2 (1:200; Chemicon) was performed on 1-week-old hippocampal cultured neuron.

Mouse brains were impregnated following the user manual of FD Rapid GolgiStain kit (FD NeuroTechnologies, Ellicott City, MD), 100 μm cryosections were stained and observed under 100× objective. The tertiary dendrites (>10 μm segment) in stratum radiatum were traced, and a serial set of pictures, which cover all spines on the dendrite, were taken and *Z*-projected by maximal intensity using NIH ImageJ software.

Electron microscopy. The fixative containing 2% formaldehyde, 2.5% glutaraldehyde, and 2 mM $CaCl_2$ in 0.1 M cacodylate buffer was perfused transcardially. The mouse brains were intact inside the skull for 1 h, and then coronal 400 μm hippocampal slices were cut by a Vibroslicer (World Precision Instruments, Sarasota, FL) inside a chamber filled with 0.1 M cacodylate buffer. Slices were soaked in 1% OsO_4 with 1.5% potassium ferrocyanide and for an additional 1 h in 1% OsO_4. Next, slices were treated following standard procedures (Harris and Sultan, 1995) and thin sectioned at 50 nm. Regions 200 μm distant from the pyramidal CA1 soma in the striatum radiatum were observed at 50,000× magnification with Jeol (Peabody, MA) 1200EX Transmission Electron Microscopy. Only synapses with clear presynaptic and complete postsynaptic structure were selected for counting and measuring by a second researcher who did not know the identity of the samples. Docked vesicles are defined as vesicles <100 nm from the presynaptic membrane. Active zone length was measured from the width of postsynaptic density as two aligned oppositely each other.

Behavioral assays. Animal behaviors were video taped and analyzed by both real-time and off-line versions of Topscan system (Clever Systems, Reston, VA).

Y-maze. The Y-maze includes three identical arms (36 cm long × 12.5 cm high × 7.5 cm wide, made of transparent Plexiglas) and a 7.5 cm hexagon as the hub in the center of the maze. Around the Y-maze, visual cues enable the animal to locate itself spatially. During the acquisition trial, one arm is blocked. A mouse is placed into the hub and allowed to freely explore the two open arms and the hub for 15 min. After an intertrial interval of 3 h, the mouse is placed in the maze with all arms open for 5 min (recall trial). The number of entries made into each arm is recorded. (Dellu et al., 1992).

Open field. An individual mouse was put into each of four test cages (50 × 50 × 40 cm) with a novel object (5-cm-diameter bottle cap) 12.5 cm from the wall. Mice were allowed to explore the cages for 15 min, and their movements were recorded.

Morris water maze (Morris, 1984) analysis was performed in a 1.2-m-diameter opaque pool in which a nontoxic tempera white paint was added. Water depth was 50 cm, and the surface was 20 cm from the ridge of the pool. Water temperature was monitored and kept at 24 ± 0.5°C throughout the training. Mice were trained to locate a submerged 10 cm platform (0.5 cm under the water) in an arbitrary quadrant of the pool

during 90 s training trials. Posters on the wall and other fixtures in the testing room served as spatial cues. Mice were allowed to stay on the platform for 15 s before they were dried and returned to their home cages. Two trials per day with a 30 min interval between trials were given at the same time of each training day. On the first day of the experiment (day 0), an individual mouse was put on the platform with a visible cue (15 cm flag) for 15 s as a primer. Mice were then placed tail-end low, facing the wall, at any one of five randomly selected points in one of three other quadrants, with approximately equal distance to the platform. During the probe trial, mice swam 60 s without a platform, and the length of stay in each quarter was analyzed. After the first probe test, the platform was put in a new position, then mice were trained another 6 d (reversal test), and then a second probe test was performed on day 18.

Results

Expression of BMP signaling pathway components in the adult mouse hippocampus

A number of previous reports have shown expression of several BMP signaling pathway members in the adult hippocampus (Soderstrom et al., 1996; Pappano et al., 1998; Scott et al., 2000), but it is not clear whether this pathway is actually active in mature neurons because some important signaling pathway components that play a role in directing neurodevelopment are shut off after maturation of the CNS. Previous *in situ* hybridization results showed that the BMPRII receptor is expressed in the hippocampus. We examined the distribution of the BMPRII receptor protein and found that is expressed in all regions of the hippocampus (CA1–CA3 and the dentate gyrus). To examine the subcellular localization of the BMPRII receptor in synaptic structures, we double stained cultured hippocampal pyramidal neurons isolated from 1-week-old mice with antibodies against the presynaptic marker synapsin I and BMPRII. We found that BMPRII is localized to both dendrites and axons. However, in culture, we see a strong colocalization of synapsin I puncta (a presynaptic marker) with BMPRII patches, suggesting that BMP signaling can potentially modulate presynaptic function (Fig. 1*E*,*F*).

To determine whether mature hippocampal cells actually receive BMP signals, we stained adult hippocampal (8 weeks old) (Fig. 1*A*) slices with three different anti-pSmad1/5 antibodies. All three gave similar patterns of immunoreactivity within the hippocampus and stained pyramidal neurons, interneurons, and astrocytes in the CA1–CA3 regions as well as the dentate gyrus (Fig. 1*B*). These observa-

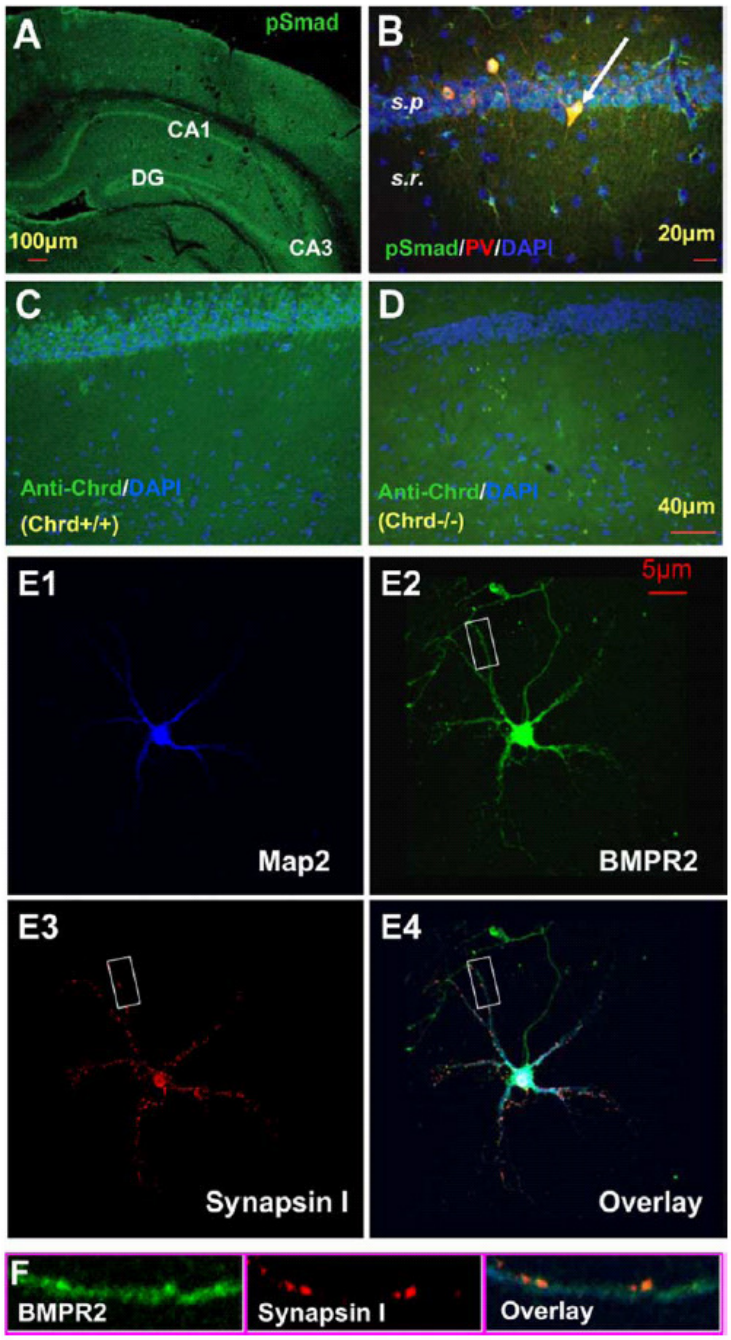

Figure 1. ***A***, Expression pattern of BMP signaling pathway components in the mouse hippocampus. Anti-pSmad staining in adult wild-type mouse hippocampus; cell body layers showed strong staining, including CA1, CA3, and dentate gyrus (DG) regions. ***B***, Anti-pSmad staining under higher magnification; signals are seen in pyramidal neurons of CA1, inhibitory neurons (parvalbumin positive), and astrocytes (typical morphology). Blue channel shows 4′,6′-diamidino-2-phenylindole (DAPI) nuclear counterstaining. Note that not all cell bodies show pSmad accumulation. Striatum pyramidal (s.p.) and striatum radiatum (s.r.) are labeled. ***C***, ***D***, Anti-Chrd staining in CA1 of $Chrd^{+/+}$ and $Chrd^{-/-}$ slices. Note the strong Chrd signal in the wild-type pyramidal cells (***C***) but not in the mutant (***D***). ***E1–E4***, BMPRII can be detected on 1-week-old hippocampal pyramidal neuronal cultured cells. ***E1***, Map2 staining of dendrites. ***E2***, ***E3***, BMPRII staining in dendrites (***E2***) and the axon synapsin I-stained synaptic structure (***E3***). ***E4***, Overlay of ***E1–E3***. ***F***, Higher magnification showed colocalization of synapsin I and BMPRII at synaptic structures.

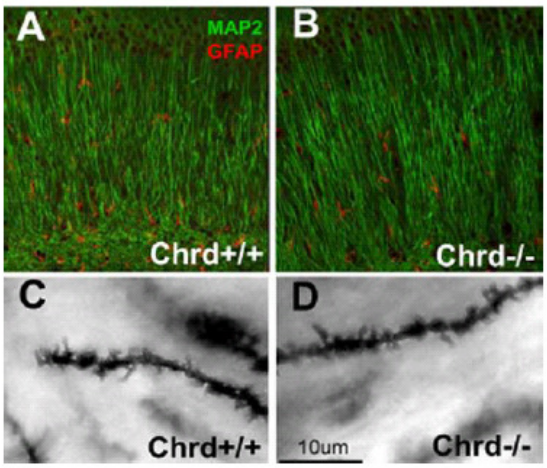

Figure 2. Normal dendritic architecture and spine density is seen in the hippocampus of *Chrd*$^{-/-}$ mice. ***A***, ***B***, Map2 and GFAP double staining of the CA1 region from *Chrd*$^{+/+}$ (***A***) and *Chrd*$^{-/-}$ (***B***) mice. Map2 staining (green) showed a similar dendrite branching pattern from both genotypes; GFAP staining (red) showed a similar distribution and density of astrocytes both genotypes. ***C***, ***D***, Golgi staining showing apical tertiary dendrites of CA1 pyramidal neurons from *Chrd*$^{+/+}$ and *Chrd*$^{-/-}$, respectively.

tions suggest that, like recent observations at the NMJ in *Drosophila* (Dudu et al., 2006), in the 8-week-old hippocampus, both presynaptic and postsynaptic cells are receiving BMP signals.

We next examined whether the BMP inhibitor chordin is also present in hippocampal tissue. Like BMPRII and pSmad, we observed strong signals from all hippocampal regions, including CA1–CA3 and the dentate gyrus. This staining is specific for chordin because slices from *Chrd*$^{-/-}$ mouse brains showed no staining (Fig. 1*C*,*D*). Because loss of chordin might be expected to increase the level of BMP signaling, we also stained chordin mutant brains with anti-pSmad antibodies. Surprisingly, we could detect no obvious differences in staining levels either by immunolocalization or on Western blots of isolated hippocampal tissue (data not shown), although small changes (<2×) or changes in only a small subset of cells might have been missed. The lack of an effect of chordin loss on steady-state levels of pMad phosphorylation, however, does not rule out that chordin loss may result in alterations in BMP signaling through non-Smad-dependent mechanisms (see Discussion).

Chrd$^{-/-}$ mice show normal hippocampal morphology and dendritic structure

Although 50% of *Chrd*$^{-/-}$ mice died perinatally in C57BL/6 background, those that survive exhibit a normal gross morphology of the CNS (Bachiller et al., 2003). We found that hematoxylin and eosin staining of *Chrd*$^{-/-}$ brain sections also showed normal gross anatomy of hippocampal structures (data not shown). Because it has been found that BMPs can stimulate dendrite growth of cultured neurons (Lein et al., 1995; Withers et al., 2000), we wanted to determine whether loss of chordin changed dendritogenesis in the hippocampus. Using anti-Map2 staining as a marker for dendrite structure, we observed no differences in dendritic morphology in the striatum radiatum of *Chrd*$^{-/-}$ mutant mice compared with wild type (Fig. 2*A*,*B*). We also examined the density of astrocytes inside hippocampus, because overexpression of BMP4 has been shown to result in an expansion of the astrocyte population (Gomes et al., 2003). Using an anti-GFAP antibody to mark astrocytes, we observed no significant difference in the pattern or density of GFAP-positive glial cells inside hippocampus of *Chrd*$^{-/-}$ animals compared with wild type (Fig. 2*A*,*B*).

Last, we wanted to examine dendritic spine morphology and density because alterations in either of these might significantly change the electrophysiological properties of hippocampal neural circuits. To test whether loss of chordin altered the spine density of hippocampal tertiary dendrites, Golgi-impregnated brains from mutant and littermate control mice were sectioned, and spine numbers were counted (double-blind study). We found no significant difference in average spine density between *Chrd*$^{-/-}$ and wild-type mice in CA1 (*Chrd*$^{-/-}$, 12.9 ± 0.6/10 μm; *Chrd*$^{+/+}$, 12.1 ± 0.6/10 μm; $p = 0.38$). In summary, our morphological assays reveal that removal of chordin has no significant effect on the general development of the hippocampus, including gross structure, glial proliferation, dendritogenesis, and spinogenesis.

Chrd$^{-/-}$ mutant mice exhibit increased paired-pulse facilitation and transmitter release

Because BMP signaling has been shown to strongly regulate glutamatergic transmission at the *Drosophila* NMJ (Aberle et al., 2002; Marques et al., 2002; McCabe et al., 2003) and because BMPs have been shown to potentiate glutamate-mediated currents in human retina neurons (Shen et al., 2004), we analyzed basic synaptic transmission inside CA1 region of hippocampus, in which the synapses are formed by axon terminals from the Schaffer collaterals of CA3 neurons onto apical dendrites of CA1 pyramidal neurons. The stimulus–response curves from *Chrd*$^{-/-}$ mutant animals and control slices overlay very well, indicating that there is no general alteration in excitatory synaptic transmission in chordin mutants (Fig. 3*A*).

We next used a paired-pulse facilitation protocol to examine short-term plasticity in chordin mutants. *Chrd*$^{-/-}$ slices show a strikingly enhanced PPF compared with littermate controls when the interpulse interval was <100 ms (Fig. 3*B*). We next studied mEPSCs by the whole-cell patch-clamp technique to differentiate between presynaptic or postsynaptic involvement effects in *Chrd*$^{-/-}$ animals. The amplitude of mEPSCs from *Chrd*$^{-/-}$ CA1 pyramidal neurons was normal compared with wild-type controls (Fig. 3*C*). However, the frequency of mEPSCs in *Chrd*$^{-/-}$ animals increased significantly (0.45 ± 0.03 vs 0.77 ± 0.08 Hz; $p = 0.003$) (Fig. 3*C*) compared with control animals. The higher PPF and mini frequency from *Chrd*$^{-/-}$ animals suggests that chordin is acting presynaptically to control transmitter release. This finding is consistent with the *Drosophila* data in which presynaptic loss of BMP signaling results in a decrease in mEPSC frequency and no change in amplitude (Marques et al., 2002). In chordin mutants, which presumably have an increased level of BMP signaling, we see an increase of mEPSC frequency and no change in amplitude.

Chrd$^{-/-}$ hippocampal synapses exhibit morphological alterations at the ultrastructural level

Because *Chrd*$^{-/-}$ mutants show altered transmitter release and short-term plasticity, we wanted to determine whether an ultrastructural change in synapse morphology might underlie these defects. To explore this issue, we examined the ultrastructure of hippocampal synapses from *Chrd*$^{-/-}$ mice and littermate controls using transmission electron microscopy (Fig. 4*A*,*B*). In a double-blind study, we found that *Chrd*$^{-/-}$ axon terminals

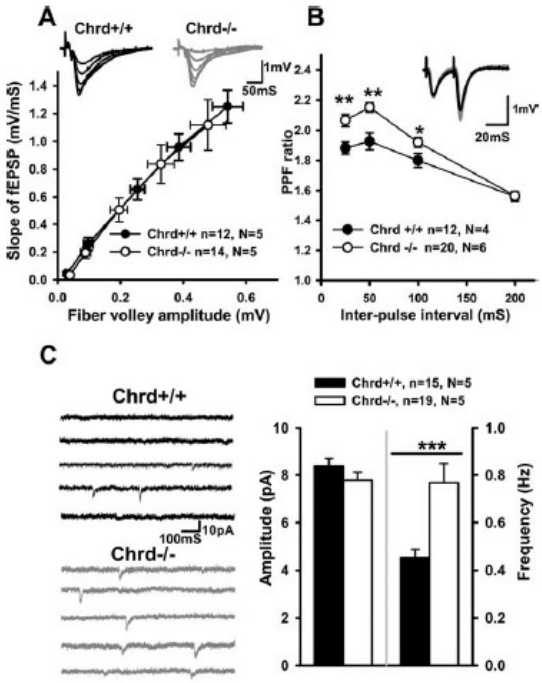

Figure 3. Increased PPF and mEPSC frequency in *Chrd*$^{-/-}$ slices. ***A***, Relationship between the slope of fEPSP and amplitude of presynaptic fiber volley for *Chrd*$^{-/-}$ and *Chrd*$^{+/+}$ mice. Data are expressed as mean ± SEM. Representative traces of fEPSPs evoked with different stimulus strengths are shown in the insets. ***B***, PPF was measured as the ratio between the slopes of fEPSPs evoked by the second and first pulses and plotted for several ISIs. Field EPSPs were evoked with a stimulus that evoked 30% of the maximal fEPSP. Values represent mean ± SEM; $*p < 0.05$, $**p < 0.01$ (unpaired *t* test). Representative traces of fEPSPs evoked with 25 mS ISI are shown in the insets. ***C***, Increase in the frequency of mEPSCs in *Chrd*$^{-/-}$ mice. Examples of mEPSCs recorded in *Chrd*$^{-/-}$ and *Chrd*$^{+/+}$ mice are shown in the left. Note the significant difference in the mean frequency of mEPSCs recorded in slices from *Chrd*$^{-/-}$ and *Chrd*$^{+/+}$ mice ($***p < 0.005$, unpaired test). Data are presented as mean ± SEM. There is no significant difference for mEPSC amplitude between genotypes.

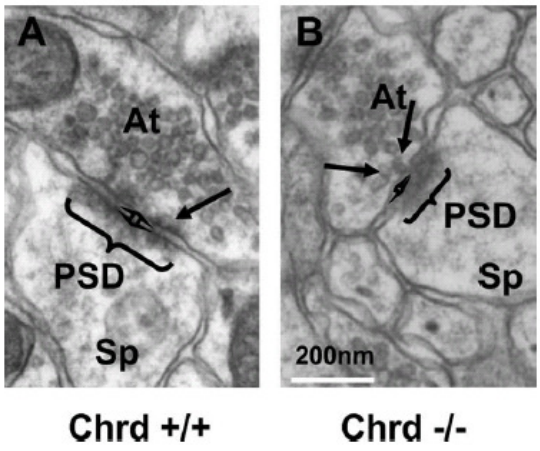

Figure 4. Ultrastructural change of hippocampal synapses in *Chrd*$^{-/-}$ mice. ***A***, Transmission electron microscopy of asymmetric synapse of *Chrd*$^{+/+}$ in CA1 region; symbol ↕ points to the synaptic cleft, and symbol { indicates the length of active zone. Arrows point to docked vesicles. At, Axon terminal; Sp, spine; PSD, postsynaptic density. ***B***, Asymmetric synapse of *Chrd*$^{-/-}$ in CA1 region. (Values are listed in Table 1.)

Table 1. Quantification of ultrastructural parameters of hippocampal synapses

	Chrd$^{+/+}$	*Chrd*$^{-/-}$
Total number of vesicles/bouton	26.4 ± 2.5	24.5 ± 2.4
Docked vesicles/synapse	1.2 ± 0.2	1.7 ± 0.2
Length of active zone (μm)	0.47 ± 0.04	0.49 ± 0.11
Docked vesicles/active zone length (DV/μm)	2.88 ± 0.71	4.97 ± 0.52*
Width of synaptic cleft (nm)	60.9 ± 4.2	46.5 ± 5.2*

Chrd$^{-/-}$ synapses of hippocampal CA1 region have more docked vesicles per active zone length ($p = 0.01$) and a narrower synaptic cleft ($p = 0.04$).

showed a significantly higher number of docked vesicles per active zone length (Table 1), consistent with the higher release probabilities (mEPSCs) from *Chrd*$^{-/-}$ boutons. We also found that the width of synaptic cleft from *Chrd*$^{-/-}$ synapses was slightly but significantly decreased, which might contribute to changes in synaptic efficacy.

Application of BMP6 but not BMP2 mimics the effects of chordin loss on mEPSCs and PPF

To examine directly whether enhanced BMP signaling produces the same changes in presynaptic release properties as those seen in *Chrd*$^{-/-}$ animals, we perfused two different BMP ligands onto C57BL/6 slices and measured mEPSC frequency and PPF. We found that, when perfused with BMP6 (2 ml/min, of 200 ng/ml for 5 min), the frequency, but not the amplitude, of mEPSCs significantly increased (Fig. 5*A*), similar to that seen in *Chrd*$^{-/-}$ slices. Interestingly, when BMP2 was perfused onto slices at the same concentration and rate as BMP6, we saw no effect on mEPSC frequency or amplitude (Fig. 5*B*). In tissue culture signaling assays, BMP6 and BMP2 produced comparable levels of Smad phosphorylation, indicating that each ligand is active for binding and canonical signal transduction (supplemental Fig. 1, available at www.jneurosci.org as supplemental material). Therefore, the difference in activity of these ligands on slices is not simply because one ligand is less active then the other for canonical signaling.

To determine whether downregulation of BMP signaling in acute slices results in the opposite effect on mini frequency, we also perfused recombinant chordin protein onto wild-type slices. In this case, we could not detect any significant change in mEPSC frequency (supplemental Fig. 2, available at www.jneurosci.org as supplemental material). It is also possible that endogenous BMP1, a metalloprotease that cleaves chordin, inactivates much of the exogenous chordin. However, cell signaling assays also showed that this commercial chordin protein does not significantly block BMP signaling in the concentration range used (supplemental Fig. 3, available at www.jneurosci.org as supplemental material). As an alternative, we examined the effects of Noggin, another structurally unrelated BMP inhibitor. In signaling assays, Noggin was a much more potent inhibitor than chordin (supplemental Fig. 3, available at www.jneurosci.org as supplemental material). We tested two physiological concentrations of Noggin on the acute slices. With the lower concentration (100 ng/ml), there was no significant effect on miniature events (supplemental Fig. 2, available at www.jneurosci.org as supplemental material), but perfusion of Noggin at 200 ng/ml significantly decreased the frequency of mEPSC ($p < 0.05$, paired *t* test) (Fig. 5*C*).

To test whether acutely enhanced BMP signaling could affect synaptic plasticity, we also incubated wild-type slices in 200

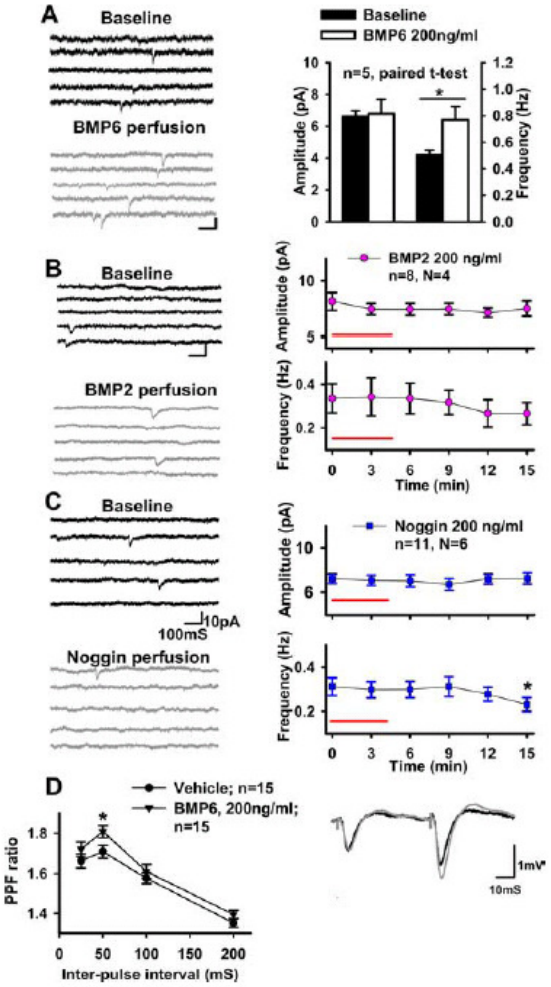

Figure 5. Effect of perfusion of BMPs and BMP antagonists on mEPSCs and PPF. ***A***, Perfusion of BMP6 on $Chrd^{+/+}$ slices increased the frequency but not the amplitude of mEPSCs. Left shows representative sweeps from control and 15 min after treatment. Right shows significant increase of frequency but not amplitude after perfusion of BMP6. ***B***, BMP2 at a similar concentration had no effect on mEPSCs after 15 min perfusion. Representative traces of mEPSCs are shown on the left. Right shows time-lapse change of amplitude and frequency of mEPSCs at 3 min analysis interval. There is no significant change of either mEPSCs amplitude or frequency. ***C***, Perfusion of Noggin, an antagonist of BMP signaling, inhibited release possibilities but not amplitude of mEPSC after 15 min (paired *t* test, $p < 0.05$). ***D***, PPF of wild-type slices treated with BMP6. Slices were incubated in a mini-interface chamber with 200 ng/ml BMP6 or vehicle for 30 min. They were then transferred to an interface recording chamber to test paired-pulse facilitation. At 50 ms ISI, BMP6-treated slices showed higher PPF. Normalized representative traces were shown as inset.

ng/ml BMP6 for 30 min and recorded paired-pulse facilitation. Like $Chrd^{-/-}$ slices, BMP6-treated slices showed a higher PPF than control slices but only at 50 ms ISI (Fig. 5*D*). Because addition of exogenous BMP6 enhances short-term plasticity and mEPSC frequency similar to that seen in *Chrd* mutants, these results are consistent with the view that loss of chordin likely produces its effects by enhancing signaling by certain BMP ligands within the hippocampus.

$Chrd^{-/-}$ hippocampal slices show an increase of high-frequency stimulation-induced LTP

LTP is widely studied throughout different regions of the CNS and is a well accepted cellular model for learning and memory (Lynch, 2004). We used both extracellular field recordings and whole-cell recordings to test whether removal of chordin would disturb normal LTP induction and expression in the hippocampus based on a presynaptic mechanism. With a standard HFS protocol (100 Hz, 1 s, 100 pulses totally), a higher field LTP is found in chordin mutant slices 1 h after induction (last 20 min average value fEPSP slope of 149.2 ± 7.7 vs 126.7 ± 4.9; $p = 0.02$) (Fig. 6*A*). In general, low-frequency presynaptic stimulation (1 Hz, 100 s, 100 pulses total) coupled with depolarization of the CA1 soma (0 mV) results in a more sensitive postsynaptic-specific LTP, and this protocol affects transmitter release less from presynaptic sites than does high-frequency stimulation (HFS) (Xu et al., 2000). Using such conditions, we induced the same level of LTP from both genotypes (140.2 ± 10.0 vs 134.9 ± 11.9; $p = 0.70$) (Fig. 6*B*). The non-enhanced LTP in $Chrd^{-/-}$ animals obtained from these patch-clamp recordings is, once again, more consistent with chordin affecting a presynaptic event.

TBS is thought to be a more physiologically relevant LTP induction protocol that mimics synaptic transmission paired with firing of postsynaptic neurons. It can induce both NMDA receptor-dependent LTP and a presynaptic calcium channel-sensitive LTP (Zakharenko et al., 2003). We found that a TBS protocol produced similar levels of LTP in both wild-type and $Chrd^{-/-}$ animals (Fig. 7*A*). Therefore, it appears that only a protocol that maximally activates presynaptic release can induce higher LTP in $Chrd^{-/-}$ slices.

To further examine this idea, we measured the depolarization envelope elicited by synaptic stimulation during the induction of LTP. For a 1 s, 100 Hz protocol, $Chrd^{-/-}$ slices showed significantly larger normalized area compared with $Chrd^{+/+}$ slices (1.58 ± 0.08 vs 1.26 ± 0.07 mV/mS; $p < 0.01$). However, one train of the TBS protocol (40 pulses in 2 s) triggered a similar depolarization envelope from the two genotypes (1.32 ± 0.06 vs 1.19 ± 0.07 mV/mS; $p = 0.17$). Together with the evidence for enhanced presynaptic function in $Chrd^{-/-}$ mice, these data suggest that the observed increases in LTP magnitude are likely a function of the enhanced depolarization provided by particularly robust glutamate release occurring in $Chrd^{-/-}$ slices during extended high-frequency stimulation (1 s, 100 Hz).

To test whether loss of chordin influenced LTP maintenance over time, we used several different stimulus protocols and examined LTP 3 h after induction. Using a four-train protocol, we found no difference in the maintenance LTP induced in $Chrd^{-/-}$ slices compared with wild type (Fig. 7*B*). However, because weaker stimulation (1 s, 100 Hz) but not stronger TBS stimulation could induce higher LTP in $Chrd^{-/-}$ slices, we reasoned that the induction might be saturated by the strong stimulus. Therefore, we also examined late-phase LTP using the weaker 1 s, 100 Hz protocol and found that, in our submerged recording chamber, $Chrd^{-/-}$ slices expressed sustained LTP for 3 h after a single train of stimulation (Fig. 7*C*), whereas $Chrd^{+/+}$ slices could not.

Together, these results suggest that $Chrd^{-/-}$ mice have intact NMDA and calcium channel-dependent LTP because the TBS protocol results in similar levels of LTP in these slices compared with controls. The inability to induce an enhanced late-phase LTP in $Chrd^{-/-}$ slices by a four-train HFS protocol also suggests that the induction process is saturated using a four-train stimulus. In contrast, however, we suggest that the higher LTP induced

by single-train HFS derives from an enhancement of presynaptic function in *Chrd*$^{-/-}$ animals that is strong enough to reach the threshold for late-phase LTP induction, whereas in wild-type animals it is not.

Chrd$^{-/-}$ mice exhibit impaired cognitive behavior

To determine whether the enhancement of presynaptic function in *Chrd*$^{-/-}$ mutants could affect cognitive behavior, we initially tested *Chrd*$^{-/-}$ mutant behavior using a two-trial Y-maze test in which performance relies on an innate tendency of a mouse to explore a novel environment but not on learning a new behavior or rule (Dellu et al., 1992). During the recall trial, which is 3 h after the acquisition phase, *Chrd*$^{-/-}$ animals entered the formerly closed (now novel) arm of the Y-maze less frequently than their littermate controls (Fig. 8*A*).

The altered performance of *Chrd*$^{-/-}$ mice might result from disturbed spatial recognition or a distortion of a basic instinctive behavior, such as rapid adaptation or a diminished exploratory instinct toward a new environment. To examine these issues further, we performed a one-trail open-field test with a novel object placed near one corner of the box. The overall ambulatory speed of *Chrd*$^{-/-}$ mice was no different from wild type (Fig. 8*B*). They also entered into an arbitrary circle area in the center of the open field with the same frequency and dwelled in the center with the same duration as wild-type mice. However, *Chrd*$^{-/-}$ mice showed hyperactivity inside the circle area. They ran faster than *Chrd*$^{+/+}$ mice in the center of the open field. Interestingly, *Chrd*$^{-/-}$ mice also showed less sniffing behavior to a novel object inside the box during the 15 min test (Fig. 8*B*, first group of bars). These results are consistent with either a decrease in innate exploratory behavior or quicker habituation to the new environment.

We next tested *Chrd*$^{-/-}$ animals in a standard Morris water maze, a well characterized hippocampal-dependent spatial learning and memory test (Morris, 1984). At the beginning of the training period, there was no difference between *Chrd*$^{-/-}$ and *Chrd*$^{+/+}$ littermate mice in their ability to find a visually cued platform within the water. However, with spatial extramaze cues, *Chrd*$^{-/-}$ mice showed a significantly improved ability to find the hidden platform. On average, it took them dramatically less time to escape from the water pool on the second day ($p < 0.001$) (Fig. 8*C*). Measurement of the swimming speed showed no significant difference between genotypes (200.5 ± 8.4 vs 180.6 ± 6.8 mm/S; $p > 0.05$). After training for 10 d, both groups of mice performed the task equally well. To test for relearning and learning flexibility, the platform was switched to an adjacent quadrant inside the pool. Under these conditions, both genotypes showed the same acquisition curve for the new task in the successive days. To evaluate spatial memory, two probe tests were given on days 11 and 18, 24 h after the end of learning or relearning trails. In this test, the platform was removed and the duration of time spent in each quadrant was measured. Both groups showed a similar high preference for exploring the former platform-containing quadrant (Fig. 8*D*). In summary, these results indicated that *Chrd*$^{-/-}$ mice have enhanced hippocampal-dependent spatial learning and less exploratory activity in a novel environment but no changes in long-term memory or motor processes.

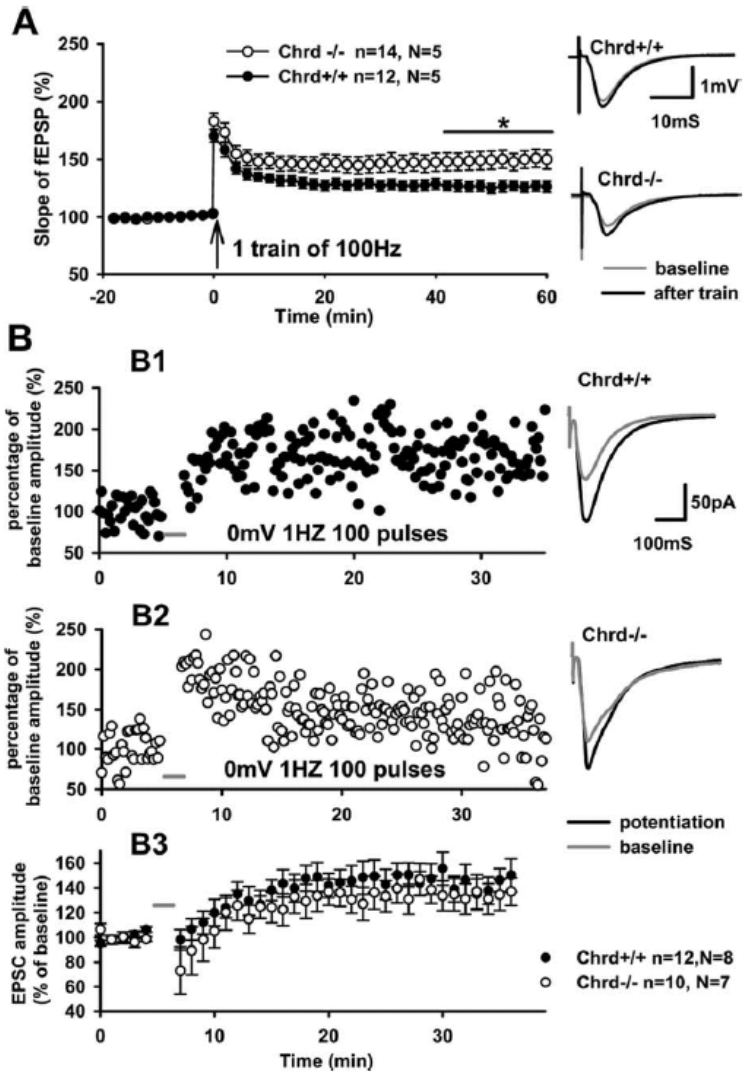

Figure 6. Increase in high-frequency tetanus-induced LTP in *Chrd*$^{-/-}$ slices. ***A***, *Chrd*$^{-/-}$ mice show higher LTP with 100Hz, 1 s protocol. Mean slope of fEPSPs recorded 0–20 min before induction of LTP was set as baseline. Number of analyzed slices (*n*) and animals (*N*) are indicated. Representative sweeps are shown on the right. ***B***, Pairing protocol-induced postsynaptic-specific LTP is normal in *Chrd*$^{-/-}$ slices. ***B1***, Sample recording from *Chrd*$^{+/+}$ slice. ***B2***, Sample recording from *Chrd*$^{-/-}$ slice. ***B3***, Accumulated data from two genotypes for pairing protocol-induced LTP. As shown in the right, there is no difference between genotypes after 30 min.

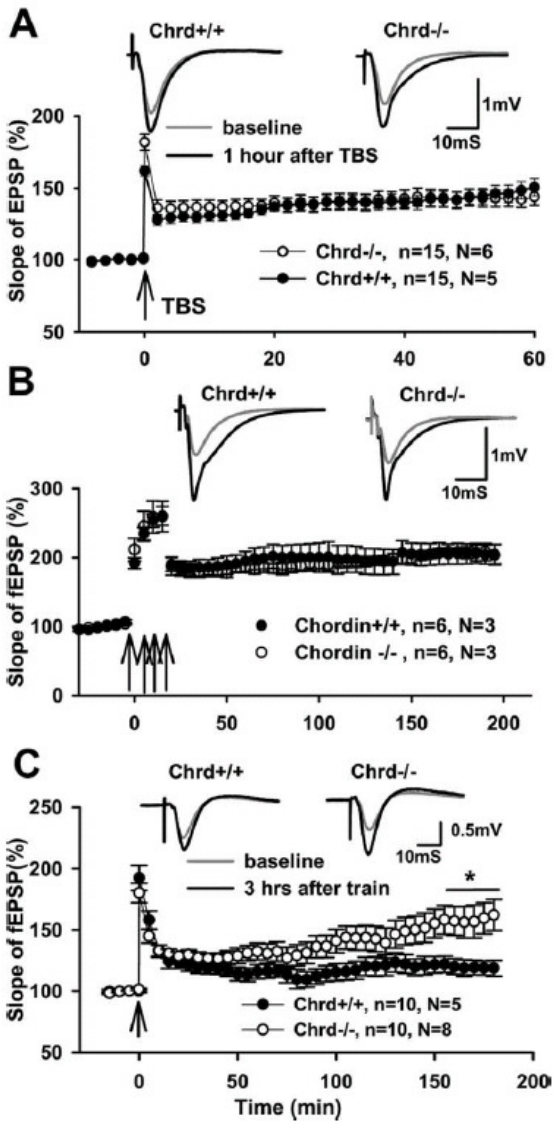

Figure 7. Transition from early-phase LTP to late-phase LTP. ***A***, TBS protocol induced a similar level of LTP in *Chrd*$^{-/-}$ and *Chrd*$^{+/+}$ slices. Mean amplitudes of fEPSPs recorded 0–10 min before induction of LTP were set as a baseline. Above the summary plot are shown an average baseline sweep and a sweep 1 h after induction. ***B***, A train of 100 Hz in 1 s given four times with a 5 min interval induces late-phase LTP at the same level from both *Chrd*$^{-/-}$ and *Chrd*$^{+/+}$ slices. Averaged sweeps of baseline and 3 h after induction are shown above the accumulated plot. ***C***, In a submerged recording chamber, early-phase LTP induced by one train of 100 Hz lasts longer than 3 h. The average slope of fEPSP of the last 20 min showed a significant difference between *Chrd*$^{-/-}$ and *Chrd*$^{+/+}$ slices. (158.8 ± 12.8 vs 120.6 ± 5.7; $p < 0.05$, *t* test)

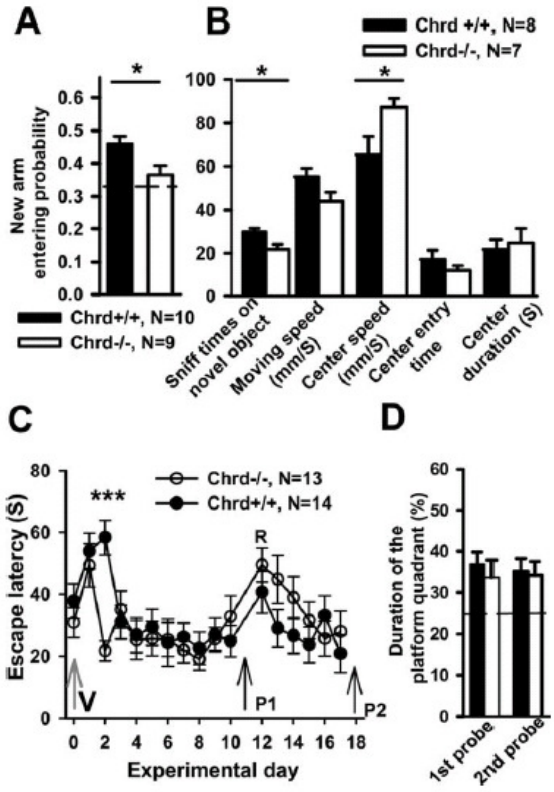

Figure 8. Cognitive behavior in *Chrd*$^{-/-}$ mice. ***A***, *Chrd*$^{-/-}$ mice showed less entry time to the formerly closed arm during a recall test of Y-maze. Dashed line is the random possibility for the new arm 0.33. ***B***, *Chrd*$^{-/-}$ mice showed less interaction with a novel object and faster running speed inside the center of an open field. *Chrd*$^{-/-}$ mice show no difference in locomotive speed in areas outside the center compared with *Chrd*$^{+/+}$ mice. *Chrd*$^{-/-}$ mice showed no significant change of center entry time and center staying time. ***C***, In a water maze test, *Chrd*$^{-/-}$ mice showed shorter escape latency on the second day of learning. ***C*** shows the escape latency plotted against training day. On day 0, (V) refers to cued platform; on days 1–17, a hidden platform was used. P1 and P2 indicate day 11 probe test and day 18 probe test. R means start of reversal test, in which the hidden platform was moved to an adjacent quadrant. ***D***, On day 11, the platform was removed from the pool and mice were given 60 s to explore the pool. Both *Chrd*$^{-/-}$ and *Chrd*$^{+/+}$ mice showed a similar higher preference for exploring the quadrant in which the platform used to be located. After the reversal on day 13, a second probe test was given on day 18, and again no difference between genotypes is seen in their preference for exploring the quadrant in which the platform used to be located. Dashed line indicates the 25% possibility of random selection for the target quadrant.

Discussion

The studies we describe here indicate that loss of the chordin, a potent inhibitor of BMP signaling that alters synaptic activity in the mouse hippocampus resulting in learning and behavior changes, and its invertebrate homolog Sog, are key regulators of BMP signaling in early development (Garcia Abreu et al., 2002). Approximately 50% of *Chrd*$^{-/-}$ null mutants survive to produce healthy breeding adults, likely attributable to functional redundancy with other BMP inhibitors such as Noggin (Bachiller et al., 2000). Our morphological analysis does not support a role for chordin in regulating spinogenesis and dendritogenesis in the hippocampus. However, at the ultrastructure level, *Chrd*$^{-/-}$ mice showed abnormal presynaptic structural organization. There was an increase of docked vesicles per active zone length and a smaller synaptic cleft width. Because the shape of axon terminal determines the vesicle release probability and cycling speed (Xu-Friedman and Regehr, 2004), the change of distribution of vesicles and synaptic width might contribute to the enhanced short-term plasticity and spatiotemporal processing (Fortune and Rose, 2001) that we see in *Chrd*$^{-/-}$ mice. Although

it is not entirely clear whether these ultrastructural changes are the result of earlier neonatal developmental differences or whether they represent later effects brought about by enhanced BMP signaling in the adult, we favor the latter because we can replicate several of the physiological effects of genetic chordin loss, such as enhanced PPF and mini frequency, by perfusing slices with BMPs. In addition, downregulation of BMP signaling by perfusion of Noggin, a potent BMP inhibitor, decreased mEPSC frequency.

Interestingly, the ultrastructural changes and differences in physiology in *Chrd*$^{-/-}$ mice are the opposite of what is seen at the *Drosophila* NMJ when BMP signaling is compromised. In *Drosophila*, a reduction in BMP signaling leads to loss of adhesion between the presynaptic and postsynaptic membranes and a decrease in mini release probability (Aberle et al., 2002; Marques et al., 2002). Although these results are from different organisms, they are consistent with the view that loss of chordin enhances BMP signaling in the nervous system.

Are the chordin effects on hippocampal function mediated by a canonical BMP signaling pathway?

Although we show here that all of the pyramidal cells in the hippocampus exhibit high levels of pSmad accumulation, we were unable to demonstrate any enhancement in the overall level of Smad1/5 phosphorylation in *Chrd*$^{-/-}$ animals by either immunohistochemistry or Western blots. We favor noncanonical pathway involvement for several reasons. First, the effects we see during perfusion of BMPs on slices are rapid and inconsistent with the time that would be required for a genomic-based transcriptional response. Second, hippocampal specific removal of Smad4, the common Smad that is thought to be required for most Smad-dependent transcriptional responses, produces no significant electrophysiological changes in the dentate gyrus (Zhou et al., 2003) or in CA1, nor does its removal alter performance in the Morris water maze (Sun et al., 2006).

In both vertebrates and *Drosophila*, the association of the BMP type II receptor with LIM kinase mediates changes in the cytoskeletal architecture at the synapse (Foletta et al., 2003; Lee-Hoeflich et al., 2004; Eaton and Davis, 2005), which could potentially contribute to the abnormal presynaptic ultrastructure in *Chrd*$^{-/-}$ mice and the effect of BMP6 on transmitter release through a non-Smad-dependent mechanism.

Another likely target for a noncanonical BMP effect is the MAPK-dependent phosphorylation of synapsin I. Mice expressing a constitutively active form of H-Ras exhibited several presynaptic changes similar to *Chrd*$^{-/-}$ mice (Kushner et al., 2005). The presynaptic effect of H-Ras activation is mediated by synapsin I, consistent with alterations in vesicle trafficking as being the primary mechanism behind the changes. The fact that TGF-β1 could phosphorylate synapsin I through MAPK (Chin et al., 2002, 2006) suggests that the serine/threonine kinase activity of BMP receptors might also be able to mediate vesicle release machinery through this mechanism. The colocalization of BMPRII and synapsin I is consistent with this possibility (Fig. 1*E*,*F*).

Another interesting attribute of the BMP signaling effects is the distinction in the responses to different ligand subfamilies. Although we see that perfusion of BMP6 can replicate some of the loss of chordin effects, BMP2, which is equally or more active on a per mole basis for stimulating Smad phosphorylation in tissue culture, is unable to stimulate PPF or enhance mini release on hippocampal slices. Similarly, BMP2 was unable to regulate ionotropic glutamate receptor activity in the retina compared with BMP7 (Shen et al., 2004). *Drosophila* Gbb (glass-bottom boat), a close relative of BMP6 and BMP7, regulates both NMJ and interneuronal synapse activity, whereas Dpp (decapentaplegic, an ortholog of BMP2 and BMP4, has no effect (Baines, 2004). Although not examined in great detail, these ligand subfamilies (BMP2/4 and BMP5/6/7) appear to have differential binding affinities for different combinations of BMP receptors, which could explain their different properties in regulating neuronal plasticity.

Presynaptic plasticity and function of BMPs

Short-term plasticity is very critical for computational functions in the cortical network (Abbott and Regehr, 2004). *Chrd*$^{-/-}$ mutants showed normal basic excitatory synaptic transmission in CA1 but produced novel presynaptic phenotypes in which both PPF and the frequency of mEPSCs increased significantly. This phenomenon conflicts with classical quantal release theory. In principle, the increase of release probability or higher frequency of mEPSC should be accompanied by a decrease instead of an increase in PPF. However, if BMP signaling regulates vesicle fusion, then it is reasonable to see an increase of mEPSC frequency and PPF at the same time, similar to that seen in Rab3a knock-out mutants (Geppert et al., 1997) or the constitutively activated H-Ras example described above.

Although postsynaptic mechanisms have received considerable attention (Malinow and Malenka, 2002), examples of presynaptic contributions to LTP have also been described (Choi et al., 2003; Kushner et al., 2005; Powell, 2006), and a unified model of presynaptic and postsynaptic contributions to LTP at the CA1 hippocampal synapses has recently been proposed (Lisman and Raghavachari, 2006). Our results also suggest that upregulation of vesicle release can enhance LTP induction under certain conditions. High-frequency stimulation of afferent fibers (100 Hz, 1 s) induced significantly larger LTP in *Chrd*$^{-/-}$ hippocampal slices than in controls. Conversely, low-frequency stimulation (paired with direct postsynaptic depolarization) or short bursts of afferent activation (TBS) induced the same level of potentiation in *Chrd*$^{-/-}$ slices and controls. Not only do we find that LTP is selectively enhanced under conditions in which demands on the presynaptic neurons are high (i.e., 100 Hz, 1 s), but also that these conditions elicit a magnified depolarization envelope whereas others (i.e., TBS) do not. These data suggest that LTP augmentation in *Chrd*$^{-/-}$ mutants is attributable to enhancement of presynaptic release properties.

TBS is a popular and "physiological" paradigm for LTP induction that is based on the close interaction of theta (4–8 Hz) and gamma (30–100 Hz) oscillations observed in the hippocampus *in vivo*. However, evidence also suggests that ongoing gamma frequency activity may contribute to memory encoding and selective attention (Varela et al., 2001; Womelsdorf et al., 2006). Our study provides an example of a correlation between LTP induced by extended gamma-frequency stimulation (100 Hz, 1 s) and spatial learning. Thus, the degree to which this high-frequency protocol may mimic *in vivo* plasticity mechanisms deserves further study.

Although *Chrd*$^{-/-}$ mice show improved learning in the water maze test, they showed impairment in the Y-maze, another spatial memory task. One obvious difference between two tests is that Y-maze is based on both intact spatial memory, knowing which arm is new according to the spatial cues around the maze, but also on the innate behavior to explore a new environment. The abnormal performance of *Chrd*$^{-/-}$ in the Y-maze might result from decreased innate exploratory/curiosity behavior. Similarly, during the open-field test, *Chrd*$^{-/-}$ mice interacted less

with a novel object, perhaps indicating they had a decreased curiosity for new objects. However, it also seems possible that, as in the water maze test, *Chrd*$^{-/-}$ mice simply learn faster and require fewer encounters before they no longer perceive the new Y-maze arm or object as novel. Additional studies will be required to distinguish between these possibilities.

Are other extracellular regulators of BMP activity also involved in mediating neural plasticity?

Chordin is unusual among BMP inhibitors because its activity is regulated by metalloproteases of the BMP-1/Tld (tolloid) family. In developmental contexts, BMP-1/Tld-like enzymes degrade chordin and thereby enhance BMP signaling (Blader et al., 1997; Marques et al., 1997). It is interesting to note in this regard that induction of long-term sensitization in *Aplysia* by application of serotonin or by behavioral training both stimulate expression of a BMP-1/Tld homolog (Liu et al., 1997). Might it be that long-term sensitization stimulated by serotonin or behavioral training in *Aplysia* is enhanced or reinforced by up regulating BMP signaling through degradation of chordin by BMP-1/Tld-like proteases? Clearly, additional *in vivo* manipulation of BMP signaling pathway components will be required to fully understand its role in modulating synaptic plasticity in different organisms.

References

Abbott LF, Regehr WG (2004) Synaptic computation. Nature 431:796–803.

Aberle H, Haghighi AP, Fetter RD, McCabe BD, Magalhaes TR, Goodman CS (2002) wishful thinking encodes a BMP type II receptor that regulates synaptic growth in *Drosophila*. Neuron 33:545–558.

Bachiller D, Klingensmith J, Kemp C, Belo JA, Anderson RM, May SR, McMahon JA, McMahon AP, Harland RM, Rossant J, De Robertis EM (2000) The organizer factors Chordin and Noggin are required for mouse forebrain development. Nature 403:658–661.

Bachiller D, Klingensmith J, Shneyder N, Tran U, Anderson R, Rossant J, De Robertis EM (2003) The role of chordin/Bmp signals in mammalian pharyngeal development and DiGeorge syndrome. Development 130:3567–3578.

Baines RA (2004) Synaptic strengthening mediated by bone morphogenetic protein-dependent retrograde signaling in the *Drosophila* CNS. J Neurosci 24:6904–6911.

Blader P, Rastegar S, Fischer N, Strahle U (1997) Cleavage of the BMP-4 antagonist chordin by zebrafish tolloid. Science 278:1937–1940.

Chin J, Angers A, Cleary LJ, Eskin A, Byrne JH (2002) Transforming growth factor beta1 alters synapsin distribution and modulates synaptic depression in *Aplysia*. J Neurosci 22:RC220(1–6).

Chin J, Liu RY, Cleary LJ, Eskin A, Byrne JH (2006) TGF-beta1-induced long-term changes in neuronal excitability in *Aplysia* sensory neurons depend on MAPK. J Neurophysiol 95:3286–3290.

Choi S, Klingauf J, Tsien RW (2003) Fusion pore modulation as a presynaptic mechanism contributing to expression of long-term potentiation. Philos Trans R Soc Lond B Biol Sci 358:695–705.

Dellu F, Mayo W, Cherkaoui J, Le Moal M, Simon H (1992) A two-trial memory task with automated recording: study in young and aged rats. Brain Res 588:132–139.

Derynck R, Zhang YE (2003) Smad-dependent and Smad-independent pathways in TGF-beta family signalling. Nature 425:577–584.

Dudu V, Bittig T, Entchev E, Kicheva A, Julicher F, Gonzalez-Gaitan M (2006) Postsynaptic mad signaling at the *Drosophila* neuromuscular junction. Curr Biol 16:625–635.

Eaton BA, Davis GW (2005) LIM Kinase1 controls synaptic stability downstream of the type II BMP receptor. Neuron 47:695–708.

Foletta VC, Lim MA, Soosairajah J, Kelly AP, Stanley EG, Shannon M, He W, Das S, Massague J, Bernard O (2003) Direct signaling by the BMP type II receptor via the cytoskeletal regulator LIMK1. J Cell Biol 162:1089–1098.

Fortune ES, Rose GJ (2001) Short-term synaptic plasticity as a temporal filter. Trends Neurosci 24:381–385.

Garcia Abreu J, Coffinier C, Larrain J, Oelgeschlager M, De Robertis EM (2002) Chordin-like CR domains and the regulation of evolutionarily conserved extracellular signaling systems. Gene 287:39–47.

Geppert M, Goda Y, Stevens CF, Sudhof TC (1997) The small GTP-binding protein Rab3A regulates a late step in synaptic vesicle fusion. Nature 387:810–814.

Gomes WA, Mehler MF, Kessler JA (2003) Transgenic overexpression of BMP4 increases astroglial and decreases oligodendroglial lineage commitment. Dev Biol 255:164–177.

Harris KM, Sultan P (1995) Variation in the number, location and size of synaptic vesicles provides an anatomical basis for the nonuniform probability of release at hippocampal CA1 synapses. Neuropharmacology 34:1387–1395.

Kushner SA, Elgersma Y, Murphy GG, Jaarsma D, van Woerden GM, Hojjati MR, Cui Y, LeBoutillier JC, Marrone DF, Choi ES, De Zeeuw CI, Petit TL, Pozzo-Miller L, Silva AJ (2005) Modulation of presynaptic plasticity and learning by the H-ras/extracellular signal-regulated kinase/synapsin I signaling pathway. J Neurosci 25:9721–9734.

Law JW, Lee AY, Sun M, Nikonenko AG, Chung SK, Dityatev A, Schachner M, Morellini F (2003) Decreased anxiety, altered place learning, and increased CA1 basal excitatory synaptic transmission in mice with conditional ablation of the neural cell adhesion molecule L1. J Neurosci 23:10419–10432.

Lee-Hoeflich ST, Causing CG, Podkowa M, Zhao X, Wrana JL, Attisano L (2004) Activation of LIMK1 by binding to the BMP receptor, BMPRII, regulates BMP-dependent dendritogenesis. EMBO J 23:4792–4801.

Lein P, Johnson M, Guo X, Rueger D, Higgins D (1995) Osteogenic protein-1 induces dendritic growth in rat sympathetic neurons. Neuron 15:597–605.

Lisman J, Raghavachari S (2006) A unified model of the presynaptic and postsynaptic changes during LTP at CA1 synapses. Sci STKE 2006:re11.

Liu QR, Hattar S, Endo S, MacPhee K, Zhang H, Cleary LJ, Byrne JH, Eskin A (1997) A developmental gene (Tolloid/BMP-1) is regulated in *Aplysia* neurons by treatments that induce long-term sensitization. J Neurosci 17:755–764.

Lynch MA (2004) Long-term potentiation and memory. Physiol Rev 84:87–136.

Malinow R, Malenka RC (2002) AMPA receptor trafficking and synaptic plasticity. Annu Rev Neurosci 25:103–126.

Marques G, Musacchio M, Shimell MJ, Wunnenberg-Stapleton K, Cho KW, O'Connor MB (1997) Production of a DPP activity gradient in the early *Drosophila* embryo through the opposing actions of the SOG and TLD proteins. Cell 91:417–426.

Marques G, Bao H, Haerry TE, Shimell MJ, Duchek P, Zhang B, O'Connor MB (2002) The *Drosophila* BMP type II receptor Wishful Thinking regulates neuromuscular synapse morphology and function. Neuron 33:529–543.

McCabe BD, Marques G, Haghighi AP, Fetter RD, Crotty ML, Haerry TE, Goodman CS, O'Connor MB (2003) The BMP homolog Gbb provides a retrograde signal that regulates synaptic growth at the *Drosophila* neuromuscular junction. Neuron 39:241–254.

Mehler MF, Mabie PC, Zhang D, Kessler JA (1997) Bone morphogenetic proteins in the nervous system. Trends Neurosci 20:309–317.

Morris R (1984) Developments of a water-maze procedure for studying spatial learning in the rat. J Neurosci Methods 11:47–60.

Moustakas A, Heldin CH (2005) Non-Smad TGF-beta signals. J Cell Sci 118:3573–3584.

Pappano WN, Scott IC, Clark TG, Eddy RL, Shows TB, Greenspan DS (1998) Coding sequence and expression patterns of mouse chordin and mapping of the cognate mouse chrd and human CHRD genes. Genomics 52:236–239.

Piccolo S, Sasai Y, Lu B, De Robertis EM (1996) Dorsoventral patterning in *Xenopus*: inhibition of ventral signals by direct binding of chordin to BMP-4. Cell 86:589–598.

Powell CM (2006) Gene targeting of presynaptic proteins in synaptic plasticity and memory: across the great divide. Neurobiol Learn Mem 85:2–15.

Rawson JM, Lee M, Kennedy EL, Selleck SB (2003) *Drosophila* neuromuscular synapse assembly and function require the TGF-beta type I receptor saxophone and the transcription factor Mad. J Neurobiol 55:134–150.

Rhinn M, Picker A, Brand M (2006) Global and local mechanisms of forebrain and midbrain patterning. Curr Opin Neurobiol 16:5–12.

Sasai Y (2001) Regulation of neural determination by evolutionarily conserved signals: anti-BMP factors and what next? Curr Opin Neurobiol 11:22–26.

Scott IC, Steiglitz BM, Clark TG, Pappano WN, Greenspan DS (2000) Spatiotemporal expression patterns of mammalian chordin during postgastrulation embryogenesis and in postnatal brain. Dev Dyn 217:449–456.

Shen W, Finnegan S, Lein P, Sullivan S, Slaughter M, Higgins D (2004) Bone morphogenetic proteins regulate ionotropic glutamate receptors in human retina. Eur J Neurosci 20:2031–2037.

Shi Y, Massague J (2003) Mechanisms of TGF-beta signaling from cell membrane to the nucleus. Cell 113:685–700.

Soderstrom S, Bengtsson H, Ebendal T (1996) Expression of serine/threonine kinase receptors including the bone morphogenetic factor type II receptor in the developing and adult rat brain. Cell Tissue Res 286:269–279.

Strasser GA, Rahim NA, VanderWaal KE, Gertler FB, Lanier LM (2004) Arp2/3 is a negative regulator of growth cone translocation. Neuron 43:81–94.

Sun M, Bofenkamp L, Deng CX, O'Connor MB (2006) Impairment of new environment cognition in mice with hippocampal deletion of Samd4. Soc Neurosci Abstr 32:750.756.

Varela F, Lachaux JP, Rodriguez E, Martinerie J (2001) The brainweb: phase synchronization and large-scale integration. Nat Rev Neurosci 2:229–239.

Withers GS, Higgins D, Charette M, Banker G (2000) Bone morphogenetic protein-7 enhances dendritic growth and receptivity to innervation in cultured hippocampal neurons. Eur J Neurosci 12:106–116.

Womelsdorf T, Fries P, Mitra PP, Desimone R (2006) Gamma-band synchronization in visual cortex predicts speed of change detection. Nature 439:733–736.

Xu B, Gottschalk W, Chow A, Wilson RI, Schnell E, Zang K, Wang D, Nicoll RA, Lu B, Reichardt LF (2000) The role of brain-derived neurotrophic factor receptors in the mature hippocampus: modulation of long-term potentiation through a presynaptic mechanism involving TrkB. J Neurosci 20:6888–6897.

Xu-Friedman MA, Regehr WG (2004) Structural contributions to short-term synaptic plasticity. Physiol Rev 84:69–85.

Zakharenko SS, Patterson SL, Dragatsis I, Zeitlin SO, Siegelbaum SA, Kandel ER, Morozov A (2003) Presynaptic BDNF required for a presynaptic but not postsynaptic component of LTP at hippocampal CA1-CA3 synapses. Neuron 39:975–990.

Zhao GQ (2003) Consequences of knocking out BMP signaling in the mouse. Genesis 35:43–56.

Zhou YX, Zhao M, Li D, Shimazu K, Sakata K, Deng CX, Lu B (2003) Cerebellar deficits and hyperactivity in mice lacking Smad4. J Biol Chem 278:42313–42320.

Rachel Herder <herde018@umn.edu>

Copyright permission request- for Ph.D. thesis

4 messages

Rachel Herder <herde018@umn.edu> Thu, Jun 21, 2012 at 5:53 PM
To: jnpermissions@sfn.org

I would like to obtain permission to reprint copyrighted materials from an article that I am a co-author on printed in the Journal of Neuroscience in 2007. I would like to reprint two figures in my Ph.D. thesis, to be published in August 2012.

Attached is my request letter. Please let me know if you have any questions. I look forward to hearing from you.

Kindest regards,
Rachel Herder

--
Rachel J. Herder
herde018@umn.edu / 303.522.3094

J.D. / Ph.D. student in Molecular, Cellular, Developmental Biology & Genetics
Joint Degree Program in Law, Health and the Life Sciences
University of Minnesota; Genetics Cell Biology & Development Department
6-160 Jackson Hall; 321 Church St. SE; Minneapolis MN 55455

Journal of Neuroscience- copyright letter.doc
25K

jn permissions <jnpermissions@sfn.org> Fri, Jun 22, 2012 at 9:00 AM
To: Rachel Herder <herde018@umn.edu>, jn permissions <jnpermissions@sfn.org>

Dear Rachel Herder,

Thank you for your email. Since you are an author on the original article listed below and directly involved in the re-use, permission is granted to reproduce the requested material listed below with NO fee in print and electronic format for use in your doctoral thesis/dissertation.

Please contact me if you have any questions or if you need another form of permission.

Respectfully,

SfN Central Office

SfN Article: *Mu Sun, Mark Thomas,* ***Rachel Herder****, M. Lisa Bofenkamp, Scott B. Selleck, and Michael B. O'Connor. (2007). Presynaptic Contributions of Chordin to Hippocampal Plasticity and Spatial Learning. The Journal of Neuroscience, 27(29):7740-7750.*

From: Rachel Herder [mailto:herde018@umn.edu]
Sent: Thursday, June 21, 2012 6:53 PM
To: jn permissions
Subject: Copyright permission request- for Ph.D. thesis

[Quoted text hidden]

Rachel Herder <herde018@umn.edu> Tue, Aug 14, 2012 at 4:11 PM
To: jn permissions <jnpermissions@sfn.org>

Dear JN Permissions,

I am writing to request a change in the journal permission that I requested a few months ago - I would like to insert the full text of the article in my Ph.D. thesis.

Originally, I had requested permission to reproduce only one figure and one table but one of my Ph.D. thesis reviewers requested that I include the entire article in an appendix of my thesis. Am I allowed make this change and insert the full text of the article?

This is the article I am referring to (I am an author):
SfN Article: *Mu Sun, Mark Thomas,* ***Rachel Herder****, M. Lisa Bofenkamp, Scott B. Selleck, and Michael B. O'Connor. (2007). Presynaptic Contributions of Chordin to Hippocampal Plasticity and Spatial Learning. The Journal of Neuroscience, 27(29):7740-7750.*

Please let me know if you have any questions.

Kindest regards,
Rachel Herder
[Quoted text hidden]

---

jn permissions <jnpermissions@sfn.org> Wed, Aug 15, 2012 at 8:18 AM
To: Rachel Herder <herde018@umn.edu>
Cc: jn permissions <jnpermissions@sfn.org>

Dear Rachel,

Thank you for letting us know of the change. Permission is granted to reproduce the requested material listed below with NO fee in print and electronic format for use in your doctoral thesis/dissertation.

Please contact me if you have any questions or if you need another form of permission.

Regards,

Chanelle Grannum

SfN Central Office

Journal of Neuroscience

***SfN Article**: Mu Sun, Mark Thomas, Rachel Herder, M. Lisa Bofenkamp, Scott B. Selleck, and Michael B. O'Connor. (2007). Presynaptic Contributions of Chordin to Hippocampal Plasticity and Spatial Learning. The Journal of Neuroscience, 27(29):7740-7750.*

From: Rachel Herder [mailto:herde018@umn.edu]
Sent: Tuesday, August 14, 2012 5:12 PM
To: jn permissions
Subject: Re: Copyright permission request- for Ph.D. thesis

[Quoted text hidden]

Figure 20: Copyright permission from Journal of Neroscience
Email correspondence with Chanelle Grannum from the SfN Central Office granting copyright permission to reprint the full text version of the Sun et al. (2007) article in this doctoral thesis.

APPENDIX C: TABLE OF PRIMERS

Here is a table of primers used in this thesis. Electronic copy left with MBO.

	Primer name	Accession /Annotation	Forward (5' - 3')	Reverse (5' - 3')	Size (bp)	Ta	Notes:
Bombyx Project	*Bm-RpL3*	AY769292.1	CGTCGTCATCGTGGTAAGGTCAAG	GGTCTCAATGTATCCAACAACACCGACAC	219	68	
	Bm-dib	NM_001043488.1	CGATACAACAGCCTACACGACAAGCTTCG	CCTTCTGCAGCCATCTACCTATTCCAATCG	221	68	
	Bm-MSBP	AY4044777.1	GGCAAGAGATTTTATGGACCGGGAGG	CCCCTAAACTGCTCTTCCCATTCTATGG	176	68	
	Bm-CYP4G25	DQ443326.1	GCTTGCTGACAAACTAAATGG	GAAAGACGAGGAGACGAGGT	167	–	Did not amplify.
	Bm-Bras1	AB176555.1	GTTCACTCGGCATCGTCTGT	CAAACAACCAGTCCCTTTATG	106	–	Did not amplify.
	Bm-iF-4Ebp	DQ443244.1	ACGCTATCCTTCGCCATCAA	ATTTACAGGGACTCTTCCTTCTCTC	106	68	
	Bm-HpC19	NM_001101727	ATACGAGGAGAAGAAGAGCGAAGT	GAACTCAACTGGGAAACAATCC	145	–	Did not amplify.
EERIE Project	*Dm-Rpl23*	NM_079089.3	GACAACACCGGAGCCAAGAACC	GTTTGCGCTGCCGAATAAGCAC	172	65	From H. Ono
	e-GFP	AF242365 (pH-Stinger)	AAGTCGTGCTGCTTCATGTG	ACGTAAACGGCCACAATGTC	186	65	
	PhmPromF1	5' *phm* (CG6578)	(AATAGATCT)GCTGCTCCTTTGTCCACAGAT				
	PhmPromF2	5' *phm* (CG6578)	(AATAGATCT)CGGCATATATTTTATGGGTCTGC				
	PhmPromF3	5' *phm* (CG6578)	(AATAGATCT)AGGTAGACGGTCGATTGAATA				
	PhmPromF3.1	5' *phm* (CG6578)	(AATAGATCT)TCGAACTGATCCCAGATTTCTAC				
	PhmPromF3.2	5' *phm* (CG6578)	(AATAGATCT)TGGGTGTAATGAATGTGCATAC				
	PhmPromF3.3	5' *phm* (CG6578)	(AATAGATCT)GATGCCGAAACCCTGTATGCT				
	PhmPromF4	5' *phm* (CG6578)	(AATAGATCT)GTATATGGTATATATGGTGTGGCA				
	PhmPromF5	5' *phm* (CG6578)	(AATAGATCT)GAGAATCTGGGAAACCAAGAAG				
	PhmPromR1	5' *phm* (CG6578)		(AATAGCTAGC)CACTTTCGATTTCCTCCTGCTC			
	PhmPromR2	5' *phm* (CG6578)		(AATAGCTAGC)CTTCTTGGTTTCCCAGATTCTC			
	PhmPromR3	5' *phm* (CG6578)		(AATAGCTAGC)TGCCACACCATATATACCATATAC			
	PhmPromR4	5' *phm* (CG6578)		(AATAGCTAGC)AAGGAGAGTGCGAAAGTAAAATT			
	ups-spok1	5' *spok* (CG41624)	TCTTATATACAAAAACCCTTTCCAACA	ATCTAGACGTACAGATGGGCAGA			
	ups-spok2	5' *spok* (CG41624)	CTAGATGCTGGATGGTTTCC	ATCAAGAGAATTCCGCTAGATAAC			
	ups-spok3	5' *spok* (CG41624)	TGATTATAGGGACCCCTACGC	TCACGCCCACACTTTTAATTT			
	ups-spok4	5' *spok* (CG41624)	CAAAAACTGTTTGCCATTCC	CGGATATCTAATGGCATTCTCTC			
	ups-spok5	5' *spok* (CG41624)	GGCTTTAAGGCGTTAGAAGAGG	ACTAATGAACTTATCAACAACCCTAAT			
	ups-spok6	5' *spok* (CG41624)	CTAGTGTGAATGCGAACGATAA	TTTTATATTTGTTTGTATCGATTTGTC			
	ups-spok7	5' *spok* (CG41624)	TTG ATG GGG CTT ATG TCA TC	TGGTTTTGTTTAACTTTTCTCTCC			
	Br1-spok for	sdm of Br site 1 in spok	CGGCGCCAGTGTGCTGGAATTCGCCCTTTCCATATGCGACGAACCCTTTCCAACAACAATAAAATTTCATAGGTCAAACGC				
	Br1-spok rev	sdm of Br site 1 in spok	GCGTTTGACCTATGAAATTTTATTGTTGTTGGAAAGGGTTCGTCGCATATGGAAAGGGCGAATTCCAGCACACTGGCGGCCG				
	Br2-spok for	sdm of Br site 2 in spok	GAGTATACTATAGATGCTGGATGGTTTCCGATACCACATATGCGACGACTTCATGATCCGGATTACTTGTCGGGTCGATCTAACCG				
	Br2-spok rev	sdm of Br site 2 in spok	CGGTTAGATCGACCCGACAAGTAATCCGGGATCTATGAAGTCGTCGCATATGTGGTATCGGAAACCATCCAGCATCTAGTATACTC				
	dib-A	3' UTR of *dib* (CG12028)	CTGATCGATCTGCGATTGCGT	TCGGATGATGGACTCCTCCCTGC			
	dib-B	5' *dib* (CG12028)	TGCTCAAAGGGGAAGAAAAGCCCC	TGGCAAAGGTGCACTGCCTCGCTTAAGATCGA			
	dib-C	intron 2 of *dib* (CG12028)	CGTCAGAATTCTGCTGCCCAAGCTCACCAGA	ACTGCAGACGAGCTCCAAAGGT			
	dib170	intron 3 of *dib* (CG12028)	GTGGGCGTGGGCAGGATTCTTAA	GTGCTGCTCCACAGCCGACAGG	170		
	dib190	intron 4 of dib (CG12028)	TCTGGTCCTTCCCTTCGGTCACG	ATTCGTATTCACGCAGCAGCTGA	190		
	dib420	intron 3+4 of *dib*	GTGGGCGTGGGCAGGATTCTTAA	ATTCGTATTCACGCAGCAGCTGA	420		
	Br1-Dib for	sdm of Br site 1 in dib	GCCCGCGTTTGCGGGAGCAGAATATGCACATTTTGCTTCTCAGGGTGAGCTCATATGCGACGACCAGCACTTTGCGGTCTCC				
	Br1-Dib rev	sdm of Br site 1 in dib	GAAGACCGCAAAGTGCTGGTCGTCGCATATGAGCTCACCCTGAGAAGCAAATGTGCATATTCTGCTCGGCCAAACGGCGGGC				
	Br2-Dib for	sdm of Br site 2 in dib	GGGTGAGCTAACGGAAAACAGATCAGCACTTTGCGGTCTCCAAAATAGTGTCCACATATGCGACGCATTGAACCGATTTGC				
	Br2-Dib rev	sdm of Br site 2 in dib	GCAAATCGGTTCAATGCGTCGCATATGTGGACCACTATTTTGGAGACCGCAAAGTGCTGATCTGTTTCCGTTAGCTCACCC				

APPENDIX D: TABLE OF FLY STOCKS

Here is a table of Fly Stocks used in this thesis. Electronic version left with MBO.

Gene	region	line	[Description]>GFP	Forward Primer	Reverse Primer	Construct	made by	vial name	X, 2, 3	RJH vial #	3G expression	RG expression	picture files	Injection company
Spookier														
	1.45 ups-spok	1	1.45 kb upstream (ups) spok				MJO-construct; RJH-balancing	1.45 ups-spok>GFP; #1	H on III; TM6 ft	RJH 1-1	no	yes-strong		Duke
	1.45 ups-spok	25	"				"	1.45 ups-spok>GFP; #25	H on III; TM6 ft	RJH 1-2	no	yes-strong		Duke
	1.45 ups-spok	37	"				"	1.45 ups-spok>GFP; #37	X	RJH 1-3	no	yes-strong		Duke
	1.45 ups-spok	58	"				"	1.45 ups-spok>GFP; #58	H on II; CyO ft	RJH 1-4	no	yes-strong		Duke
	ups-spok1	32	(-1 to -300) ups spok	tct tat ata caa aaa ccc ttt cca	atc tag acg tac aga tgg gca ga		RJH	ups-spok1-32>GFP		n/a-dead stock	yes	yes		Duke
	ups-spok1	33a	"	"	"		RJH	ups-spok1-33a>GFP	H on III	RJH 1-5	yes	yes-strong		Duke
	ups-spok1	74c	"	"	"		RJH	ups-spok1-74c>GFP	H on III	RJH 1-6	yes	yes-strong		Duke
	ups-spok1	80a	"	"	"		RJH	ups-spok1-80a>GFP	H on II	RJH 1-7	yes	yes-strong		Duke
	ups-spok1	84a	"	"	"		RJH	ups-spok1-84a>GFP	H on II	RJH 1-8	yes	yes-strong		Duke
					atc aag aga att ccg cta gat									
	ups-spok2	13	(-190 to -463) ups spok	cta gat gct gga tgg ttt cc	aac		RJH	ups-spok2-13>GFP	over CyO'	RJH 1-9	yes	no		Duke
	ups-spok2	34a	"	"	"		RJH	ups-spok2-34a>GFP	over CyO'	RJH 1-10	yes	no		Duke
	ups-spok2	40	"	"	"		RJH	ups-spok2-40d>GFP	H on III	RJH 1-11	yes	no		Duke
	ups-spok3	1	(-314 to -601) ups spok	tga tta tag gga ccc cta cgc	tca cgc cca cac ttt taa ttt		RJH	ups-spok3-1>GFP	H on III	RJH 1-12	yes	no		Duke
	ups-spok3	2	"	"	"		RJH	ups-spok3-2>GFP	H on II	RJH 1-13	yes	no		Duke
	ups-spok3	4	"	"	"		RJH	ups-spok3-4a>GFP	X	RJH 1-14	yes	no		Duke
	ups-spok3	7	"	"	"		RJH	ups-spok3-7>GFP	--	n/a-dead stock	yes	no		Duke
	ups-spok3	45b	"	"	"		RJH	ups-spok3-45b>GFP	H on III	RJH 1-15	yes	faint		Duke
	ups-spok3	56	"	"	"		RJH	ups-spok3-56>GFP	H on II	RJH 1-16	yes	no		Duke
	ups-spok3	76	"	"	"		RJH	ups-spok3-76>GFP	H on III	RJH 1-17	yes	no		Duke
	ups-spok4	11a	(-467 to -737) ups spok	caa aaa ctg ttt gcc att cc	cgg ata tct aat ggc att ctc tc		RJH	ups-spok4-11a>GFP	H on II; CyO ft	RJH 1-18	yes	no		Duke
	ups-spok5	20	(-610 to -901) ups spok	ggc ttt aag gcg tta gaa gag g	act aat gaa ctt atc aac aac cct aat		RJH	ups-spok5-20>GFP	H on III	RJH 1-19	yes	no		Duke
	ups-spok5	21b	"	"	"		RJH	ups-spok5-21b>GFP	X	RJH 1-20	no	no		Duke
	ups-spok5	23a	"	"	"		RJH	ups-spok5-23a>GFP	H on III	RJH 1-21	yes	no		Duke
	ups-spok5	84	"	"	"		RJH	ups-spok5-84>GFP	H on II	RJH 1-22	yes	no		Duke
					ttt tat att tgt ttg tat cga ttt									
	ups-spok6	30a	(-745 to -1017) ups spok	cta gtg tga atg cga acg ata a	gtc		RJH	ups-spok6-30a>GFP	X	RJH 1-23	no	no		Duke
	ups-spok7	Id	(-901 to -1191) ups spok	ttg atg ggg ctt atg tca tc	tgg ttt tgt tta act ttt ctc tcc		RJH	ups-spok7-Id>GFP	H on III	RJH 1-24	yes	no		Duke
	ups-spok7	5a	"	"	"		RJH	ups-spok7-5a>GFP	over TM6	RJH 1-25	yes	no		Duke
	ups-spok7	17	"	"	"		RJH	ups-spok7-17>GFP	H on II; CyO ft	RJH 1-26	yes	no		Duke
	ups-spok7	56	"	"	"		RJH	ups-spok7-56>GFP	H on III	RJH 1-27	yes	no		Duke
	ups-spok8	--	(-1056 to -1336) ups spok	ttt ggg cgg ttc tca ttt ta	act ttt tcg tca tcg cca tt		RJH+OZ							Duke
						primers								
	ups-spok9	--	(-1203 to -1450)	aca acc atc ggt cag cac ag	ggg cta aat ctt ccg ata agc	didn't work	RJH+OZ							
	spok1M-6	1					RJH+OZ	ups-spok1-M6-1>GFP	III	RJH 1-72	yes-faint	yes-strong		Best Gene
	spok1M-6	2					RJH+OZ	ups-spok1-M6-2>GFP	III	RJH 1-73	yes-faint	yes		Best Gene
	spok1M-6	3					RJH+OZ	ups-spok1-M6-3>GFP	X	RJH 1-74	yes	yes-strong		Best Gene
	spok1M-6	4					RJH+OZ	ups-spok1-M6-4>GFP	III	RJH 1-75	no	yes-strong		Best Gene
	spok1M-6	5					RJH+OZ	ups-spok1-M6-5>GFP	III	RJH 1-76	no	no		Best Gene
	spok1M-6	6					RJH+OZ	ups-spok1-M6-6>GFP	III	RJH 1-77	no	no		Best Gene
	spok1M-6	7					RJH+OZ	ups-spok1-M6-7>GFP	III	RJH 1-78	yes	yes-strong		Best Gene
	spok1M-6	8					RJH+OZ	ups-spok1-M6-8>GFP	III	RJH 1-79	yes	yes-strong		Best Gene
	spok1M-6	9					RJH+OZ	ups-spok1-M6-9>GFP	III	RJH 1-80	yes	yes-strong		Best Gene
	spok1M-6	10					RJH+OZ	ups-spok1-M6-10>GFP	X	RJH 1-81	yes-faint	yes-strong		Best Gene
	spok1M5	1					RJH+OZ	ups-spok1-M5-1>GFP	2	RJH 1-94	yes	yes-faint		Best Gene
	spok1M5	2					RJH+OZ	ups-spok1-M5-2>GFP	3	RJH 1-95				Best Gene
	spok1M5	3					RJH+OZ	ups-spok1-M5-3>GFP	2	RJH 1-96	yes	yes-strong		Best Gene
	spok1M5	4					RJH+OZ	ups-spok1-M5-4>GFP	X	RJH 1-97	yes	yes-strong		Best Gene
	spok1M5	5					RJH+OZ	ups-spok1-M5-5>GFP	2	RJH 1-98	yes	yes-strong		Best Gene
	spok1M5	6					RJH+OZ	ups-spok1-M5-6>GFP	3	RJH 1-99	yes	yes-strong		Best Gene
	spok1M4	1					RJH+OZ	ups-spok1-M4-1>GFP	2	RJH2-01	yes	yes		
	spok1M4	2					RJH+OZ	ups-spok1-M4-2>GFP	3	RJH2-02				
	spok1M4	3					RJH+OZ	ups-spok1-M4-3>GFP	2	RJH2-03	yes	yes		
	spok1M4	4					RJH+OZ	ups-spok1-M4-4>GFP	x	RJH2-04	yes	yes		
	spok1M4	5					RJH+OZ	ups-spok1-M4-5>GFP	2	RJH2-05				
	spok1M4	6					RJH+OZ	ups-spok1-M4-6>GFP	2	RJH2-06	yes	yes		
	spok1M4	7					RJH+OZ	ups-spok1-M4-7>GFP	2	RJH2-07				
	spok1M4	8					RJH+OZ	ups-spok1-M4-8>GFP	2	RJH2-08	yes	yes		
	spok1M3	1					RJH+OZ	ups-spok1-M3-1>GFP	x	RJH 1-90	yes	yes		Best Gene
	spok1M3	2					RJH+OZ	ups-spok1-M3-2>GFP	2	RJH 1-91	yes	yes		Best Gene
	spok1M3	3					RJH+OZ	ups-spok1-M3-3>GFP	x	RJH 1-92				Best Gene
	spok1M3	4					RJH+OZ	ups-spok1-M3-4>GFP	2	RJH 1-93	yes	yes		Best Gene
Phantom														
	1.196 bp						lab stock?			--				
	800bp phm (F2-R1)					pMBO 2453	lab stock; ecd 3; #73	phm>GFP.nls F2-22A2 (800 bp)		RJH 1-28		[yes]-MJ		
	700 bp phm (F3+R1)					pMBO 2454	lab stock			--		[yes]-MJ		
	600 bp phm (F3-R2)					pMBO2467	lab stocks			--		[yes]-MJ		
	250 bp phm (F3+R3)					pMBO2468	lab stocks			--		[yes]-MJ		
	600 bp phm (F3.1-R1)					pMBO2464	lab stocks			--		[yes]-MJ		
	500 bp phm (F3.2-R1)					pMBO2465	lab stocks			--		[yes]-MJ		
	69 bp phm					pMBO 2491	lab stock; ecd 5; #5	phm>GFP.nls.291>482 (F3.21-R4) (69 bp)		RJH 1-29		[yes]-MJ		
	400 bp phm (F3.3-R1)					pMBO 2466	lab stocks					[no]-MJ		
	400 bp phm (F4-R1)					pMBO 2455	lab stocks					[no]-MJ		
	150 bp phm (F5-R1)					pMBO 2456	lab stocks					[no]-MJ		
	69-phm.mot-1	3a					KR-DZ,RJH balance	69-phm.mot-1-3a>GFP	H on III	RJH 1-30	yes	no		Duke
	69-phm.mot-1	30a					KR-DZ,RJH balance	69-phm.mot-1-30a>GFP	over TM6	n/a-dead stock	yes	no		Duke
	69-phm.mot-1	31a					KR-DZ,RJH balance	69-phm.mot-1-31a>GFP	H on III; TM6 ft	RJH 1-31	yes	no	Used in PPT	Duke
	69-phm.mot-1	31c					KR-DZ,RJH balance	69-phm.mot-1-31c>GFP	H on III; TM6 ft	RJH 1-32				Duke
	69-phm.mot-1	43b					KR-DZ,RJH balance	69-phm.mot1-43b>GFP	H on III	RJH 1-33	yes	no		Duke
	69-phm.mot-1	55a					KR-DZ,RJH balance	69-phm.mot1-55a>GFP	H on III	RJH 1-34	no	no		Duke
	69-phm.mot-1	61b					KR-DZ,RJH balance	69-phm.mot1-61b>GFP	H on III	n/a-dead stock	yes	no		Duke
	69-phm.mot-2	7a					KR-DZ,RJH balance	69-phm.mot2-7a>GFP		RJH 1-35	yes-in some anim	no		Duke
	69-phm.mot-2	11c					KR-DZ,RJH balance	69-phm.mot2-11c>GFP	H on II; CyO ft	RJH 1-36	yes	no		Duke
	69-phm.mot-2	17b					KR-DZ,RJH balance	69-phm.mot2-17b>GFP	H on II; CyoO' ft	n/a-dead stock	yes	no	Used in PPT	Duke
	69-phm.mot-2	22a					KR-DZ,RJH balance	69-phm.mot2-22a>GFP	over TM6	RJH 1-37	yes	yes		Duke
	69-phm.mot-2	29b					KR-DZ,RJH balance	69-phm.mot2-29b>GFP	H on II; CyO ft	RJH 1-38	yes	no		Duke
	69-phm.mot-2	33c					KR-DZ,RJH balance	69-phm.mot2-33c>GFP		RJH 1-39	yes	no		Duke
	69-phm.mot-3	16c					KR-DZ,RJH balance	69-phm.mot-3-16c>GFP	H on III	RJH 1-40	yes	no		Duke
	69-phm.mot-3	33a					KR-DZ,RJH balance	69-phm.mot-3-33a>GFP	H on II	RJH 1-41	yes	no		Duke
	69-phm.NC	3a					KR-DZ,RJH balance	69-phm.NC-3a>GFP	H on III	RJH 1-42	No	no		Duke
	69-phm.NC	11b					KR-DZ,RJH balance	69-phm.NC-11b>GFP	H on III; TM6 ft	RJH 1-43	faint	faint		Duke
	69-phm.NC	15					KR-DZ,RJH balance	69-phm.NC-15>GFP	H on II	RJH 1-44	faint	faint		Duke
	69-phm.NC	18b					KR-DZ,RJH balance	69-phm.NC-18b>GFP	over TM6	RJH 1-45	yes	yes	Used in PPT	Duke
	69-phm.NC	24a					KR-DZ,RJH balance	69-phm.NC-24a>GFP	H on III	RJH 1-46	faint	faint	Used in PPT	Duke
	69-phm.NC	39					KR-DZ,RJH balance	69-phm.NC-39>GFP		RJH 1-47	faint	faint		Duke
	69-phm.mot4	21b					KR-DZ,RJH balance	69-phm.mot4-21b>GFP	H on III	RJH 1-48	yes	faint	used in PPT	Duke
	69-phm.mot4	26c					KR-DZ,RJH balance	69-phm.mot4-26c>GFP	H on II	RJH 1-49	yes	faint		Duke
	69-phm.mot4	27					KR-DZ,RJH balance	69-phm.mot4-27>GFP		RJH 1-50	no	no		Duke
	69-phm.mot4	44					KR-DZ,RJH balance	69-phm.mot4-44>GFP	H on III	RJH 1-51	yes	yes-medium		Duke
	69-phm.mot5	19a					KR-DZ,RJH balance	69-phm.mot5-19a>GFP	H on II; CyO ft	RJH 1-52	yes	strong	Used in PPT	Duke
	69-phm.mot5	44a					KR-DZ,RJH balance	69-phm.mot5-44a>GFP	H on II	n/a-dead stock	yes	strong		Duke
dlb														
	dlb-A	86	3' UTR of dlb gene	ctgatcgatctgcgattgcgt	tcggatgatggactcctccctgc		Abdi/RJH	dlb A-86>GFP	over FM7	n/a-dead stock	no	no		Duke
	dlb-B+C	12	5' ups dlb + intron 2	tgctcaaaggggaagaaaagcccc	atggcaaaggtgcactgcctgcttaagatcga and ac		Abdi/RJH	dlb B+C-12>GFP	H on II; CyO ft	RJH 1-53	yes	no		Duke
	dlb-B+C	18	5' ups dlb + intron 2	"	"		Abdi/RJH	dlb B+C-18>GFP	over CyO	n/a-dead stock	yes	no		Duke
	dlb-B+C	45	5' ups dlb + intron 2	"	"		Abdi/RJH	dlb B+C-45>GFP	H on II; CyO ft	RJH 1-54	yes	no		Duke
	dlb-B+C	61	5' ups dlb + intron 2	"	"		Abdi/RJH	dlb B+C-61d>GFP	over CyO	RJH 1-55	yes	no		Duke
	dlb170(BG8643	1	dlb 3rd intron	GTGGGCGTGGGCAGGATTCTTAA	GTGCTGCTCCAGCCGACAGG		RJH/DZ	dlb170-1>GFP	2	RJH 1-56	yes-faint	no		Best Gene
	dlb170(BG8643	2		"	"		RJH/DZ	dlb170-2>GFP	2	RJH 1-57	yes	no		Best Gene
	dlb170(BG8643	3		"	"		RJH/DZ	dlb170-3>GFP	2	RJH 1-58	yes	no		Best Gene
	dlb170(BG8643	4		"	"		RJH/DZ	dlb170-4>GFP	2	RJH 1-59	yes	no		Best Gene
	dlb170(BG8643	5		"	"		RJH/DZ	dlb170-5>GFP	2	RJH 1-60	yes	no		Best Gene
	dlb170(BG8643	6		"	"		RJH/DZ	dlb170-6>GFP	3	RJH 1-61	yes-faint	no		Best Gene
	dlb170(BG8643	7		"	"		RJH/DZ	dlb170-7>GFP	X	RJH 1-62	yes	no		Best Gene
	dlb190 (BG864	1	dlb 4th intron	TCTGGTCCTTCCCTTCGGTCACG	ATTCGTATTCACGCAGCAGCTGA		RJH/DZ	dlb190-1>GFP	2	RJH 1-63	yes	yes		Best Gene
	dlb190 (BG864	2					RJH/DZ	dlb190-2>GFP	2	RJH 1-64	yes	yes		Best Gene
	dlb190 (BG864	3					RJH/DZ	dlb190-3>GFP	x	RJH 1-65	yes	yes-faint		Best Gene
	dlb190 (BG864	4					RJH/DZ	dlb190-4>GFP	x	RJH 1-66	yes	yes-strong		Best Gene
	dlb190 (BG864	5					RJH/DZ	dlb190-5>GFP	2	RJH 1-67	yes	yes-faint		Best Gene
	dlb190 (BG864	6					RJH/DZ	dlb190-6>GFP	3	RJH 1-68	yes	yes-faint		Best Gene
	dlb190 (BG864	7					RJH/DZ	dlb190-7>GFP	x	RJH 1-69	yes	yes		Best Gene
	dlb190 (BG864	8					RJH/DZ	dlb190-8>GFP	2	RJH 1-70	yes	yes		Best Gene
	dlb190 (BG864	9					RJH/DZ	dlb190-9>GFP	2	RJH 1-71	yes	yes		Best Gene
	dlb420 (BG870	1	dlb 3rd to 4th intron	GTGGGCGTGGGCAGGATTCTTAA	ATTCGTATTCACGCAGCAGCTGA		RJH/DZ	dlb420-1>GFP	2	RJH 1-82				Best Gene
	dlb420 (BG870	2					RJH/DZ	dlb420-2>GFP	2	RJH 1-83	yes	yes-strong		Best Gene
	dlb420 (BG870	3					RJH/DZ	dlb420-3>GFP	x	RJH 1-84	yes	yes-strong		Best Gene
	dlb420 (BG870	4					RJH/DZ	dlb420-4>GFP	x	RJH 1-85	yes	yes-strong		Best Gene
	dlb420 (BG870	5					RJH/DZ	dlb420-5>GFP	x	RJH 1-86	yes	yes-strong		Best Gene
	dlb420 (BG870	6					RJH/DZ	dlb420-6>GFP	x	RJH 1-87	yes	yes-strong		Best Gene
	dlb420 (BG870	7					RJH/DZ	dlb420-7>GFP	x	RJH 1-88				Best Gene
	dlb420 (BG870	8					RJH/DZ	dlb420-8>GFP	x	RJH 1-89	yes	yes-strong		Best Gene

[
[